



UNIVERSITY OF
BIRMINGHAM

Scanning Tunnelling Microscopy and Spectroscopy Investigation of C₆₀ on Au(111) and HOPG Surfaces.

by
Megan Grose

A thesis submitted to the University of Birmingham
for the degree of Doctor of Philosophy

Nanoscale Physics Research Laboratory
School of Physics and Astronomy
University of Birmingham
December 2021

UNIVERSITY OF
BIRMINGHAM

University of Birmingham Research Archive

e-theses repository

This unpublished thesis/dissertation is copyright of the author and/or third parties. The intellectual property rights of the author or third parties in respect of this work are as defined by The Copyright Designs and Patents Act 1988 or as modified by any successor legislation.

Any use made of information contained in this thesis/dissertation must be in accordance with that legislation and must be properly acknowledged. Further distribution or reproduction in any format is prohibited without the permission of the copyright holder.

Abstract

In this thesis the investigation of C_{60} on Au(111) and highly oriented pyrolytic graphite (HOPG) surfaces is performed using scanning tunneling microscope (STM) imaging and scanning tunneling spectroscopy (STS). For C_{60} on Au(111) the relative heights and orientations of bright and dim fullerene molecules are examined, for C_{60} on HOPG the relative heights of the dim molecules are discussed. It was found that the C_{60} orientation most commonly found for dim molecules on Au(111) was with the hexagon facet of the C_{60} molecule adhered to the substrate. This orientation was also the most frequently observed when analysing the orientation of individual molecules within islands of C_{60} . The least commonly observed orientation was the pentagon facet of the fullerene adjacent to the substrate. The height analysis of C_{60} on HOPG found two groups of heights of 0.25 nm and 1.4 nm corresponding to the C_{60} monolayers being raised due to Au islands forming below the C_{60} monolayer and as a result of second layer C_{60} molecules. STS experiments on Au(111) and HOPG substrates at 77 K confirm results from prior studies; displaying that for HOPG the two unit cells have different local density of states (LDOS), and for Au(111) varying packing structures on the surface display differing responses. The STS spectra for A and B HOPG atoms show at larger negative bias the B atom has a larger conductance but for low bias and large positive bias the A atom has larger conductance. For Au(111) spectra the face centered cubic (FCC) component displays a higher conductance around -0.2 V, hexagonal close packed (HCP) shows this peak shifted to -0.3 V. Finally the STS investigation of C_{60} on Au(111) is detailed and the results presented. The Au/ C_{60} spectra were not reproducible and no conclusions could be drawn from the data.

Dedication

To the younger version of myself who thought this would be a good idea, you got through it.

Acknowledgements

Firstly I must thank EPSRC for providing the funding for this work and my supervisor Dr Quanmin Guo for the support he has provided throughout the PhD. I would like to thank Dr Wolfgang Theis for his help and the difficult questions he regularly asked and Dr Alex Pattison who I met in the first year of our undergraduate degree and has been a wonderful friend all the way through the PhD. To all of my family and friends who have supported me throughout this PhD thank you and I love you. I would like to specifically thank my parents for their support throughout my studies particularly for their help proof reading this document. My sisters though they hate listening to me talk about physics have also been very supportive over the last 4 years. I would not have been able to get through the pandemic without Lizzie and Julia, our weekly calls are often the highlight of my week. Thank you to my dressmaking benefactor and bestie Freddie for her ongoing friendship throughout undergrad and this PhD, she is my biggest cheerleader. I also wish to thank Georgina, my soul sister, the PhD was made bare-able because we shared the experience. I could not have done this without her and regular cuddles with Björn and Rufus. Finally I want to thank my partner Jonny, for help during the PhD and this thesis but also for his company and support in the day to day. He calms me down on a regular basis, forces me to breathe and watches trashy TV with me. I can not thank him enough for the love and support he has given me.

Table of Contents

List of Figures	9
List of Acronyms	22
1 Introduction	24
1.1 Gold, Graphite and C_{60}	25
1.2 Applications of C_{60}	26
1.3 Thesis Layout	28
2 Literature Review and Background Theory	29
2.1 C_{60}	29
2.2 Gold and Au(111)	32
2.2.1 Au(111) steps	37
2.3 HOPG	39
2.4 C_{60} on surfaces	40
2.4.1 C_{60} on Au(111)	42
2.4.2 C_{60} on HOPG	47

2.5	Scanning Tunelling Microscopy Theory	49
2.6	Scanning Tunneling Spectroscopy	55
2.6.1	STS Theory	55
2.6.2	Electronic Orbitals	57
2.6.3	STS measurements in previous work	58
3	Experimental Techniques	64
3.1	Low Temperature - STM Setup	64
3.1.1	Preparation chamber	67
3.1.2	Analysis chamber	73
3.2	Sample preparation	74
3.2.1	Substrate preparation	74
3.2.2	Gold C ₆₀ sample preparation	76
3.2.3	HOPG C ₆₀ sample preparation	77
3.2.4	Au adatom deposition onto C ₆₀ Au(111) and C ₆₀ HOPG samples	77
3.3	Tip production	78
3.4	STS methodology	80
4	Investigation of C₆₀ on Au(111)	81
4.1	Experimental Method	82
4.2	Results and Discussion	83
4.2.1	Bright and Dim C ₆₀ molecules	86
4.2.2	C ₆₀ molecules orientation	90

4.3	Summary	101
5	Investigation of C_{60} on HOPG	103
5.1	Experimental Methods	104
5.2	Results and Discussion	105
5.2.1	Bright Molecules	106
5.2.2	Dim molecules	111
5.2.3	Orientation	116
5.3	Summary	119
6	Scanning Tunneling Spectroscopy Studies of Au(111), HOPG and C_{60} on Au(111).	120
6.1	Experimental Method	121
6.1.1	STS Tips	121
6.1.2	Lock-in	123
6.1.3	Analysis	124
6.2	Results and Discussion	125
6.2.1	Spectroscopy measurements on Au(111)	125
6.2.2	HOPG	138
6.2.3	C_{60} on Au(111)	152
6.3	Summary	156
7	Conclusion	158

7.1	STM investigation of C_{60} on Au(111)	159
7.2	STM investigation of C_{60} on HOPG	162
7.3	Comparison of results from C_{60} on HOPG and Au(111)	163
7.4	STS investigation of Au(111), HOPG and C_{60} on Au(111)	165
7.4.1	Comparison of STS and STM Investigations	168
7.5	Suggestions for future work	168
Bibliography		170

List of Figures

2.1	A diagram of a C_{60} molecule where the circles represent the carbon atoms and the bonds between are represented by straight lines.	31
2.2	a) A diagram of an FCC unit cell. b) Diagram of an HCP unit cell. c) Diagrams of 100, 110 and 111 lattice planes shown on a simple cube. .	33
2.3	Image of the Au(111) surface showing the herringbone reconstruction pattern.	34
2.4	Diagram showing the positions of the atoms and the corresponding height profile of one row of those atoms. The atoms on the surface layer (black dots) and the atoms in the layer below (white circles) are shown to demonstrate how the top atoms move from FCC to HCP over the course of the reconstruction.	35
2.5	Annotated STM images showing the reconstruction pattern and the different elbow types in more detail.	36

2.6	The left image shows a step where the discommensuration line (DL)s form U-turns and a single DL runs parallel to the bottom edge of the step. The right image shows a step edge where the DLs continue through the step.	37
2.7	a) A diagram showing the top down view of the atomic positions for an island on an FCC surface, light grey circles are top layer atoms and dark grey are the layer beneath.b) The side view of the atomic positions for the two types of micro-facets labeled in a)	38
2.8	Diagram of the C_{60} molecule in 3 rotations and the corresponding structure seen when STM imaging. The C_{60} molecule with 5 fold symmetry has a pentagon face adjacent to the sample; the 2 fold symmetry occurs when the molecule has a bridge (bond between two hexagons) bonded to the surface; and the three fold symmetry is when the molecule has a hexagonal face bound to the surface of the substrate.	41
2.9	C_{60} molecules (circles) orientation with respect to the gold atoms beneath (crosses). The unit cell of the arrangement is illustrated with a dark lined shape in each of the diagrams. The darker grey C_{60} molecules are to represent the fact that every 3 C_{60} molecules occupies the same lattice site.	43

2.10	An STM image showing a C ₆₀ island formed on an Au(111) surface with various bright and dim molecules shown throughout the image. The image shows all four phases described above: R0°, R14°, R30° and, R34°. The white line at the bottom right corner shows the direction of the DL on the gold surface.	45
2.11	Figure showing a schematic view of an STM and the basic electronic layout.	50
2.12	Figure showing tunneling through a simple 1D square barrier.	51
2.13	This image shows Bardeen's approach to the system by separating the tip and surface into two separate systems.	53
2.14	A diagram of molecular orbitals of a molecule. The lower orbitals are filled and the top few orbitals are empty, given some energy, electrons can move into the unoccupied orbitals and transition back releasing that energy, often in the form of light (a photon).	58
2.15	STS spectrum from Au(111) showing the difference in curves from a terrace and a step.	59
2.16	Graph showing the difference in STS spectrum at different current set points (inversely proportional to the height of the STM tip).	61
2.17	Graph of $\frac{dI}{dV}$ and the density functional theory (DFT) comparison for C ₆₀ on Au(111) and C ₆₀ on Ag(100)	63

3.1	A schematic of the low temperature scanning tunneling microscope (LT-STM) used in this project, viewed from above.	65
3.2	A simplified schematic of the LT-STM used within these experiments illustrating the sample movement within the system.	66
3.3	Diagram of the C ₆₀ evaporator.	69
3.4	Diagram showing the the E-beam evaporator used to evaporate gold onto samples within these experiments. The cut out section at the top of the shield is to illustrate the structure underneath for clarity.	70
3.5	a) A typical background spectrum from the residual gas analyser in the LT-STM system. b) an RGA spectrum taken whilst argon was leaked into the chamber, a large peak at 40 m/z can be seen which corresponds to the atomic mass of argon (39.95u). The other large peak at 20 m/z is due to the Ar ²⁺ ion.	72
3.6	A schematic of the setup used for etching tungsten wire into tips. . . .	78
4.1	A 100×100 nm image of 0.7 ML C ₆₀ on Au(111) taken at 137 pA and 1.5 V. The image shows a large island of C ₆₀ molecules that crosses multiple steps and contains examples of bright and dim C ₆₀ molecules. The reconstruction of the Au(111) substrate is visible on the bare gold at the bottom of the image.	84

4.2	An 137×48 nm image showing 0.7 ML C_{60} coverage on step edges at two different contrasts. The image is taken at 165 pA and 700 mV. The left image shows the C_{60} molecules in focus and in the right image the resolution of the DLs is clearer. The molecules form preferentially on FCC areas of the step.	85
4.3	a) Graph of the height profiles taken over four points on a C_{60} island. The inset shows the location of each height profile taken. b) Image showing an area of a C_{60} island on Au(111) the 3 dim molecule locations and one bright molecule are highlighted by white circles these molecules' depth/height was measured and is shown in a). The image is $21 \text{ nm} \times 9 \text{ nm}$ taken at 1.97 V and 222 pA.	86
4.4	Histogram of the depth of different dim molecules across multiple samples with a smoothing fit applied to show any obvious peaks. The peaks on the smoothing fit are at 32 and 70 pm depth below the monolayer height.	88
4.5	A table showing diagrams of the C_{60} molecule orientation, a simplified orbital structure diagram of what would be observed through the STM and STM images of the corresponding orientations.	91
4.6	A 7.8×4.3 nm image (taken at 1.42 V and 123 pA) showing the electronic lobe structure of C_{60} molecules within a small island of C_{60} . The red circle represents the "hexagon down" orientation, the green represents the "bridge down" and the blue represents the "pentagon down" orientations.	92

4.7	a) A 10×6 nm image taken at 1.42 V and 124 pA showing the orientation of C_{60} molecules within an island. The blue box on the image corresponds to the enlarged image just below and the white line indicates the line that the height profile was obtained at. The molecules in the enlarged portion of a) are numbered and correspond to the numbers on the graph in b). b) A graph showing the height of multiple C_{60} molecules along the line shown in a).	93
4.8	A pie chart showing the proportion of the orientations observed for dim molecules within multiple STM images. Each segment of the pie chart has examples taken from different STM images of the dim molecules as examples.	96
4.9	Images showing the different phases in one STM image of a C_{60} island on Au(111). a) A 40×40 nm image taken at 708 mV and 112 pA of 0.6 ML coverage C_{60} . The white boxes correspond to the two enlarged areas b) 34×16.5 nm and c) 29×11 nm. The green line on image a) and c) corresponds to the direction of the reconstruction lines of the gold substrate. d) takes the four different lines (blue green black and grey) from the previous images and compares the angles between each of them and hence the phases of those islands.	98

4.10	This figure shows the frequency of each orientation of C_{60} molecule for different phase islands of C_{60} . The first graph shows the data taken from various C_{60} islands with 0° phase difference to the gold lattice below. The second graph shows the data from two $R14^\circ$ islands and the final two graphs contain data collated from an $R30^\circ$ island and an $R34^\circ$ island.	99
5.1	A 100×50 nm image of the C_{60} -Au HOPG surface. The C_{60} molecules cover the majority of the sample with the bare HOPG only visible through gaps in the C_{60} monolayer. This image was taken at 1.5 V and 152 pA with 0.75 ML C_{60} and 1 minute Au deposition.	106
5.2	a) A 79×56 nm image of three types of bright features in an STM image of an HOPG sample with 0.75 ML C_{60} and 2 minutes Au deposition. Taken at 2.5 V and 110 pA. b) The corresponding height profiles along the lines indicated on (a). The black line profile is taken along the line labeled a and the blue profile is taken along the profile b. Heights of the features are labeled on the figure.	107
5.3	Histogram showing the number of bright molecules found at different heights. The red curve is a smoothing fit applied to show any major peaks detected.	109

5.4	Diagram showing possible arrangements of the C_{60} molecules and the gold adatoms on the HOPG surface. Figure a) shows a single layer Au island and c) shows a double layer gold island sitting on the surface of the HOPG substrate. Diagrams b) and d) show two possible arrangements for two single layers of gold islands forming between the two C_{60} layers. These diagrams are for illustration purposes and the atoms shown are not to scale with one another.	110
5.5	A 23x20 nm size image of the C_{60} monolayer on HOPG with dim molecules and one bright molecule. Taken at 1.5 V and 114 pA, the sample had 0.75 ML C_{60} deposition and 1 minute Au.	112
5.6	Height profiles a-d of the molecules labeled on 5.5. The heights of the features are labeled on the graph in the corresponding colour to each trace.	112
5.7	Histogram of the number of dim molecules found at different heights. The red curve is a smoothing fit that shows only one peak in the distribution.	113
5.8	Images of the orientation of dim molecules in a C_{60} monolayer. a) 18x10 nm taken at 1.5 V and 114 pA. b) 21x8 nm taken at 1.5 V 114 pA. Both samples had 0.75 ML C_{60} and 1 minute Au deposition.	116

5.9	Figure showing the effect of a C_{60} molecule's orientation adsorbed on the STM tip when scanning Si(111). The top image of a, b and c shows a model of the C_{60} molecule showing the face that is adjacent to the substrate in yellow: a) bridge site between two hexagons b) bridge between hexagon and pentagon facets and c) a pentagon facet bonded to the sample. The large STM image in the centre of a b and c is an STM image showing how these orientations appear in a scan. The bottom left image is a zoomed in version of the image above focusing on one molecule and the bottom right image is the same but with a higher contrast so the orbital shape can be more easily resolved.	118
5.10	Image of C_{60} molecules on HOPG taken with C_{60} adsorbed onto the tip. a) 5.3x2.8 nm taken at 1 V and 112 pA on sample with 25 minutes C_{60} and 1 minute Au. b)15.5x3.5 nm taken at 1.5 V and 146 pA on sample with 25 minutes C_{60} and 1 minute Au deposition, the red arrow indicates the line where the tip changed state.	118
6.1	a)Image of an etched W tip magnified with an optical microscope, showing the basic shape of a good tip. b) Image of a recrystallised and heated wire in the wire etching holder, the brighter section at the end of the wire is where the tungsten oxide layers have been removed, it appears a brighter silver to the rest of the tungsten wire.	123

6.2	a) Graph of the IV sweep performed during the spectroscopy measurement. b) Graph showing $\frac{dI}{dV}$ against V for the same bias sweep as in a). The data for both these graphs was taken on the bare HOPG surface. .	125
6.3	a) Graph showing the differential current vs voltage curve averaged from multiple Au(111) spectra. b) Graph showing the normalised differentiated current data for Au(111). The peaks observed on this graph are located at -0.53 V , -0.33 V , $+0.34\text{ V}$ and 0.58 V . The spectrum was taken at 200 mV set-point voltage and 0.2 nA	126
6.4	Figure showing the electronic structure, typical I-V and $\frac{dI}{dV}$ curves for metals, semi-metals, semiconductors and insulators.	127
6.5	Graph showing the STS spectra averaged over 15 FCC positions on the Au(111) surface. The spectra were taken at 500 mV and 1 nA set-point. The surface state peaks on this graph are at approximately -0.36 V and -0.2 V . The vertical lines on the graph help to highlight peaks that are at similar voltages to experiments found in the literature and to guide the eye.	129
6.6	Graph showing STS data averaged from 26 HCP sites taken at 500 mV and 1 nA set-point. Main peaks observed in this spectrum are observed at -0.31 V and -0.39 V . The vertical lines on this graph are used as a guide to show the shape of the curve at certain voltages that have been previously associated to peaks or troughs in conductance	130

6.7	Graph showing the averaged STS data from DL sites averaged over 22 spectra, taken at 500 mV 1 nA . Peaks of this spectra are highlighted with vertical lines on the graph indicating their position. The -0.31 V peak is due to the surface state of the gold.	131
6.8	Graph showing the comparison between FCC HCP DL and an averaged spectra over various positions of Au(111) surface. Peaks highlighted are at -0.6 V, -0.3 V, -0.2 V, 0.34 V and 0.57 V	132
6.9	Graph showing STS of step edge sites and the averaged Au signal from figure 6.3 taken at multiple points on a terrace. The terrace spectra taken at 500 mV 1 nA averaged over 34 spectra, and the step edge spectra taken at 500 mV 1 nA averaged over 18 spectra (upper edge) and 10 spectra (bottom edge).	135
6.10	STS taken at the top and bottom of a step on the Au(111) surface. Spectra taken at 500 mV and 1 nA averaged from 18 and 10 data sets respectively. The peak positions are at -0.49 V (lower step edge) and -0.34 V (upper edge).	136
6.11	a) Graph of normalised edge spectra from -1 V to 1 V. b) Enlarged portion of (a) from -1 V to -0.2 V with peaks highlighted at -0.49 V and -0.34 V. Upper step edge spectra averaged over 18 curves, taken at 500 mV 1 nA. Lower edge spectra averaged over 10 curves, taken at 500 mV 1 nA.	137

6.12	STS profile from the HOPG surface averaged over 34 spectra and taken at 100 mV and 1 nA set-point.	139
6.13	Graph showing STS curves on HOPG at different set-point voltages. The positive and negative biases are shown in the same colour with the positive bias as a solid line and the negative bias presented as a dashed line.	140
6.14	Graphs showing the unnormalised (left) and normalised (right) STS spectra taken at positive and negative 100 mV set-point voltages and 1 nA . The blue line represents +100 mV and the red line represents -100 mV.	142
6.15	Graph showing the curves averaged over multiple spectra taken at 300 mV 200 mV and 100 mV set-point voltages and 1 nA. a) differential current b) normalised differential current.	143
6.16	Image showing the HOPG surface atoms. The left hand image shows the triangular lattice and the right hand side image shows the hexagonal lattice, over both images a diagram of 6 carbon atoms is superimposed to show the rough positions of the atoms that make up the image.	144
6.17	Image showing the layers of carbon atoms, their arrangement and the top down view of the surface layer of carbon atoms. The A type atoms are shown as black dots and the B type atoms are shown as white dots. The unit cells for A and B atoms are shown with red triangles.	145

6.18	a) Graph showing the averaged spectra produced for -100 mV and 100 mV on the two types of triangular lattice. b) Graph showing the averaged spectra produced for -200 mV and 200 mV on the two triangular lattice atoms. Peaks have been shifted vertically for clarity.	146
6.19	Graph showing the spectra of A and B atom types taken at 200 mV 1 nA set-point.	148
6.20	Graph showing the I-V response at bright and dim spots on 1 layer (a and b) 2 layer (c) and 3 layer (d) superlattice lattices. The Blue circle shows the position where the red curve was taken and the yellow circle shows the position of where the black curve was measured.	150
6.21	Images of triangular lattice and hexagonal lattice observed via STM imaging and the corresponding $\frac{dI}{dV}$ spectra for each lattice. a) triangular lattice b) spectra from the triangular lattice area c) hexagonal lattice d) spectra from the hexagonal lattice.	151
6.22	Figure showing graphs of the STS spectra from C_{60} molecules adsorbed on the Au111 substrate, averaged from 9 spectra taken at 700 mV 0.2 nA set-point.	153
6.23	Figure showing a graph of the STS spectra from C_{60} molecules adsorbed on the Au111 substrate. The data was averaged from 3 data sets taken at 1.5 V 0.2 nA set-point.	154

List of Acronyms

AFM atomic force microscope.

DFT density functional theory.

DL discommensuration line.

DOS density of states.

EELS electron energy loss spectroscopy.

FCC face centered cubic.

FEL fast entry lock.

HCP hexagonal close packed.

HOMO highest occupied molecular orbital.

HOPG highly oriented pyrolytic graphite.

IRRAS infrared reflection-absorption spectroscopy.

LDOS local density of states.

LT-STM low temperature scanning tunneling microscope.

LUMO lowest unoccupied molecular orbital.

RGA residual gas analyser.

SAM self assembled monolayers.

STM scanning tunneling microscope.

STS scanning tunneling spectroscopy.

TSP titanium sublimation pump.

UHV ultra high vacuum.

UPS ultraviolet photoelectron spectroscopy.

XPS X-ray photoelectron spectroscopy.

Chapter 1

Introduction

Nanotechnology is the study of materials and their applications at the nanometer scale ($\times 10^{-9}$ m). In 1981 the STM was invented by Binnig and Rohrer at IBM ^[1], this invention opened up the field of nanotechnology for study and was awarded the Nobel prize in 1986. The STM was the first instrument that allowed the study of atomic surfaces and is still one of the main tools used in surface science today. The STM, unlike an optical microscope uses a probe and quantum tunnelling electrons to “view” the desired sample. Other probe microscopes have developed from this invention such as the atomic force microscope (AFM) and are also key to the field of surface science.

STS is an expansion to the method of imaging with the STM. Tunnelling microscopy allows for images to be generated using a tunnelling current that travels between the tip (probe) and the sample. A current is measured at each lateral position and plotted in a matrix to provide an ‘image’ detailing topography of the surface being scanned.

Spectroscopy is a process of probing matter with a wave, usually electromagnetic radiation, and studying the interaction. For example, illuminating a substance with light consisting of a range of wavelengths, then observing either the absorption or emission of specific wavelengths can provide information on the constituents of the substance. In the case of STS the tunnelling electrons energies are varied by adjusting the bias voltage across the STM. The corresponding tunnelling current is measured for each voltage and a spectrum of current vs voltage is produced. This technique has advantages over other spectroscopy techniques used in surface science such as X-ray photoelectron spectroscopy (XPS) as the spectra can be measured at a very specific point on the sample and probes the local effects as opposed to measuring the surface as a whole.

1.1 Gold, Graphite and C₆₀

One area that can be examined with an STM is the adsorption of molecules and formation of monolayers on surfaces. Self assembled monolayers (SAM) are a field of research where molecules are deposited onto a surface on which their arrangement and bonding can be examined. Many combinations of substrates and different types of molecule have been studied previously; from metals and organic molecules^[2] to semiconductors^[3] and metal adlayers^[4]. This thesis will focus on the study of the C₆₀ molecule on gold and HOPG surfaces.

Gold and HOPG substrates are often used in surface science as they are relatively inert^[5]

and provide flat surfaces suitable for the STM^[6]. The Au(111) surface in particular is a good candidate as it has a distinct pattern that forms on the surface which can be used as a template for molecules adhere to^[7]. HOPG is a form of graphite that is atomically flat over large scales and is easy to prepare and clean due to its structure. The bonds between layers of graphite are much weaker than the bonds within a plane and therefore it is easy to remove top surface layers just using sticky tape.

The C_{60} molecule is an allotrope of carbon, other forms of carbon include graphite, diamond and graphene. C_{60} as the name suggests is formed of 60 carbon atoms and is arranged in a similar shape to a football technically called a truncated icosahedron. C_{60} can also be referred to as Buckminsterfullerene or “Bucky balls”, these names derive from the architect Buckminster Fuller, since the molecular structure of C_{60} is reminiscent of the geodesic domes Fuller designed^[8]. The molecule was discovered unintentionally in 1985^[9] when performing an experiment irradiating graphite with a laser aiming to form long chain carbon structures. Curl, Kroto and Smalley were awarded a Nobel prize for C_{60} ’s discovery in 1996 which has led to the discovery of a new class of carbon structure “fullerenes”.

1.2 Applications of C_{60}

C_{60} has been investigated in many applications ranging from catalysis^[10], electronics^[11], self assembled monolayers (SAM)’s to healthcare (both diagnostic and therapeutic

uses)^[12]. One of the applications driving the study of C_{60} molecules on surfaces is their potential electronic applications. C_{60} molecules have previously been investigated as possible single molecule transistors^[11], research on the way the molecules behave on varying surfaces and arrangements could lead to their use as building blocks for future circuitry.

C_{60} has been studied on a variety of metal surfaces, it has been found to alter the surface reconstruction of most metals it adheres to and readily forms an organised monolayer^[13]. On gold the C_{60} molecule has been studied as a monolayer and as a sub monolayer where magic number clusters have been found to form^[14]. Magic number clusters are so named due to the enhanced stability of the clusters containing specific numbers of atoms compared to similar sized clusters that don't have the "magic number" of atoms. In this case the term "magic number" does not reference the number of fullerene molecules in the cluster but the combination of a specific number of gold adatoms and C_{60} molecules^[15]. The C_{60} molecule has been previously studied by STM and STS on the gold substrate, the results that have been previously obtained will be built upon and compared to the results achieved within this thesis. When C_{60} has been deposited on HOPG and examined it was found that C_{60}/Au magic number clusters still formed but as part of a matrix of C_{60} molecules as opposed to individually^[16]. This work will continue the investigation of the C_{60} gold matrix that forms on HOPG. STS investigations of Au(111) and HOPG have been completed in the past and the results observed will be compared to the results obtained in this thesis. The STS spectra

obtained from multiple positions on the Au and HOPG surface will be compared and finally the STS spectra of C_{60} on Au(111) will be compared to the base Au(111) spectra. While previous experiments have been completed using STS and STM on C_{60} /gold and C_{60} /HOPG surfaces the main focus of these experiments is to increase the understanding of the C_{60} -Au magic number clusters that can form on both substrates and the orientation and conductance across different areas of these clusters. The use of low temperature scanning can help to provide information on the orientation of the C_{60} molecules with respect to the substrate below and the STS experiments can provide the information on local density of states within the cluster.

1.3 Thesis Layout

The literature review section of this thesis will contain more information on C_{60} , gold and HOPG surfaces as well as a discussion of relevant previous research. After this the experimental chapter will provide more detailed information about the techniques and equipment used throughout the experiments within this work. The results chapters will be split as follows: first the STM investigation of C_{60} on Au(111) will be discussed; secondly the experiments of C_{60} on HOPG will be posited; and finally the STS experiments on Au(111), HOPG and C_{60} on Au(111) will be analysed. A conclusion chapter will summarise the results presented within this work and any postulates for future work will be detailed.

Chapter 2

Literature Review and Background Theory

In this chapter the theory behind the instruments and methods will be discussed along with the background information on materials used throughout this thesis. Also discussed here will be relevant experiments undertaken previously in similar or related areas to provide context.

2.1 C_{60}

C_{60} was discovered in 1985 by Kroto et al. ^[9], it is a football shaped molecule comprised of 60 carbon atoms. The C_{60} molecule belongs to a class of carbon structures known as fullerenes which are defined as hollow spheroidal molecules comprised of car-

bon atoms^[17].

Other fullerenes can be produced in varying sizes which are denoted by the number within their name, for example, the molecule C₇₀, C₈₀ etc. which are comprised of 70 and 80 carbon atoms respectively. The discovery of fullerenes was the one of the first of various nanocarbon structures, with nanotubes (1991^[18]) and graphene (2004^[19]) following in its wake.

C₆₀ along with other carbon allotropes has been suggested for many different applications ranging from electronic devices to uses in healthcare. The potential use of C₆₀ in electronic applications stems from the work by Park et al.^[11] where the C₆₀ molecule behaved as a transistor between two gold electrodes. C₆₀ molecules also have uses as electron acceptors in organic photovoltaic devices such as solar cells^{[20],[21]}. The medical applications often rely less on the electronic properties of the molecule but more on its size and relative ease of functionalisation (adding on functional groups to the molecule). It can be used in both therapeutic and diagnostic cases, a therapeutic example is the use of the C₆₀ cage as a mechanism for drug delivery^[12]. Due to its hollow structure the C₆₀ molecule can be utilised as a carrier of other molecules such as proteins or metals, this type of functionalised C₆₀ molecule is known as an endofullerene. These endofullerenes can be used in diagnostics as contrast agents in magnetic resonance imaging, and radiotherapy techniques^{[22][23]}. Another application of C₆₀ molecules is utilising the orientational organisation it can exhibit on different surfaces, for example the work on the Au(111)^[24]. More information on the orientation of C₆₀ molecules on surfaces is

discussed later in this chapter in sections 2.4.1 and 2.4.2.

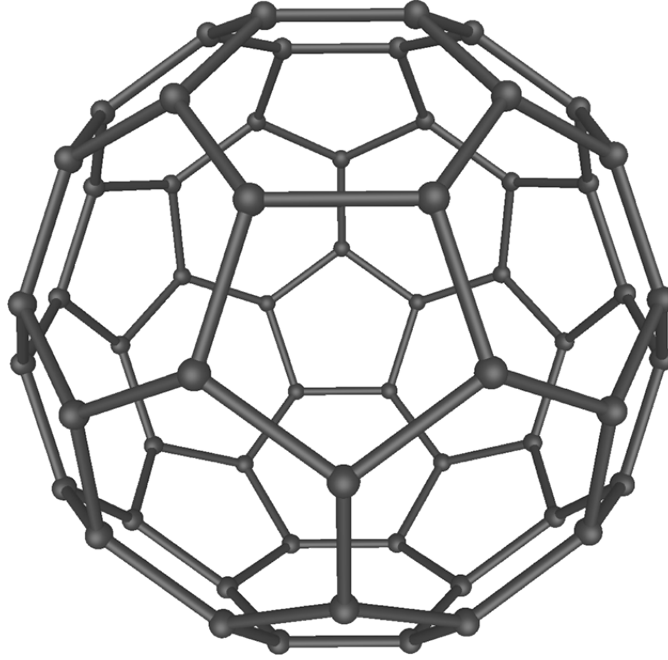


Figure 2.1: A diagram of a C_{60} molecule where the circles represent the carbon atoms and the bonds between are represented by straight lines. Sourced from[25].

The structure of C_{60} is similar in shape to a football made up of 12 pentagons and 20 hexagons, also known as a truncated icosahedron. A molecular diagram of this structure can be seen in figure 2.1. The molecule is a ≈ 1 nm sphere and has a similar electronic structure to graphene [26], where the exact size of the carbon cage excluding the surrounding electron cloud is 0.7 nm. The size observed when scanning with a scanning tunneling microscope can vary due to the molecule's orientation, its position on the substrate and the type of substrate examined. C_{60} molecules' height when adsorbed onto an Au(111) surface was found to be between 4.9- 7.3 Å by Yang et al. [27] whereas the height observed by Guo et al. [28] on a highly oriented pyrolytic graphite (HOPG) surface is 8 Å. More information about C_{60} on surfaces can be found later in

this chapter in section 2.4.

2.2 Gold and Au(111)

Gold is particularly useful for nanoscale applications due to its lower reactivity, surfaces do not oxidise easily so producing a clean surface is relatively easy compared to other substrates^[29]. Gold substrates can provide large flat terraces^[30] which is convenient for depositing other materials onto, as imaging on a flat surface often yields better results than surfaces with an abundance of steps. Bulk gold has a face centered cubic (FCC) lattice structure and the structure of the sample surface can be along the $\{111\}$, $\{100\}$, and $\{110\}$ crystallographic planes. A diagram of these planes and the FCC lattice structure is shown in figure 2.2. The surface used throughout this thesis is the (111) surface.

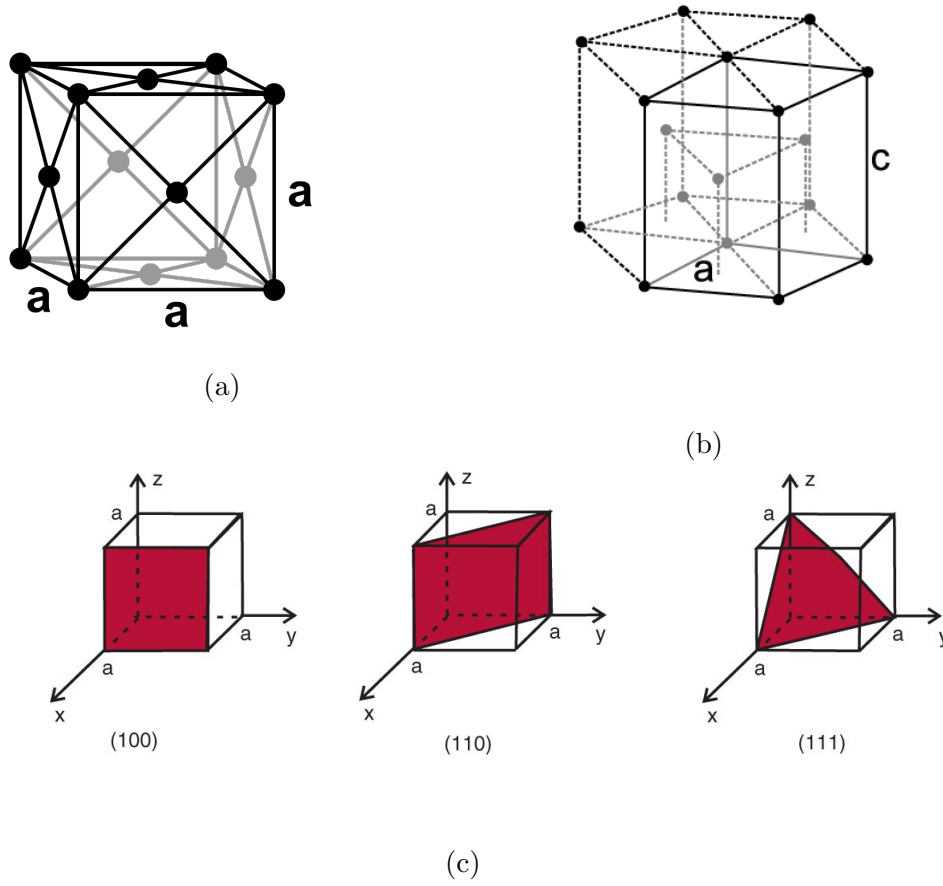


Figure 2.2: a) A diagram of an FCC unit cell, sourced from [31] b) Diagram of an hexagonal close packed (HCP) unit cell, sourced from [32] c) Diagrams of 100, 110 and 111 lattice planes shown on a simple cube, sourced from [33]

Au(111) is often used as a substrate within the field of nanotechnology, particularly in aiding the formation of self assembled monolayers^[7], this is due to the unique surface reconstruction that the Au(111) surface exhibits($22 \times \sqrt{3}$). The 111 reconstructed surface is the most thermodynamically stable when compared to its 100 and 110 surfaces^{[34][35]}. The reconstruction on the 111 surface forms in a herringbone pattern (shown in figure 2.3). This reconstruction is caused by gold atoms contracting along the $\langle 110 \rangle$ direction so that 23 atoms compress into 22 lattice sites^[36].

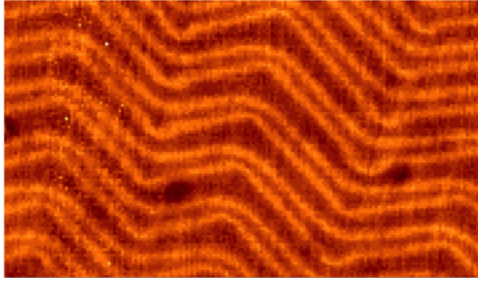


Figure 2.3: Image of the Au(111) surface showing the herringbone reconstruction pattern.

The contraction of the surface atoms results in some sitting slightly higher than their neighbours, around $0.15\text{-}0.25\text{ \AA}$ ^[30]. This height difference is a result of the lattice site the atoms are sitting in. The contraction forces the surface atoms to shift slightly from their FCC lattice sites when allowing the extra (23rd) atom to sit in the space that 22 would normally occupy. Therefore, the position the atoms sit in relative to the atoms on the layer below is shifted. Looking at the 23 atoms relative to the layers of atoms below, they are initially in an FCC position and are shifted until they are in an HCP position. They then migrate back to an FCC position, this can be seen in figure 2.4. The areas between the two crystal structures where the atoms are not sitting in a conventional lattice site are slightly raised compared to the HCP and FCC areas, this is called a discommensuration line (DL). These lines can be thought of as the top layer forming ridges as it is compressed (similar to the way cardboard would if you applied pressure to it perpendicular to its surface).

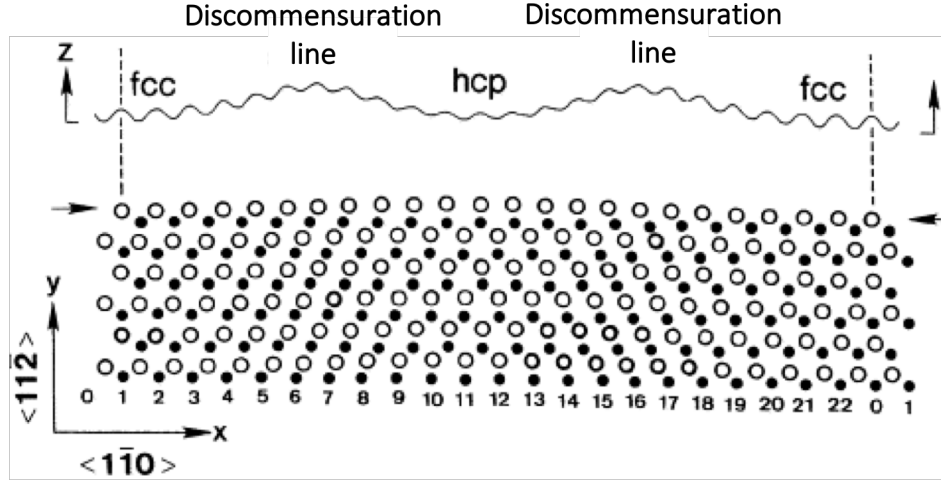


Figure 2.4: Diagram showing the positions of the atoms and the corresponding height profile of one row of those atoms. The atoms on the surface layer (black dots) and the atoms in the layer below (white circles) are shown to demonstrate how the top atoms move from FCC to HCP over the course of the reconstruction. Sourced from [37].

Since bulk gold has an FCC structure the FCC packed areas on the surface are more favourable and account for a higher percentage of the surface than the HCP areas^[34]. This can be seen in images of the reconstruction (figure 2.3) as the distance between a pair of discommensuration lines is smaller than the distance between two adjacent pairs. The distance between pairs (the repeating unit distance) is 63 \AA and the distance between 2 lines that make up a pair is around 44 \AA ^[30].

The corners of the reconstruction lines are referred to as elbow sites, this is where the discommensuration lines change direction by 120° . The change in direction of two DLs results in one DL having a “bulged elbow” and one having a “pinched elbow” ^[38] (figure 2.5). The types of elbow sites can form on either HCP or FCC sites and the

distribution between the two is even, for example in one line of elbows the pinched site might be on an HCP packed area of the surface but in the next line of elbows that occur the pinched elbow would be on an FCC region. Several studies have found that when material is deposited on the Au(111) surface the elbow sites are the preferential adsorption sites^{[39][40]}.

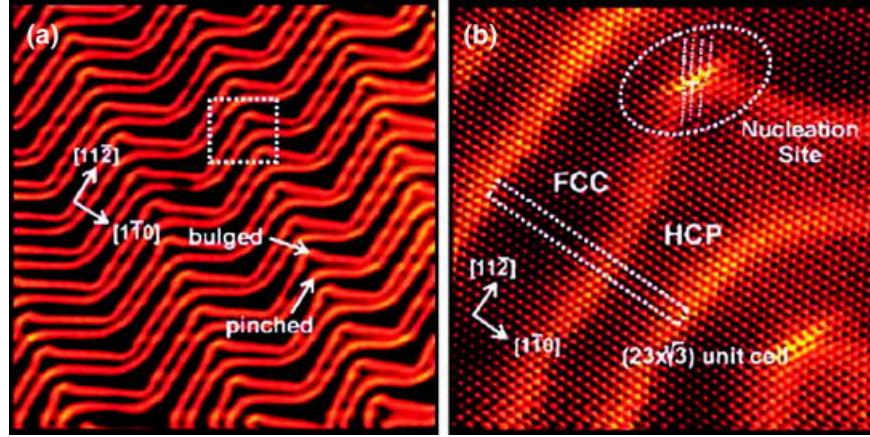


Figure 2.5: Annotated scanning tunneling microscope (STM) images showing the reconstruction pattern and the different elbow types in more detail. Sourced from [41] adapted for [42].

When examined in further detail it has been shown that the bulged elbows are more desirable sites for adsorption, since the atoms are compressed the most at this point in the reconstruction.^[38] More atoms in the region, results in more electrons occupying the site so the electron density of that area is higher than surrounding areas^{[38][43]}.

When the energy of the reconstructed surface is studied and compared to the energy of the atoms in their bulk lattice positions, it is shown that the FCC and HCP regions have a lower energy than the DLs^{[34][35][36]}. The FCC regions have a slightly lower energy ($\approx 10\text{ meV}$) than the HCP regions which makes sense since FCC is the bulk crystal

structure for gold. However, the DL atoms have considerably higher energy than the bulk atom conditions they were compared to by $\approx 33 \text{ meV}$.

2.2.1 Au(111) steps

On an Au(111) substrate two types of step can be observed; one where the DL's pass through and one where there is a single DL alongside the step (with many U turns adjacent to the step edge)^[30]. Examples of these steps can be seen in figure 2.6.

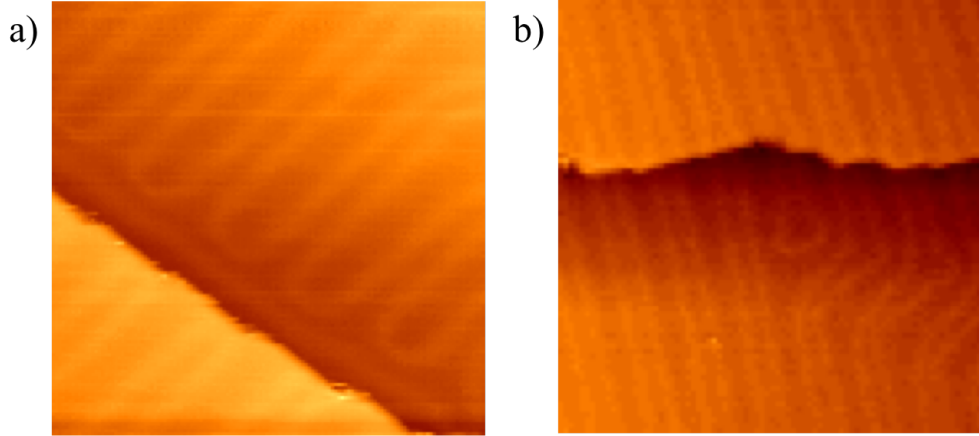


Figure 2.6: The left image shows a step where the DLs form U-turns and a single DL runs parallel to the bottom edge of the step. The right image shows a step edge where the DLs continue through the step.

The difference between the two step types is a result of the micro-facet of the step in question. When examining the atomic structure of a 111 plane from above (figure 2.7a) it can be seen that 2 kinds of close packed steps are present, one with a $\{111\}$ micro-facet and one with a $\{100\}$ micro-facet. This difference is shown more clearly in a diagram with the perspective along the plane of the surface (figure 2.7b). The $\{111\}$

step has the atom on the lower level in the hollow site between the two atoms above, and the $\{100\}$ step has the atoms on the top and lower level directly in line.

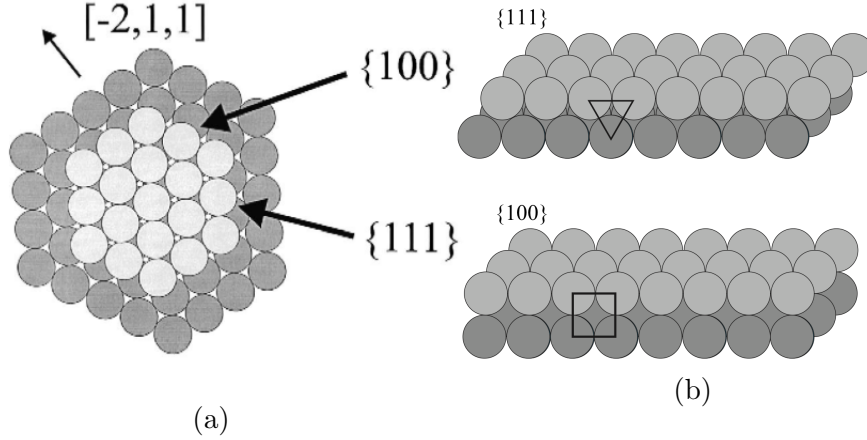


Figure 2.7: a) A diagram showing the top down view of the atomic positions for an island on an FCC surface, light grey circles are top layer atoms and dark grey are the layer beneath. Adapted from [40]. b) The side view of the atomic positions for the two types of micro-facets labeled in a).

Previous work illustrates that the DL lines pass through $\{111\}$ steps and the DLs form U turns at $\{100\}$ microfaceted steps, this was found to be true for a range of temperatures^[44]. As discussed previously Au(111) is an FCC crystal in bulk form, only the top surface layer reconstructs and shifts from the bulk spacing positions. This means that the atoms on the layer directly underneath the step are in FCC positions^[45]. The reconstruction line that runs parallel to the $\{100\}$ steps forms to allow the atoms adjacent to the lower edge of the step to also be in an FCC structure. The $\{111\}$ steps have a lower step energy than the $\{100\}$ steps^[46], and they are more frequent on the surface than $\{100\}$ steps.

2.3 HOPG

Highly Oriented Pyrolytic Graphite (HOPG) is commonly used in nanotechnology: as a monochromator in X-ray diffractometry^[47]; as a calibration sample for scanning probe microscopes; and as a substrate for electrochemical experiments^[48]. HOPG is a synthetic form of carbon produced by hot pressing (applying a high heat and temperature) to form pyrolytic carbon, this is then annealed to improve the crystallinity of the graphite. The resulting HOPG has a very small angular distribution of its comprising graphite layers. The large atomically flat crystallites of graphite, within the HOPG sample, are useful for calibrating scanning probe microscopes^[6], where the distance between carbon atoms can be measured to calibrate scanning distances in the xy plane. It is largely a chemically inert sample with high thermal stability in and out of vacuum^[47]. The properties of HOPG are similar to that of a graphite single crystal but with larger crystal domains and fewer impurities. The properties of graphite differ depending on the plane in question, for example along the plane the electrical resistance is low and perpendicular to the graphite plane the resistance is much higher.

As a substrate HOPG can be used as a template to form either islands or nanoparticles when metals are deposited on its surface. One major advantage to using HOPG as a substrate is the ability to clean the surface by cleaving. Graphite is comprised of multiple hexagonally close packed planes of carbon atoms, the bonds within a plane (x-y plane) are much stronger than bonds between planes (z axis). These weak bonds allow the top few graphite layers to be easily removed from the surface leaving a fresh

clean surface of the substrate ready for the next investigation. This cleaving process is discussed in more detail in section 3.2.1.

HOPG has been used as a substrate for many different surface science studies including metal deposition^[49] and as a substrate for fullerene nanostructures to be deposited on^{[28],[50],[51]}, which will be discussed in section 2.4.2.

2.4 C₆₀ on surfaces

C₆₀ has been deposited on a variety of surfaces with the intention of studying its geometric and electronic properties. One of the potential uses for C₆₀ is its possible ability to be a component in future circuitry, for this reason much research has been done on C₆₀ on metal and semiconductor surfaces. C₆₀ can form ionic, covalent or van der Waals bonds with surfaces depending on the material of the substrate. On Cu(111) and Ag(111) surfaces an ionic bond is formed^{[52][13]}, on Pt(111) surfaces covalent bonds form^[53] and on graphite and semiconductor surfaces van der Waals forces are responsible for the chemisorption of C₆₀^{[54][55][56]}. When C₆₀ is deposited on some metal surfaces it can alter the reconstruction of the surface, vacancies are created on the surface that the C₆₀ molecules bond on top of^[57]. For metals like silver, aluminium, copper and platinum the fullerene sits directly above the vacancies that are created^{[58][59][52][57]}. Reconstruction of the metal surface layer by the addition of vacancy islands when C₆₀ is deposited, is more common than it remaining unaltered^[13], which conversely is the

case for the Au(111) surface, discussed further in section 2.4.1.

On platinum surfaces the C_{60} molecules form islands with 2 different phases with respect to the Pt(111) surface; $(2\sqrt{3} \times 2\sqrt{3})R30^\circ$ ^[60] and $(\sqrt{13} \times \sqrt{13})R13.9^\circ$ ^[57]. As stated earlier on copper, aluminium, and silver surfaces vacancies form on the surface and the C_{60} molecules form superstructures pinned by these vacancies, $(2\sqrt{3} \times 2\sqrt{3})R30^\circ$ for Ag(111)^[58], (6×6) structure for Al(111)^[59] and (4×4) structure with 7 atom vacancies for Cu(111)^[52].

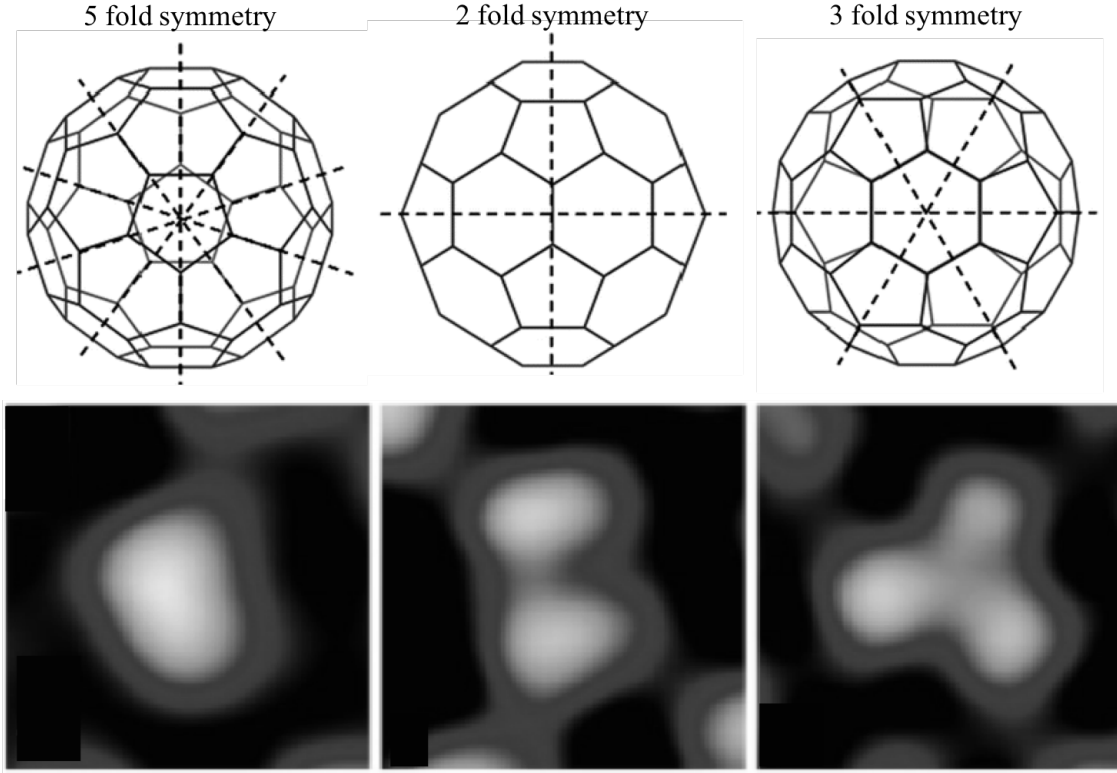


Figure 2.8: Diagram of the C_{60} molecule in 3 rotations and the corresponding structure seen when STM imaging. The C_{60} molecule with 5 fold symmetry has a pentagon face adjacent to the sample; the 2 fold symmetry occurs when the molecule has a bridge (bond between two hexagons) bonded to the surface; and the three fold symmetry is when the molecule has a hexagonal face bound to the surface of the substrate. Images adapted from [13] and [24].

At room temperature the adsorbed C_{60} molecule rotates, whereas at low temperatures the C_{60} molecule has less kinetic energy and is “pinned” to the surface. C_{60} can be oriented in different positions with respect to the surface beneath, these are shown in figure 2.8. The molecule can be adsorbed onto the surface with a pentagon adjacent to the surface, a hexagon face bound to the surface or a bond between two faces could be the facet the surface binds to^[60]. Many DFT studies have confirmed what has been observed experimentally that the orientation most common is when a hexagonal face of the C_{60} molecule is bound to the substrate surface^{[61][52][13][57]}. This orientation has 3 fold symmetry similar to possible bonding sites: atop and hollow sites on an FCC(111) surface. The corresponding symmetry between the bonding sites and the molecular orientation means that “hexagon down” is the most common C_{60} orientation observed on 111 surfaces^[13]

2.4.1 C_{60} on Au(111)

When C_{60} is deposited onto the Au(111) surface in small quantities the C_{60} molecules adsorb along step edges and elbow sites of the reconstruction as these areas have the highest electron density.^[62] Some research where molecules are adsorbed on gold show preferential binding to FCC regions of step edges over HCP regions when submonolayer coverage is deposited^[63]. When larger amounts of C_{60} molecules are deposited, monolayers form with HCP packing structure. These monolayers can have several different orientations with respect to the positions of the gold atoms beneath them: in

phase($R0^\circ$), rotated 30° ($R30^\circ$), rotated 34° ($R34^\circ$) and rotated 14° ($R14^\circ$). A diagram of the 4 different phases of C_{60} on gold can be seen in figure 2.9. These phases can be identified on STM images if the gold reconstruction is visible, the C_{60} islands' direction can be compared to the gold reconstruction and therefore the phase identified.

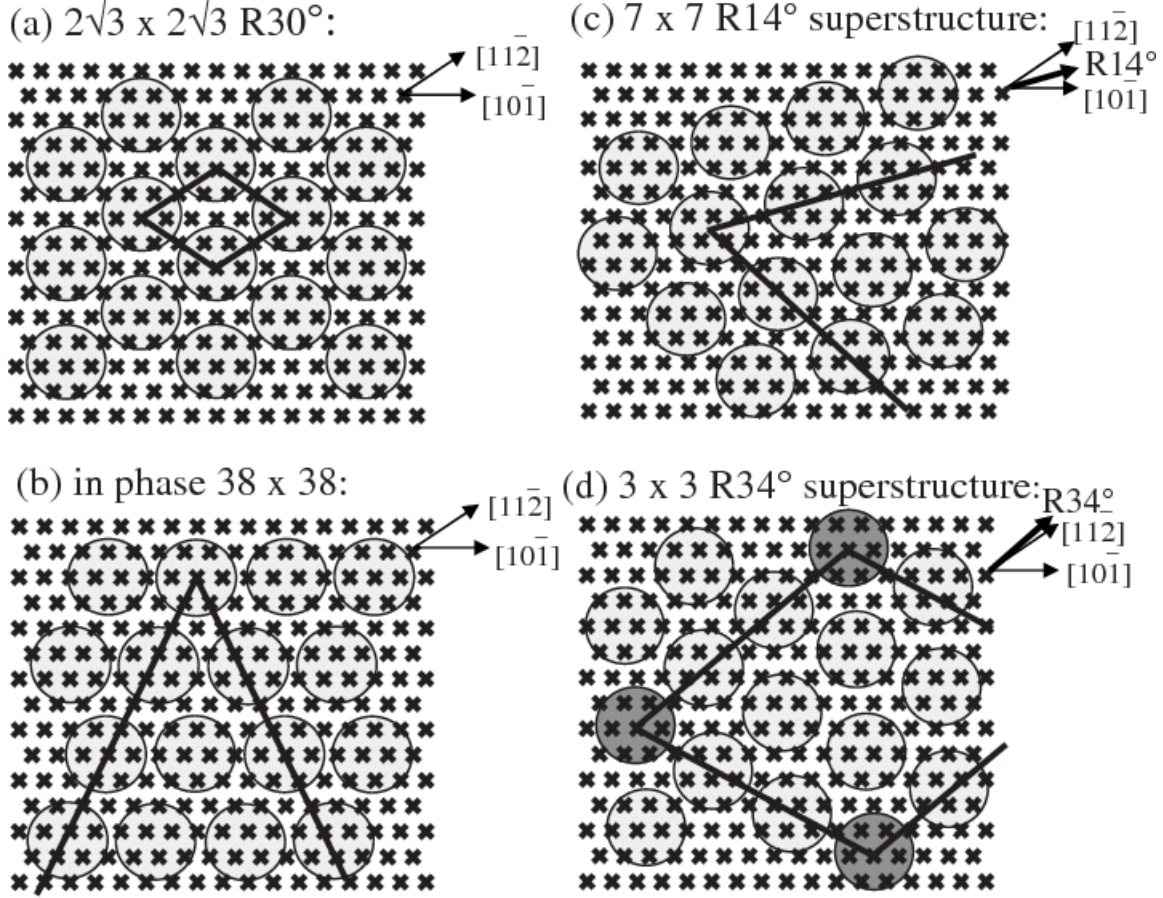


Figure 2.9: C_{60} molecules (circles) orientation with respect to the gold atoms beneath (crosses). The unit cell of the arrangement is illustrated with a dark lined shape in each of the diagrams. The darker grey C_{60} molecules are to represent the fact that every 3 C_{60} molecules occupies the same lattice site. Image sourced from [64].

Bright and dim C_{60} molecules have been observed on C_{60} islands deposited on gold surfaces^[65], the fullerene's brightness compared to surrounding molecules can be due to multiple factors. An STM image of bright and dim C_{60} molecules can be seen in

figure 2.10. One explanation for the apparent height difference could be just that, a height difference; some C_{60} molecules could be sitting on a vacancy in the gold surface below or conversely sat directly on top of an adatom. This is the case for some bright and dim molecules, however, if the sample is heated so the gold atoms have enough thermal energy to diffuse, these bright and dim molecules should also diffuse and not stay constant^[66]. Another possible explanation for the dim and bright molecules could be the orientation of the C_{60} molecule discussed in the previous section (2.4). Work done by Gardener et al. ^[64] examined the relation between these bright and dim molecules and the voltage applied while scanning those areas. Some bright and dim molecules were found to have a bias dependence and the polarity of the scanning voltage dictated whether the molecule in question appeared dim or bright. The C_{60} molecules that are dim potentially have a stronger electronic bonding to the surface than the normal height molecules and the bright molecules. The $R34^\circ$ phase was observed to have a superstructure comprised of dim molecules; this can be used to identify phases of the C_{60} islands if the gold reconstruction is not visible.

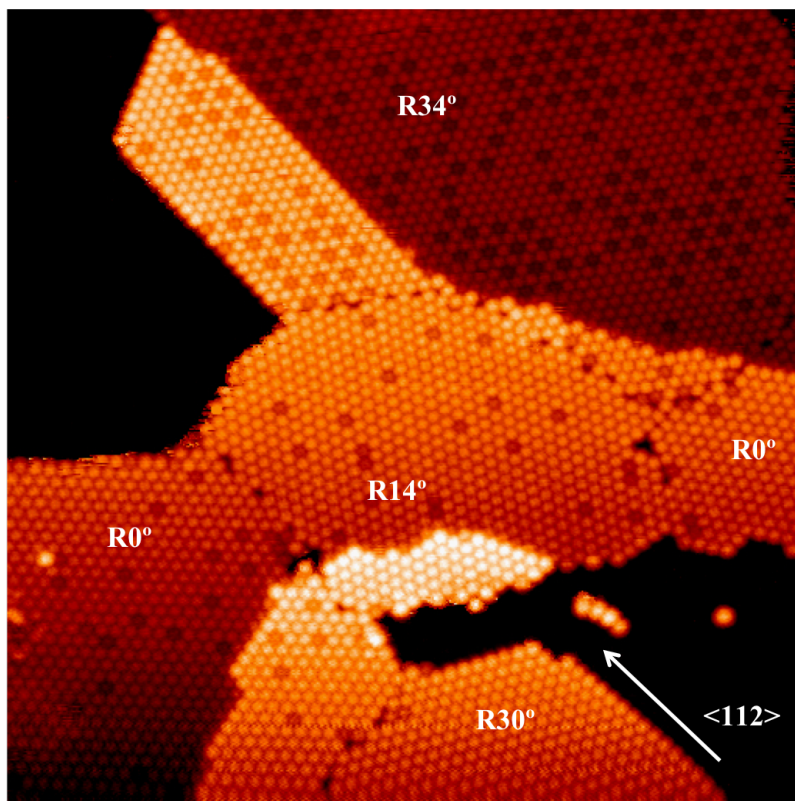


Figure 2.10: An STM image showing a C_{60} island formed on an Au(111) surface with various bright and dim molecules shown throughout the image. The image shows all four phases described above: $R0^\circ$, $R14^\circ$, $R30^\circ$ and, $R34^\circ$. The white line at the bottom right corner shows the direction of the DL on the gold surface. Image adapted from [67].

Unlike on other metal surfaces no periodic vacancies are created when C_{60} is adsorbed onto Au(111) and occasionally the herringbone reconstruction can be imposed on or “seen through” the C_{60} monolayer adsorbed on top^[68].

The instances where the reconstruction “shows through” the C_{60} adlayer have been found when the C_{60} molecules are in $R30^\circ$ phases. The packing direction of the C_{60} molecules aligns with the reconstruction lines found on the Au(111) surface^[62] which is one of the factors thought to allow the reconstruction to remain unchanged. The

alignment of the packing direction and DLs makes this phase energetically favourable and one of the more commonly observed packing orientations. The in phase orientation of the C_{60} molecules has 38 gold atoms to 11 C_{60} molecules, the lattice constant mismatch is low here so this phase is another frequently observed phase.

Magic number clusters

When less than a full monolayer of C_{60} is deposited at low temperatures onto the Au(111) surface, small C_{60} islands nucleate at the elbow sites of the herringbone pattern^[69]. When gold adatoms are deposited onto a surface decorated with small C_{60} clusters at the elbow sites, magic number clusters can be formed^[14]. The most common size of cluster found on the surface by Xie et al. was $(C_{60})_7Au_{19}$ where 19 gold atoms form a small island that 6 C_{60} molecules bond in a ring around and the seventh C_{60} molecule sits on top of the gold island. A slightly different C_{60} and Au structure has also been investigated on Au(111) where C_{60} rings form around Au islands on the gold elbow sites, this structure was found to form in similar sizes to the magic number clusters but without the C_{60} molecule adsorbed to the top of the gold island^[70]. In the paper by Xie et al.^[14] and then later in the work by Rookni-Fard et al.^[71] it was observed that clusters form preferentially on bulged elbows rather than pinched elbow sites.

Atomic manipulation of these clusters has been attempted and it has been found that C_{60} -Au clusters form magic number clusters after manipulation^[72]. In the experiment

by Kaya et al. the STM tip was driven into the clusters so that the clusters broke apart and when they reassembled it was in one of the magic number cluster sizes suggesting that they are more energetically favourable. The STM tip can be used to remove single C_{60} molecules from clusters and when the C_{60} molecule is pushed out of its position it adheres to the side of the cluster ^[73]. The C_{60} clusters are stable at room temperature up to 400 K, they are also stable when adding extra C_{60} molecules as they add to the edge of the cluster expanding the ring structure of the cluster. However, when adding extra gold to the surface with magic number clusters the gold islands that sit beneath the clusters expand and this leads to complete restructuring of the clusters^[74] The clusters when formed are also stable enough to diffuse thermally as one^[75]. These magic number clusters bind more strongly to the gold surface than either the C_{60} molecule islands or the gold islands alone.

2.4.2 C_{60} on HOPG

C_{60} deposition on HOPG has been examined in multiple studies over the past couple of decades. C_{60} bonds to HOPG via van der Waals bonds, there is no charge transfer between the fullerene and the substrate, unlike on metal surfaces.^[76] Since the van der Waals bond is a relatively weak bond compared to covalent or ionic bonding the mobility of the fullerenes on the graphite is quite high.^[77] Although individual C_{60} molecules are mobile on the surface, the mobility of large islands of C_{60} has not been found ^[78] and the shear stress between C_{60} islands and HOPG has been found to be 0.2 GPa^[50].

Many initial experiments featured on the mechanism of growth of C_{60} monolayers on the HOPG substrate, it was found that C_{60} on HOPG has a layer by layer growth mode^{[51][79]} in an HCP packing structure^[77]. The first monolayer of C_{60} bonds strongly with the HOPG surface and is stronger than the C_{60} monolayer and any subsequent monolayers, this is shown by temperature programmed desorption studies where the temperature for removal of the 1st layer is higher than 2nd or 3rd monolayers^[51]. Along with monolayers C_{60} has also been found to form clusters^[80], spherical^[76] and fractal islands^[79] depending on the surface preparation. Some studies show that steps are nucleation points for the growth of C_{60} islands^[81] and others show that the steps act as a diffusion barrier for the C_{60} molecules and are not nucleation sites^{[79][76]}.

Some research has been done either comparing the C_{60} -HOPG substrate to C_{70} -HOPG sample, or combining the two molecules on one substrate. Okita et al. found that the C_{70} monolayer forms as a bilayer as opposed to the monolayer found for C_{60} ^[50]. Guo et al. deposited a C_{60} monolayer then a C_{70} monolayer with the intention of creating van der Waals heterojunctions.^[28]

Guo et al. have also studied C_{60} and Au on HOPG with the aim of recreating the magic number clusters found on gold, on HOPG^[16]. The clusters were found to occur on the surface however, instead of isolated clusters forming at nucleation sites on the surface a monolayer of C_{60} was formed with the clusters contained within. These clusters appear as raised C_{60} molecules, similar orientations to previously found cluster sizes were observed. The height difference between the raised C_{60} molecules and the

monolayer was 0.27 nm which corresponds nicely to the height of a single layer gold island 0.24 nm. Other heights of bright molecules were observed, for example 0.62 nm, which is believed to correspond to a double layer of gold atoms below the raised C₆₀ molecule. The other heights were measured on second and third monolayers and were a combination of C₆₀ molecules binding on top of already raised molecules on the layer below and potentially Au islands forming between C₆₀ molecule layers.

2.5 Scanning Tunelling Microscopy Theory

The experiments discussed in this thesis are all completed using a scanning tunneling microscope, the principles behind its operation will be discussed in this section.

Optical microscopes work by reflecting light off a sample and then use lenses to alter the path of the light before it enters the observers eye, making the object appear bigger than if examined without the lens. Optical microscopes are limited by the wavelength of light and the resolution limit of these microscopes is $0.25\text{ }\mu\text{m}$. In order to view objects smaller than this other types of microscopes are needed such as the electron microscope or the STM. A scanning electron microscope and an STM both use electrons rather than light to image samples, this allows a much smaller resolution than optical microscopes. As the name suggests the STM uses quantum tunneling of electrons to “view” the sample being examined.

The STM can be simplified to a metal probe that scans across the surface of a sample

taking current measurements at every point in an x-y grid. The metal probe or “tip” is shaped into a point that ends with one single atom at the apex - the experiments within this thesis use a tungsten tip that is electrochemically etched to an atomically sharp point, more details on this process can be found in section 3.3. The tip is positioned above the sample with a small distance (typically ≈ 1 nm) between the apex and the sample surface. A potential difference is applied between the tip and the sample so one is negatively charged and the other positive. The tip is close enough to the sample for quantum tunneling effects to be present; the electrons can tunnel between the tip and the sample completing the circuit and allowing a current measurement to be taken. Quantum tunneling will be discussed in more detail later in this section.

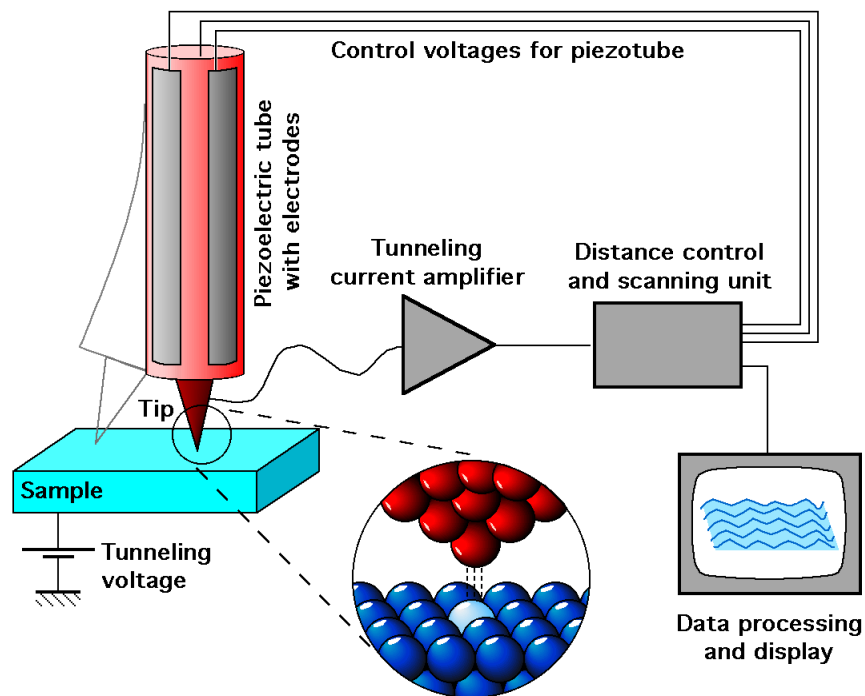


Figure 2.11: Figure showing a schematic view of an STM and the basic electronic layout. Figure sourced from [82] (Michael Schmid, TU Wien).

The microscope can be used in two modes, constant current and constant height mode. In constant current mode the height of the tip is adjusted to keep the tunneling current constant, whereas in constant height mode the current varies to keep the height of the tip constant. The tip moves across the area of interest in a line by line fashion, recording the current or height at a set number of points along each line. These current/height values are then used to create a topological map of the surface. Since the current is used to create an image (it is used in the feedback loop for the constant height mode) the sample that is being investigated must be conductive. The disadvantage of constant height mode, is, when scanning over large features on the surface it is possible for the tip to crash into these features. To control the height and lateral position of the tip a piezoelectric motor is used, a voltage is applied to the piezoelectric crystal and the crystal is “stretched”. This voltage application corresponds to a very precise movement of the crystal allowing nanometer precision in the control of the STM tip. Figure 2.11 shows the experimental set up of an STM.

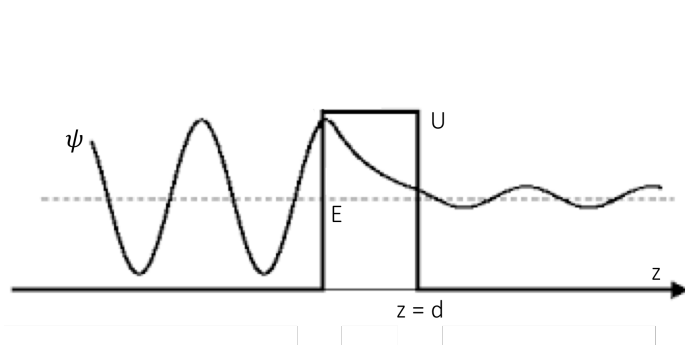


Figure 2.12: Figure showing tunneling through a simple 1D square barrier.

A simple example of quantum tunneling is a wavefunction tunneling through a 1D bar-

rier (shown in figure 2.12). In this example a wavefunction travels towards a potential barrier, classically the wavefunction would be completely reflected from the barrier and no signal would permeate the barrier. However, when quantum mechanics is considered the wavefunction decays exponentially through the barrier and passes through to the other side. The classical situation can be thought of as a ball being thrown at a wall and bouncing back whereas in the quantum realm the ball would also pass through the wall.

The tunneling between sample and tip can be modelled as a simple barrier, shown in figure 2.12, where the wavefunction of the electron before the barrier has the form,

$$\psi(z) = \psi_0 e^{\pm ikz},$$

and the wavefunction of the electron inside the barrier is an exponential decay with the form:

$$\psi(z) = \psi_0 e^{-\kappa z}.$$

The wavenumber k and decay constant κ are defined as:

$$k = \frac{\sqrt{2m(E - U)}}{\hbar}, \quad \kappa = \frac{\sqrt{2m(U - E)}}{\hbar}.$$

where m is the mass of the electron, E is the energy of the electron with wavefunction ψ and U is the height of the barrier.

The tunneling current across the barrier is proportional to the probability of finding an electron on the other side of the barrier. At a point $z = d$ after the barrier

$$I \propto |\psi(d)|^2 \equiv |\psi_0|^2 e^{-2\kappa d}.$$

As can be seen by the equation above, the tunneling current decays exponentially with the increase of width of the barrier d . In 1961 Bardeen proposed a method that used perturbation theory to include the electronic structure of the tip and sample into the tunneling model^[83]. In Bardeen's model the tip and sample can be thought of as two separate systems with known potentials and wavefunctions shown in figure 2.13.

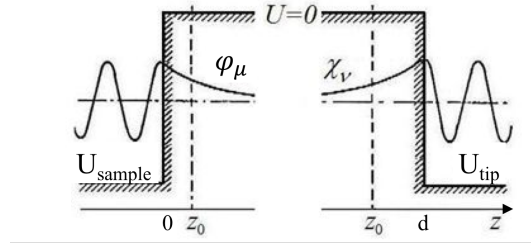


Figure 2.13: This image shows Bardeen's approach to the system by separating the tip and surface into two separate systems. Image adapted from [84].

For the sample and tip subsystems the time dependant Schrödinger equations are:

$$\begin{aligned} i\hbar \frac{\partial \Psi(z, t)}{\partial t} &= \left[\frac{-\hbar^2}{2m} \frac{\partial^2}{\partial z^2} + U_{\text{sample}}(z, t) \right] \Psi(z, t) \\ i\hbar \frac{\partial \Psi(z, t)}{\partial t} &= \left[\frac{-\hbar^2}{2m} \frac{\partial^2}{\partial z^2} + U_{\text{tip}}(z, t) \right] \Psi(z, t), \end{aligned}$$

where $U_{\text{tip/sample}}$ is the potential of either the tip or sample. The Schrödinger equation

that describes the combined system is written below.

$$i\hbar \frac{\partial \Psi(z, t)}{\partial t} = \left[\frac{-\hbar^2}{2m} \frac{\partial^2}{\partial z^2} + U_{tip}(z, t) + U_{sample}(z, t) \right] \Psi(z, t) \quad (2.1)$$

The spatial wavefunction for the sample φ_μ , its corresponding energy eigenvalue E_μ , wavefunction χ_ν and eigenvalue E_ν for the tip are the solutions to the respective Hamiltonian listed above. When the sample and tip are far apart φ_μ and χ_ν decay into the vacuum, but when the two systems are brought close together electrons can tunnel between the two systems. The wavefunction can then be described as

$$\Psi = \chi_\nu e^{\frac{-iE_\nu t}{\hbar}} + \sum_{\mu=1}^{\infty} c_\mu(t) \varphi_\mu e^{\frac{-iE_\mu t}{\hbar}}. \quad (2.2)$$

Inserting this wavefunction (equation 2.2) into the Schrödinger equation for the combined system (equation 2.1) gives:

$$i\hbar \frac{dc_\mu(t)}{dt} = \int_d \chi_\nu U_{tip} \varphi_\mu^* d\mathbf{V} e^{-i(E_\nu - E_\mu)t/\hbar}.$$

From this the matrix element is defined as:

$$M_{\nu\mu} = \int_d \chi_\nu U_{tip} \varphi_\mu^* d\mathbf{V}.$$

It can be assumed that the tunneling is elastic therefore electrons can only tunnel into states with the same energy $E_\nu = E_\mu$. If a bias V is applied to the tunnel junction and

the density of states of the tip and sample ($\rho_{sample}, \rho_{tip}$) are assumed not to vary near the Fermi energy (E_F) the tunneling current is:

$$I = \frac{2\pi e^2}{\hbar} |M_{\nu\mu}|^2 \rho_{tip}(E_F) \rho_{sample}(E_F) V. \quad (2.3)$$

The full derivation of the tunneling current can be found in work by Chen^[84], Gottlieb et al. ^[85] and Lounis ^[86].

When looking at the equation for the current 2.3 one can see that the current measured by the STM is proportional to the density of states of both the sample and the tip near the Fermi energy ($\rho_{tip}(E_F), \rho_{sample}(E_F)$) This relationship is key to scanning tunneling spectroscopy (STS) where the local density of states (LDOS) of the sample is examined.

2.6 Scanning Tunneling Spectroscopy

2.6.1 STS Theory

Scanning tunneling spectroscopy probes the electronic structure of the sample by keeping either current, voltage or height constant while measuring the relationship between the other two parameters.^[87] Therefore, there are three modes of STS: I-V spectroscopy where the height is kept constant; I-d where the voltage is kept constant and the relationship between distance and height is examined; and V-d where the current is kept constant and the height of the tip with relation to voltage is measured. The spec-

troscopy used in this experiment is I-V spectroscopy.

The advantage of scanning tunneling spectroscopy over other spectroscopic analysis tools such as ultraviolet photoelectron spectroscopy (UPS), electron energy loss spectroscopy (EELS) and infrared reflection-absorption spectroscopy (IRRAS) is that those techniques examine the electronic structure over a large area of the surface, the nature of the STM allows precise local spectroscopic information to about 5 Å surrounding the tip^[88].

As stated previously the spectroscopy used within this thesis is I-V spectroscopy which can be presented as I-V graphs or $\frac{dI}{dV}$ plotted against V. The electronic information that STS can provide is the density of states of the sample. How $\frac{dI}{dV}$ relates to the density of states of the sample is detailed in equations 2.4 to 2.6.

If equation 2.3 is summed over all possible states and the electrons in the tip and the sample abide by the Fermi distribution ($f(E) = (1 + e^{(E-E_F)/k_B T})^{-1}$) then, when a bias V is applied to the junction

$$I = \frac{4\pi e}{\hbar} \int_{-\infty}^{\infty} [f(E_F - eV + \epsilon) - f(E_F + \epsilon)] |M|^2 \rho_{sample}(E_F - eV + \epsilon) \rho_{tip}(E_F + \epsilon) d\epsilon. \quad (2.4)$$

If $K_B T$ is very small then the Fermi function can be simplified to a step function so the current equation becomes:

$$I = \frac{4\pi e}{\hbar} \int_0^{eV} |M|^2 \rho_{sample}(E_F - eV + \epsilon) \rho_{tip}(E_F + \epsilon) d\epsilon. \quad (2.5)$$

If this equation is then differentiated with respect to V while the density of states of the tip is assumed to be constant, and the matrix element is assumed not to vary much near the Fermi energy, those terms are insignificant and

$$\frac{dI}{dV} \propto \rho_{sample}(E_F - eV). \quad (2.6)$$

2.6.2 Electronic Orbitals

Since the STM can examine the electronic structure of molecules a brief explanation of terms is required. In the section below the lowest unoccupied molecular orbital (LUMO) and highest occupied molecular orbital (HOMO) are illustrated, figure 2.14 shows a diagram of an molecule's molecular orbitals with the HOMO and LUMO labeled.

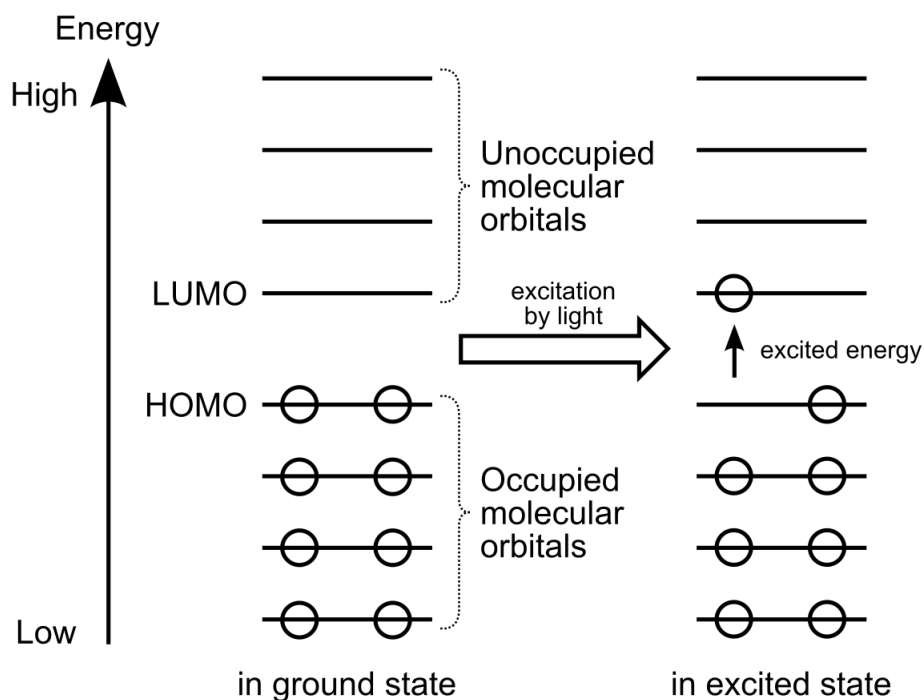


Figure 2.14: A diagram of molecular orbitals of a molecule. The lower orbitals are filled and the top few orbitals are empty, given some energy, electrons can move into the unoccupied orbitals and transition back releasing that energy, often in the form of light (a photon). From [89].

2.6.3 STS measurements in previous work

STS on Au(111)

STS measurements taken on Au(111) show a surface state peak at around -300 mV ^[90] due to the almost free electrons on the surface. The effect of monatomic steps has also been researched and it has been found to decrease the intensity of the surface state peaks, effectively acting as an energy barrier^{[91][90][92]}.

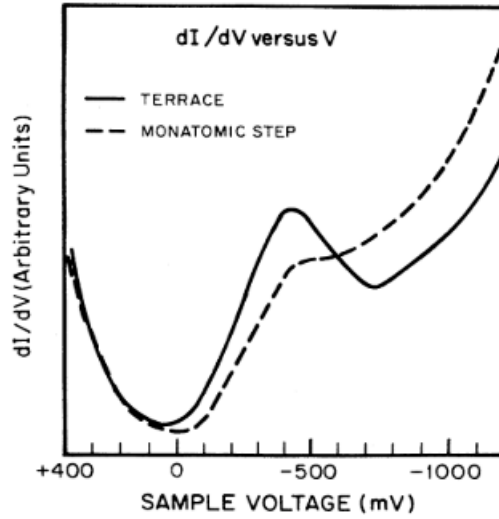


Figure 2.15: STS spectrum from Au(111) showing the difference in curves from a terrace and a step. From [92].

When scanning the Au(111) surface no features of the surface such as the DL or vacancy islands were found to cause energy shifts to any of the peaks of the $\frac{dI}{dV}$ curve^[93]. Photoemission studies^{[94][95]} can support the observations made by STS as the work by Reinert et al. completed on the surface state of Au(111) surface^[96] demonstrates. They found that the Shockley surface state peak is present around -500 mV and the peaks observed at -300 mV are also due to the surface state.

Molecules or monolayers have also been studied with STS on Au(111), Labonté et al. examined various SAMs and found that the conductance gap varied based on the different monolayer deposited. The thickness of the monolayer and the bonding of the molecule to the gold substrate was also found to impact this gap.^[97] Katoh et al. performed STS measurements of a single molecule magnet deposited on Au(111) and how the molecule's conductance curve compared to Au(111).^[98] A change in a molecule's

configuration can also alter its STS spectrum, it can cause an increase or decrease in the conductance gap and also introduce new peaks at different energies^[63]. Koslowski et al.^[99] investigated terthiophene molecules adsorbed on Au(111) and compared the STS curves taken above the terthiophene molecules with the bare gold surface. The difference from the well known peak positions on the gold surface, such as the Shockley state peak at -0.5 eV was used to describe the electronic properties of the terthiophene molecule.

STS on HOPG

STS measurements on a clean HOPG surface when taken further away from the sample show a dip at 200 mV and as the tip sample distance is decreased the dip position shifts to ≈ 300 mV. This is thought to be due to the HOPG surface layer being deformed due to the tip. The bonds between layers of graphite are significantly weaker than interplane bonds and so the top layer of atoms is thought to separate from the bulk by its attraction to the STM tip. ^[100]

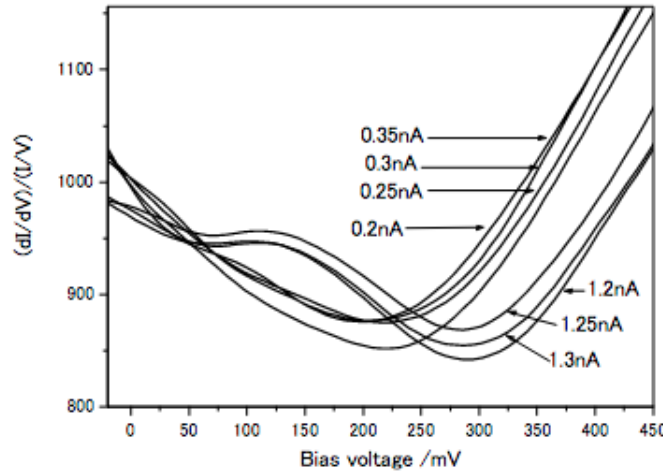


Figure 2.16: Graph showing the difference in STS spectrum at different current set points (inversely proportional to the height of the STM tip). From[100].

HOPG has also been studied using STS as a substrate for both gold thin films and fullerenes. The Au thin films have different spectrums to bulk Au and take on more characteristics of the bulk HOPG spectrum, although the peak at -500 mV remains. When examining the I-V curves for the Au-HOPG sample there are peaks on the curve that are evenly spaced which could indicate a coulomb blockade. These changes to the spectrums created when comparing the substrate and the adsorbate indicate that there is some inter-colation between the metal and the HOPG in this case.^[101] Klinger et al. surveyed a variety of fullerenes on HOPG and found that the STS curves for the smaller fullerenes showed that they behaved in a semi metallic manner, whereas the larger molecules behaved as semiconductors. A semiconductor STS spectrum can be identified by a band gap around 0 V and a metal like substance would have a non 0 $\frac{dI}{dV}$ value around 0 V^[102].

STS on C₆₀

A study of C₆₀ on the Cu(111) surface compared the STS curves for C₆₀/Cu without the Cu surface reconstruction and with the reconstruction. The positions of the peaks were shifted closer to the Fermi energy(E_F) for the reconstructed spectrum compared to unreconstructed. This confirms previous research suggesting that the reconstructing of the copper surface when C₆₀ is adsorbed is more energetically favourable than when not reconstructing.^[52] Another study of C₆₀ on Cu(111) illustrated that four peaks are found for C₆₀ on Cu(111) surfaces, and the LUMO splits into two peaks due to a charge transfer between the C₆₀ molecule and the Cu surface. This study also found that when examining the spectrums from C₆₀ molecules on differing adsorption sites the STS peaks' energies were shifted slightly. This indicates that the bonding energy in different sites is not the same.^[103]

Perez-Jimenez et al. examined the STS of C₆₀ on Au(111); the spectrums of bright and dim C₆₀ molecules were compared and it was found that the dim molecule binds more strongly to the surface. In this study the bright molecule was assumed to be on an atop site and the dim on a hollow/bridge site. The spectrum of the dim molecule had a broadening of its peaks which corresponds to a stronger binding to the surface.^[104] Lu et al. also examined C₆₀ on Au(111) and compared it to C₆₀ on Ag(100). Similar to studies of C₆₀ on Cu(111) the C₆₀-Ag spectrum showed splitting of the LUMO, whereas the gold surface with C₆₀ molecules had no splitting. This indicates that the charge transfer between the C₆₀ and Ag and between the C₆₀ and Cu is stronger than the C₆₀

and Au. The peaks for C_{60} -Au(111) surface are observed at ≈ -1.7 V, 1 V, and 2.2 V.^[105]

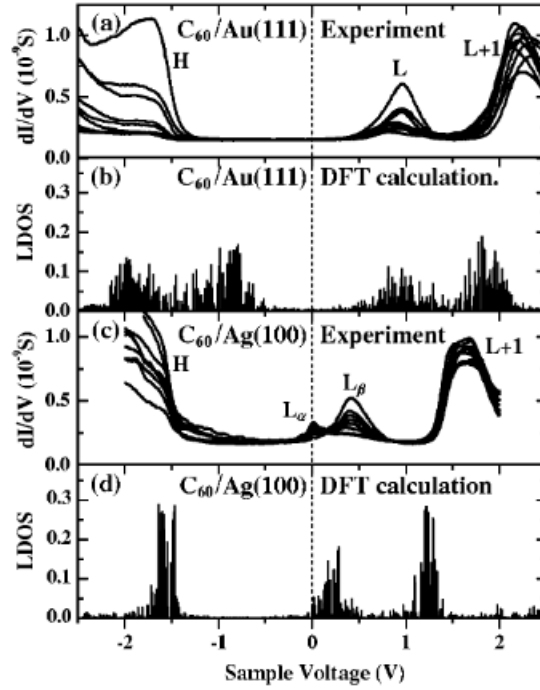


Figure 2.17: Graph of $\frac{dI}{dV}$ and the density functional theory (DFT) comparison for C_{60} on Au(111) and C_{60} on Ag(100). From [105].

The work described from the literature was built upon within the experiments in this thesis, the main aim was to expand the knowledge of the sub molecular arrangement of C_{60} gold magic number clusters both through low temperature STM and STS experiments.

Chapter 3

Experimental Techniques

This chapter will discuss the overarching equipment and experimental techniques used throughout this thesis, specific techniques only used in one section will be discussed in the relevant chapter. The main piece of apparatus used in these experiments was an Omicron low temperature scanning tunneling microscope (LT-STM). Detail on the physics used in the operation of the scanning tunneling microscope (STM) can be found in section 2.5.

3.1 Low Temperature - STM Setup

The LT-STM used in these experiments comprised of two chambers, an analysis chamber and a preparation chamber, a diagram of this setup is shown in figure 3.1. The analysis chamber is where the tunneling microscope is located and the preparation

chamber is where samples are produced and cleaned. The system operates at ultra high vacuum (UHV) from 10^{-9} to 10^{-12} mbar to keep samples at optimum conditions for long periods of time. To operate in this regime several pumps are attached to the system to maintain the low pressure, these pumps include one Varian turbomolecular pump connected to the preparation chamber, as well as an ion pump and a titanium sublimation pump (TSP) in each chamber.

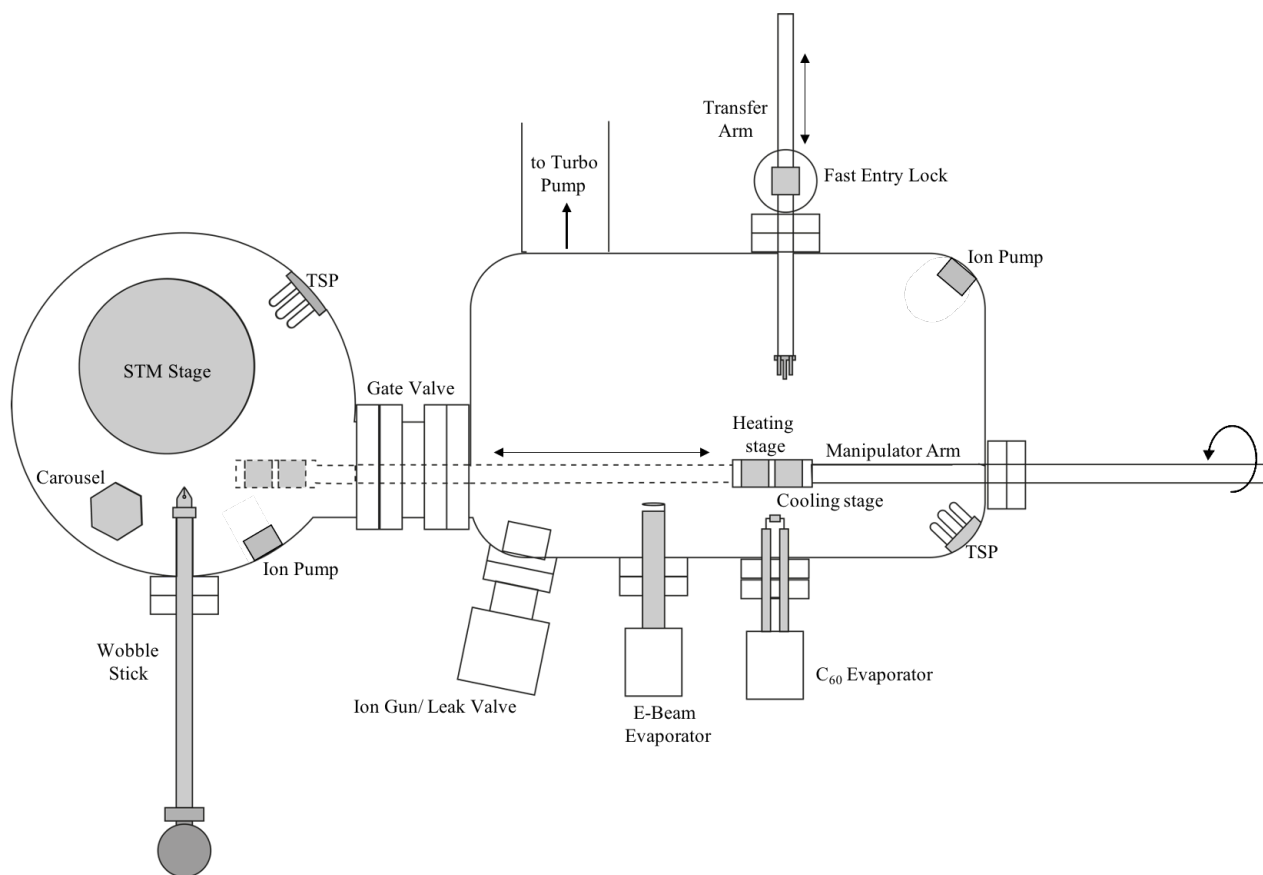


Figure 3.1: A schematic of the LT-STM used in this project, viewed from above.

The preparation chamber can be isolated from the analysis chamber with a gate valve. This allows the analysis chamber to maintain high level vacuum when depositing onto

samples or inserting and removing samples from the preparation chamber. Samples are inserted or removed from the system via a fast entry lock (FEL) attached to the preparation area. The FEL can be pumped independently of the rest of the system and when a low enough pressure is achieved a valve can be opened connecting the preparation chamber to the FEL.

To move samples around the chamber the system contains multiple arms: the manipulation arm, the transfer arm and the wobble stick, details of sample movement mechanisms are shown in figure 3.2.

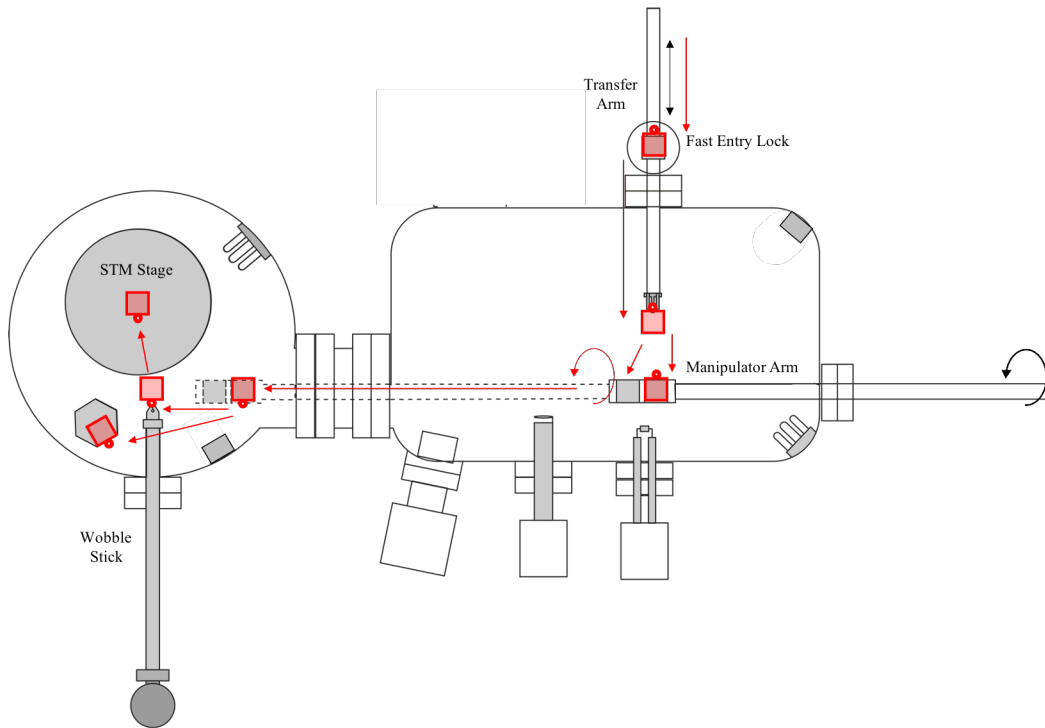


Figure 3.2: A simplified schematic of the LT-STM used within these experiments illustrating the sample movement within the system.

The transfer arm is used to move samples into the STM system, from the FEL to the preparation chamber. The manipulation arm is where the heating and cooling stages

are located, it can move between the preparation and analysis chambers and rotate 360°. The wobble stick is a fully articulated arm with a pincer on the end that can grab samples and move them from the manipulation arm into the carousel for storage or into the STM stage. In the analysis chamber there is a carousel used for storing samples when not in the microscope stage, this allows samples to be kept in vacuum conditions which can help prevent surfaces from deteriorating.

3.1.1 Preparation chamber

The preparation chamber as the name suggests is mostly used for preparing samples for scanning. The chamber contains various evaporators, an ion gun and a residual gas analyser (RGA). The heating and cooling of samples is often performed when the manipulation arm is within the preparation chamber and the gate valve between the two chambers is closed, this is so the analysis chamber can maintain a higher vacuum and therefore keep the samples in better condition.

The evaporators attached to the preparation chamber in these experiments were: a C₆₀ evaporator (discussed in more detail later in this section); and a SPECS E-beam evaporator. The ion gun is attached to a leak valve on the chamber so that the valve can be used for vapour deposition when the ion gun is not in use, and as an ion gun when operational. The main use of the ion gun in this experiment is to clean samples between experiments. Further detail on this process is found in section 3.2.1.

C₆₀ Evaporator

The C₆₀ evaporator is a simple resistive heating thermal evaporator. A pocket made from tantalum foil was created and attached via tungsten wire to two power pins on a CF feedthrough flange. A current is passed through the poles on the flange and therefore across the pocket which causes resistive heating to occur. A k-type thermocouple is attached to the pocket to measure the temperature while evaporating, when the pocket is at the desorbing temperature of C₆₀ (380 K) the C₆₀ can be deposited on the sample, a diagram of the evaporator is shown in figure 3.3. The design of this pocket was a modification of a similar design previously used in the group. The main differences in this iteration is the use of wires to attach the pocket to the copper rods of the flange, as opposed to the tantalum foil strips used in past designs. This alteration allowed for much smaller currents to be used to provide the heating, as both the surface area of the pocket is far smaller, and the resistance is higher in the new design. This enabled the evaporator to be powered off the pre-existing power supply in the STM control rack as opposed to another external power supply.

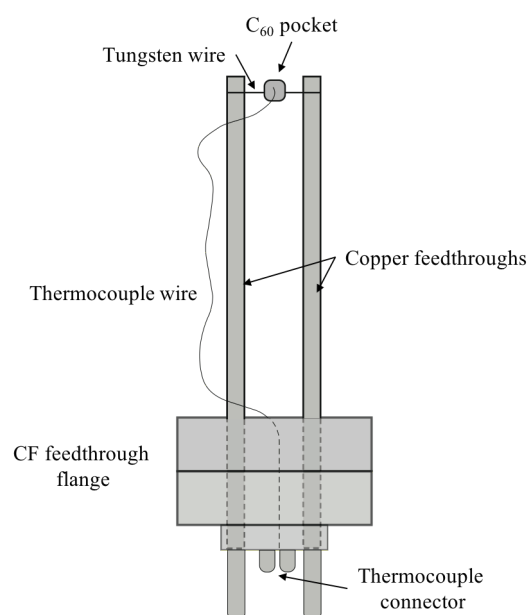


Figure 3.3: Diagram of the C₆₀ evaporator.

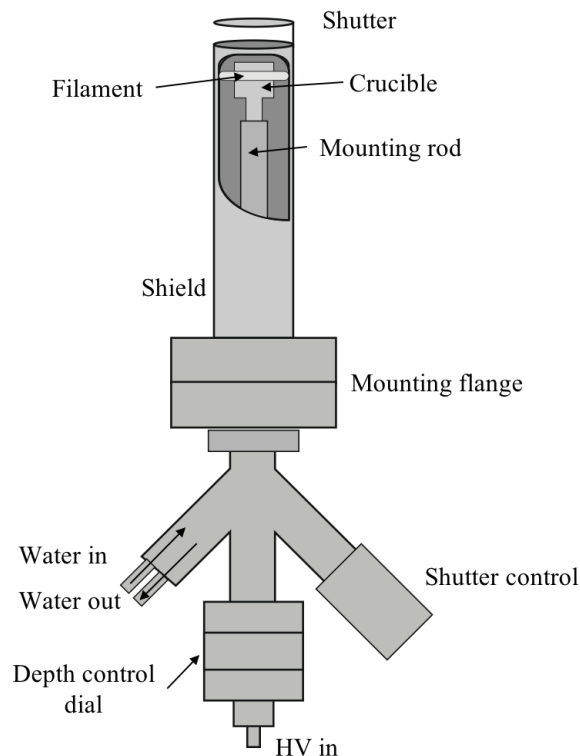


Figure 3.4: Diagram showing the the E-beam evaporator used to evaporate gold onto samples within these experiments. The cut out section at the top of the shield is to illustrate the structure underneath for clarity.

E-beam evaporator

Similarly to the C_{60} evaporator, the E-beam evaporator is another example of physical vapour deposition, where instead of resistive heating an electron beam is used to heat the sample and cause the material to evaporate. The high energy electron beam is focused onto the material to be evaporated (in these experiments gold). The electrons bombard the sample and transfer their kinetic energy to the material heating it up to a point where the material can evaporate and a vapour is released into the chamber.

The evaporator can be fitted with: a rod of material that either sublimates or produces a vapour before its melting point temperature is released (such as platinum); or a crucible to hold metals with a lower melting point such as gold. In these experiments the copper crucible was used to hold a small coil of 99.99% gold wire. This evaporator employs a water cooling system when running to prevent the copper crucible heating and possibly contributing to and contaminating the evaporation material. A diagram of this evaporator can be found in figure 3.4.

Residual Gas Analyser

The RGA is used within these experiments to verify the substances being deposited in the chamber and to help ascertain the cleanliness of the chamber. An RGA is a mass spectrometer that measures the mass to charge ratio (M/z) of any molecules present within the chamber. The components of an RGA within the vacuum system are an ion source, a quadrupole, and a detector; this connects via a vacuum feedthrough port to a computer so the spectrum measured can be read. The ion source ionises any residual gasses within the chamber and the quadrupole separates these molecules by their mass, the quantity of each mass is collected by the detector in the form of a voltage. A typical RGA spectrum from the chamber used within this experiment is shown in figure 3.5, the x axis is the mass of the gas molecule and the y axis is representative of the amount of each substance within the chamber.

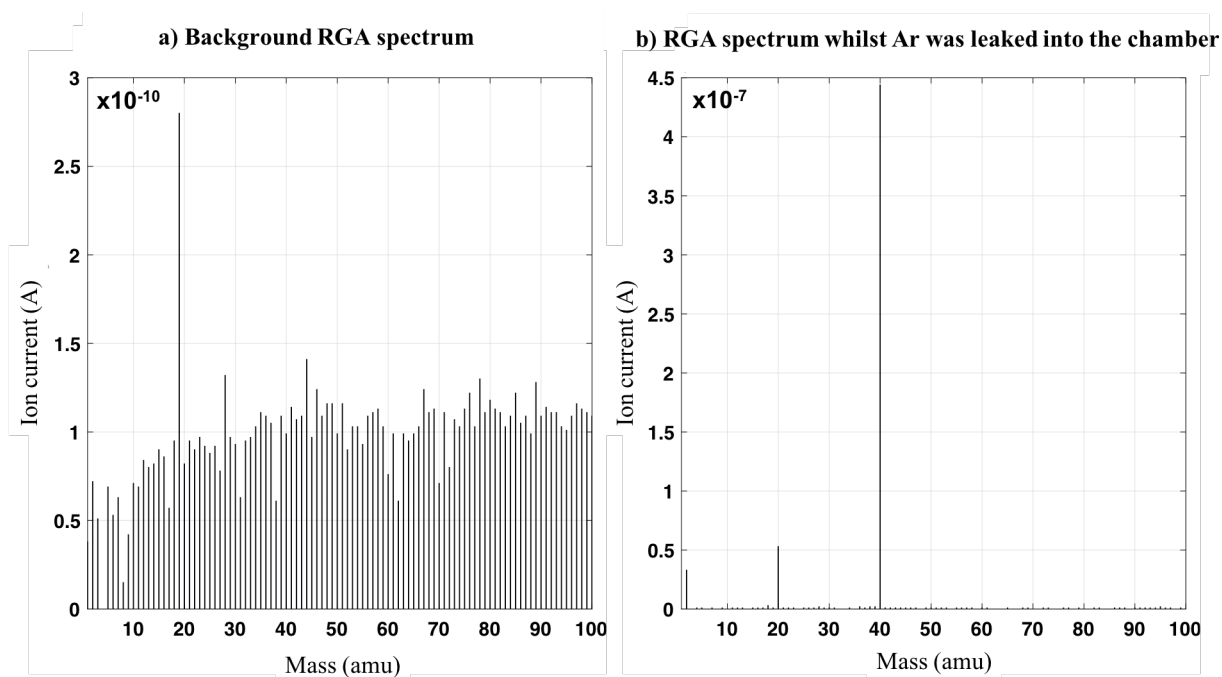


Figure 3.5: a) A typical background spectrum from the residual gas analyser in the LT-STM system. b) an RGA spectrum taken whilst argon was leaked into the chamber, a large peak at 40 m/z can be seen which corresponds to the atomic mass of argon (39.95u). The other large peak at 20 m/z is due to the Ar^{2+} ion.

Ion gun

As previously discussed the ion gun was used mostly for sample cleaning within these experiments. The ion gun is connected to a gas valve which provides the molecules that ionise - in this case argon. The ion gun contains a filament which is heated to produce electrons which then ionise the argon gas as it passes through the gun. The argon ions are then accelerated and focused with the use of electromagnetic lenses. The typical beam energy and other settings can be found in section 3.2.1.

Manipulation arm

As mentioned above the manipulator arm can travel between both chambers, most of the preparation of samples is completed with the manipulator in the preparation chamber. The arm has two sample stages: a heating stage where a sample can be heated by direct current or indirect heating methods; and a cooling stage where the sample can be cooled by passing liquid nitrogen through pipes along the arm that are connected to the copper block of the cooling stage. A sample can be placed in either the heating or cooling stage and the manipulation arm can rotate to any angle desired, this is used for angling the sample so it faces a particular evaporator or the ion gun within the chamber. In the experiments detailed in this thesis the heating stage was used in the sample cleaning process discussed in section 3.2.1 and the cooling stage was used when certain samples were prepared (section 3.2.4).

3.1.2 Analysis chamber

The analysis chamber contains the STM stage, the carousel and the cryostat. The cryostat is composed of an inner and an outer chamber; the outer chamber is used to prolong the low temperature of the inner chamber as it provides an extra layer between the ambient temperature of the room and the temperature of the inner cryostat. This design requires that the outer cryostat should be filled with cryogenic liquid regularly as

it evaporates faster than the inner cryostat. Within this thesis liquid nitrogen cooling was used when scanning, however, the LT-STM can also utilise liquid helium to reach lower scanning temperatures. The inner cryostat is in direct thermal contact with the sample stage allowing for an efficient heat transfer to the sample. The carousel is a rotating sample holder that has 6 slots and can store either tips or samples when not in use.

The STM stage is suspended from springs attached to the cryostat housing, this helps to damp any vibrations that could interfere with the signal from the tip when scanning the sample surface. The stage also has an eddy current damping system built around the stage to further stabilise for clearer measurements. The stage has thermal shielding which can be closed around the stage to help keep temperatures more stable, the shields can be rotated with the wobble stick so that the openings allow for the sample to be transferred to and from the STM stage.

3.2 Sample preparation

3.2.1 Substrate preparation

The two substrates used within this experiment are a single crystal Au(111) sample and highly oriented pyrolytic graphite (HOPG).

Au(111) single crystal

The gold substrate used in this experiment was a single crystal Au(111) sample attached to a molybdenum sample plate with tantalum strips spot welded to keep the sample secure. When the gold sample is entered into the chamber it is cleaned via a process of sputtering then annealing. The sputtering parameters used in this experiment were $\approx 1 \times 10^{-6}$ mbar for 5 minutes, which led to a sputtering current of around $13\mu\text{A}$. The gold is then annealed at 1.5A for 15 minutes which corresponds to a temperature of $\approx 600\text{ K}$ on the surface of the sample. The annealing process allows any impurities in the sample to rise to the surface of the sample and sputtering uses Ar^+ ion bombardment to remove the top few layers. After a few repeats of both annealing and sputtering, the quantity of impurities on the sample is greatly reduced or hopefully removed entirely. Before deposition of any materials on top of the clean Au(111) sample the sample was scanned to check for impurities. If the sample was determined to be clean by examining the image then other materials could then be deposited onto the sample, if not then more cycles of sputtering and annealing were repeated.

HOPG preparation

The HOPG samples used within this thesis are 10mm square; to prepare the HOPG for use it is cleaved to produce a clean flat surface that can then be deposited on. To cleave the sample, scotch tape is applied to the surface and the back of a pair of tweezers is run across the tape to ensure it is adhered fully to the graphite sample. The tape is

then removed and several layers of graphite are removed with the tape leaving a fresh surface for use. This cleaving technique is possible due to the weak bonds between layers within the graphite sample. After the sample is cleaned it can be spot welded in the same way as the gold sample to a molybdenum sample plate and entered into the LT-STM vacuum system through the FEL to be deposited onto.

3.2.2 Gold C_{60} sample preparation

The Au(111) sample was cleaned using the techniques described above (section 3.2.1) then the C_{60} was deposited using the C_{60} evaporator. Applying a direct current of approximately 7 A to the C_{60} pocket allows the C_{60} to reach its desorbing temperature and to evaporate from the pocket. The length of time the C_{60} evaporator had a current applied, directly correlates to the amount of C_{60} deposited onto the surface of the substrate. The amount of C_{60} on the substrate was determined using images from various areas on the sample and this then influenced the amount of time used for subsequent depositions. For example if an image had approximately 0.5 ML coverage of the fullerene that deposition time could be assumed to give around 0.5 ML coverage in future. After scanning of the sample and related experiments had been performed (either at room temperature or 77 K) the sample was heated up to above the C_{60} evaporation temperature (≈ 600 K) to remove the C_{60} from the surface, the sample was then put through a few cycles of sputtering and annealing to clean the sample.

3.2.3 HOPG C₆₀ sample preparation

The HOPG was cleaved as detailed above (section 3.2.1) and entered into the vacuum system. The C₆₀ evaporator was used to deposit C₆₀ molecules onto the HOPG substrate and the sample could then be moved into the analysis chamber to be scanned. Unlike the Au(111) sample C₆₀ is mobile on the HOPG surface so to scan these samples lower temperatures (77 K) were needed to limit the fullerene's kinetic energy and "pin" them to the surface. To remove the C₆₀ from the graphite surface the sample was annealed (above 600 K) until the C₆₀ was removed from the surface.

3.2.4 Au adatom deposition onto C₆₀ Au(111) and C₆₀ HOPG samples

To deposit Au adatoms onto the surface of C₆₀ Au or C₆₀ HOPG samples the substrates needed to be kept at lower temperatures to lower the kinetic energy of the gold atoms. The sample was placed in the cooling stage of the manipulator and liquid nitrogen was passed through pipes connected to the stage, cooling it to 77 K. The E-beam evaporator containing gold in a crucible was then used to deposit gold adatoms onto the surface. The manipulator was kept at cryogenic temperatures and moved into the analysis chamber where the sample was transferred to a cooled STM stage.

3.3 Tip production

STM tips used in these experiments are etched from tungsten wire using sodium hydroxide (NaOH). A 2 molar NaOH solution is made and placed in a beaker, a tungsten wire is then inserted into the beaker to be etched. The setup for the etching process is a simple electrochemical cell and is shown in figure 3.6. In this setup the wire that is etched to become the tip is the anode and a second wire is placed in the solution to act as the cathode.

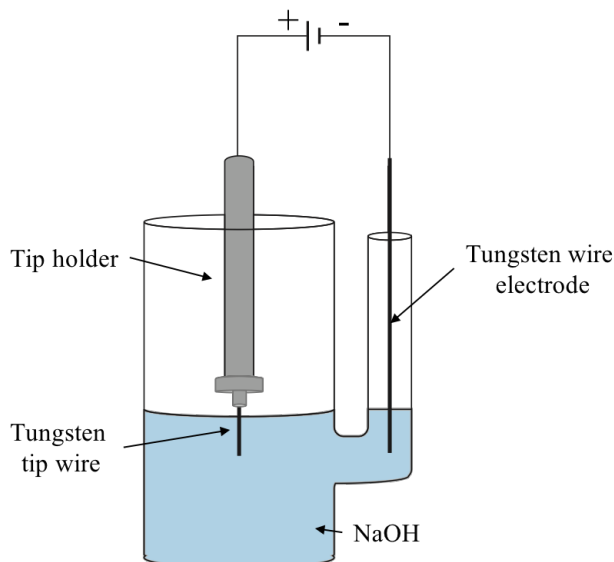
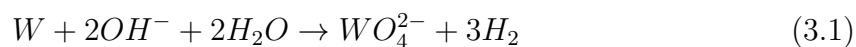
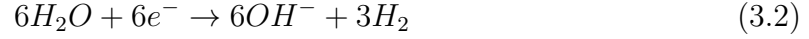


Figure 3.6: A schematic of the setup used for etching tungsten wire into tips.

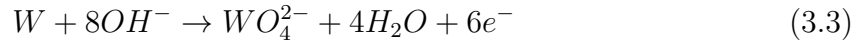
The process of etching the tungsten wire is a simple redox reaction where the tungsten wire is oxidised with the overall chemical equation as follows,



The reaction at the cathode is a reduction reaction where the equation is:



and the equation at the anode is:



When the tip is entered into the STM system, the tip is heated in the heating stage of the sample to 425 K to remove any impurities on the tip. Ideally the tip would be heated to a much higher temperature to remove the oxide layer formed on the surface of the tip, but in this system the temperature is limited by the tip holder mechanism. The tip is inserted into a tip holder with a magnetic base. If the tip holder were to be heated up to the necessary temperatures to remove any oxide layer, the magnet would be damaged and demagnetised. The oxide layer on the tungsten tips was removed in a separate vacuum system where it could be heated by applying a direct current across it reaching the desired temperature of 1000 K. The tip was then removed from this chamber and inserted into the magnetic holder before being inserted into the STM system. During this process the tip was exposed to air but this was kept to a few minutes to prevent the oxide layer that inevitably forms from becoming too thick. Tungsten oxides form slowly at room temperature^[106] but more readily as the temperature is increased, so although not all oxides have been removed using this procedure, the thickness of the

oxide layer on the tip post heating is thinner than before.

For some of the measurements in this thesis the tips were recrystallised before etching and heating. This was done by heating a tungsten wire by applying a current across it gradually, increasing the current until the tungsten wire snaps and breaks the circuit. The ends of the tungsten wire near the break are crystalline due to the localised heating at that point. These tips were used to increase the stability of the tip particularly when taking scanning tunneling spectroscopy (STS) measurements.

3.4 STS methodology

Spectroscopy was performed within some experiments in this thesis. The process consists of the STM tip being positioned over a specified point on the surface, whilst the tip is kept at a constant height a voltage sweep is applied between the tip and the sample and the current readings at those voltages are measured. This method allows the user to produce a spectrum and examine the local density of states (LDOS) on the surface of the substrate. Different samples will have different characteristic peaks similar to other forms of spectroscopy. The STS measurements taken in the experiments detailed in this work were taken using a lock in amplifier built into the nanonis system used for STM imaging. The use of a lock in amplifier reduces the noise on the signal so any signature peaks are clearer. Data processing of the I-V data is discussed in section 6.1.3.

Chapter 4

Investigation of C_{60} on Au(111)

In this chapter the results of the investigation of C_{60} fullerenes on Au(111) will be discussed and compared to similar studies found within the literature. C_{60} has been studied on Au(111) and magic number clusters were found to form at low coverages, discussed in more detail in section 2.4.1. The C_{60} /Au sample is stable at room temperature and the gold surface provides large flat terraces for C_{60} islands to form on top. One of the main advantages to using Au(111) as a substrate is its herringbone reconstruction pattern. The elbow sites of the discommensuration line (DL)'s can act as a template for clusters to form upon and can produce organised arrays of clusters^[69]. Though no isolated magic number clusters were studied in this work, this experiment follows on from similar work previously performed at NPRL^{[69],[14],[70],[71],[72],[73],[74],[75]}. This chapter contains height analysis of various C_{60} islands that formed on the surface and a discussion of the potential causes of the variation. The orientation of the C_{60}

molecules with relation to the gold surface and its potential link to the phase of the C_{60} monolayer is discussed.

4.1 Experimental Method

Au(111) samples were used to calibrate the the height measured by the scanning tunneling microscope (STM) tip as the step height is known to be 0.24 nm ^[30]. Si(111) samples were also prepared and used for lateral calibration of the STM images. The Au(111) surface was prepared as described in 3.2.1 by cycles of sputtering and annealing until a clean surface was achieved. The C_{60} molecules were then deposited onto the sample using the apparatus described and method detailed in section 3.2.2. Differing amounts of C_{60} were deposited onto the samples by evaporating for various periods of time. The coverage deposited varied from 0.3 ML to 0.8 ML . Gwyddion was used to analyse the STM images that were produced and height profiles of specific parts of the image were extracted using this software. The coverage of the samples in ML was also calculated using Gwyddion by calculating the surface cover (area of monolayer coverage/area of the image size) of a variety of images taken at different areas of the sample then averaged. This information was then used to inform the deposition time for future depositions.

4.2 Results and Discussion

Figure 4.1 shows a gold sample with 0.7 ML C_{60} coverage. When C_{60} is deposited on Au(111) it adheres to the lower step edges initially and islands grow from the steps as a nucleation site^[62].

When gold adatoms are deposited on the sample at low temperatures they form islands on the elbow sites and step edges due to the higher electron density at those sites. The C_{60} and Au adatoms on Au(111) samples ($C_{60}/Au/Au(111)$) behave differently to $C_{60}/Au(111)$ samples as the added Au adatoms act as extra nucleation sites for clusters. At large amounts of C_{60} deposition it is more common to observe larger islands as opposed to C_{60} -Au clusters. Some samples examined had large islands of C_{60} with a few raised molecules that could be due to small gold islands bonded to the Au(111) substrate. This is similar to results found previously in other literature of a $C_{60}Au$ matrix on HOPG^[16].

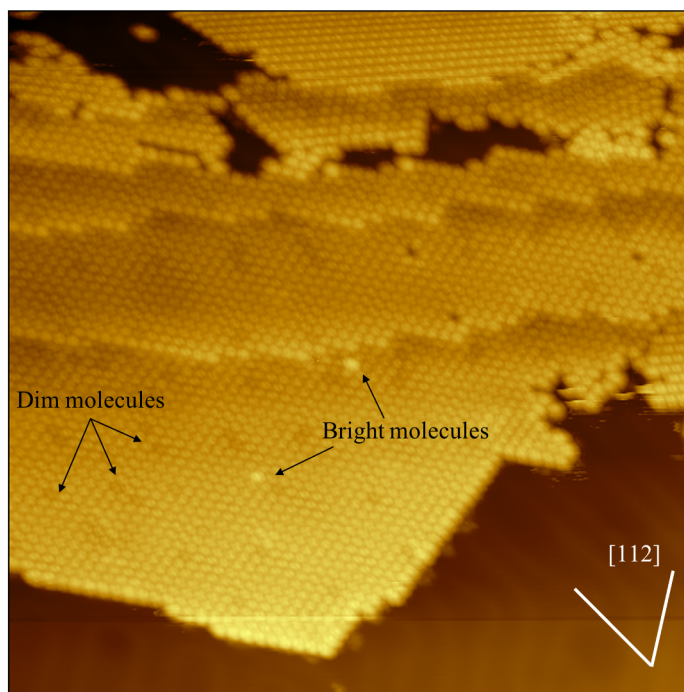


Figure 4.1: A 100×100 nm image of 0.7 ML C_{60} on Au(111) taken at 137 pA and 1.5 V. The image shows a large island of C_{60} molecules that crosses multiple steps and contains examples of bright and dim C_{60} molecules. The reconstruction of the Au(111) substrate is visible on the bare gold at the bottom of the image.

C_{60} on Step Edges

When the C_{60} molecules are deposited on Au(111) they bond to the step edges, figure 4.2 shows step edges on a gold sample with 0.7 ML of C_{60} . The left side of the figure has the contrast adjusted so the C_{60} molecules can be seen and the image on the right has the contrast adjusted so the gold reconstruction (DL) is visible. As discussed in section 2.2 the distance between DL is different in the areas of FCC and HCP packing, 63 Å between neighbouring pairs and 44 Å between the pair^[30]. The face centered cubic (FCC) areas of the sample correspond to the gap between two pairs of DL's and the

hexagonal close packed (HCP) region is between two DL's. In figure 4.2 the larger areas between two pairs are the sections that the C_{60} molecules have adhered to, leaving the HCP regions bare. Similar to work by Sk et al.^[63] and Altman et al.^[62], discussed in the literature review the C_{60} molecules form preferentially on FCC areas of the steps.

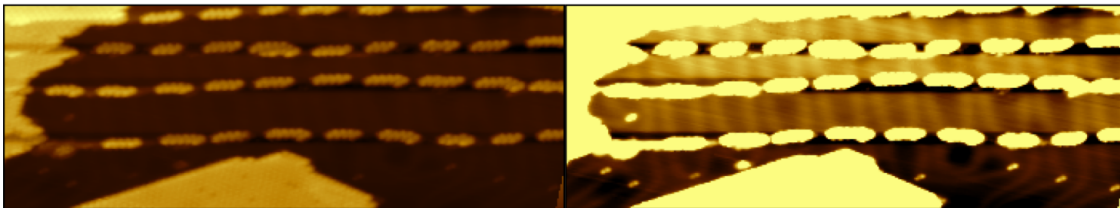


Figure 4.2: An 137×48 nm image showing 0.7 ML C_{60} coverage on step edges at two different contrasts. The image is taken at 165 pA and 700 mV. The left image shows the C_{60} molecules in focus and in the right image the resolution of the DLs is clearer. The molecules form preferentially on FCC areas of the step.

When the coverage is under a monolayer the C_{60} molecules decorate the step edge in sections at the FCC structure of the gold step.

In section 2.2.1 the two types of step that form on Au(111) are discussed. The $\{111\}$ micro-facet steps are found to be longer and straighter in STM images than the $\{100\}$ micro-facet steps. This is thought to be due to the smaller energy needed to modify the reconstruction for the $\{111\}$ steps compared to the $\{100\}$ steps^[45]. The $\{111\}$ steps can be identified on an image as the reconstruction lines appear to go through the steps and the $\{100\}$ steps have the DLs make U-turns before the edge of the step. Figure 4.2 is an example of $\{111\}$ micro-facet steps as the reconstruction lines appear to pass through the steps.

4.2.1 Bright and Dim C_{60} molecules

A variation in heights of the fullerenes was observed when analysing the C_{60} and gold samples, this can be seen in figure 4.3b and in figure 4.1.

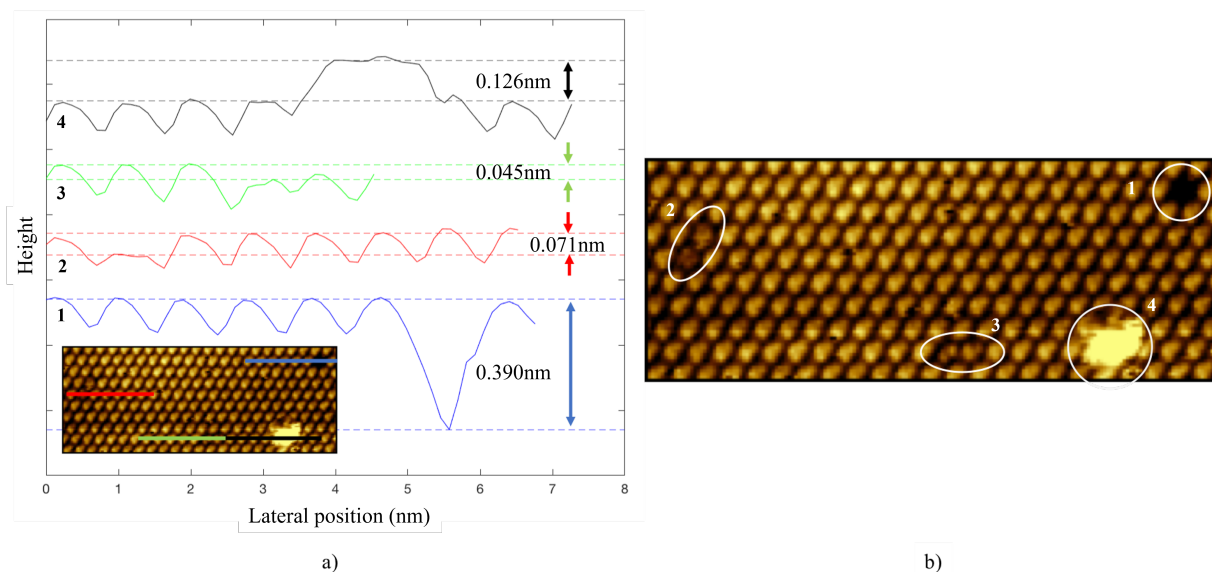


Figure 4.3: a) Graph of the height profiles taken over four points on a C_{60} island. The inset shows the location of each height profile taken. b) Image showing an area of a C_{60} island on Au(111) the 3 dim molecule locations and one bright molecule are highlighted by white circles these molecules' depth/height was measured and is shown in a). The image is 21 nm \times 9 nm taken at 1.97 V and 222 pA.

Figure 4.3b shows an area of an image which contains examples of dim molecules and raised molecules. There are two varieties of dim molecules illustrated one is a vacancy or hole (absence of a C_{60} molecule in the monolayer) this is represented by a circle in the top right corner of the image. The dim molecule which is represented by the blue height profile in the figure above is most likely a vacancy in the C_{60} layer and has a depth of 390 pm. The other pairs of dim molecules highlighted by white ovals in figure 4.3b are due to either topological or electronic effects: the molecules could appear dim

due to a stronger interaction or due to them sitting in a vacancy in the surface layer below. Dim molecules in figure 4.3 were observed at 45 pm and 71 pm depth. The bright molecules shown in figure 4.3b (white circle at the bottom right of the image) are raised by 126 pm (compared to the surrounding monolayer) which is smaller than the height of a monatomic gold step (approximately 240 pm) this height could be due to impurities on top or below the C_{60} island. When a molecule is raised by the height of a gold step it is likely to be due to a small gold island forming underneath the C_{60} monolayer and raising the molecules that sit on top, similar to work done by Guo et al.^[16] The blurring of the raised area is due to the tip either dragging molecules across the image slightly or the tip having molecules adsorbed onto it and those interacting with the sample affecting the image. The energy of a C_{60} - C_{60} bond is 0.85 eV^[107], when the C_{60} molecule is in a monolayer environment the molecule bonds with all molecules that surround it and the electron density is spread over the surrounding molecules. When a molecule is adsorbed as a second layer molecule or is raised compared to the monolayer surface, the electron density of that fullerene is distributed differently to the molecules in the first layer^[108].

In all images examined depths were found ranging in height from 20 pm to 100 pm. Bright molecules in all images analysed were found to be at a few heights above the C_{60} island height the heights were distributed from 30 pm to 1.4 nm above the average height of the C_{60} surface.

Dim C₆₀ molecules

The depth of the dim molecules found within islands was measured for multiple images. These heights were then collated and plotted in a histogram (figure 4.4) to see if any groupings of heights occurred. The curve plotted on the bar graph is a smoothing fit, it compares the heights of one bar to its neighbours and plots the average height across neighbouring columns. This type of fit can be used to help identify any statistically significant peaks from the data spectrum and helps prevent reading into the data and identifying peaks where there is little evidence.

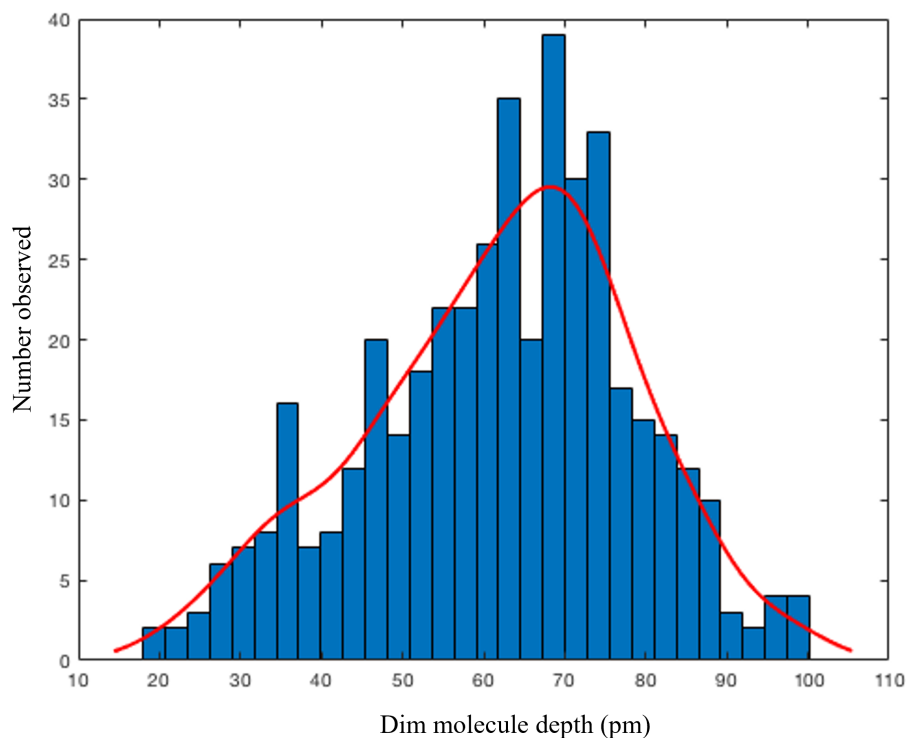


Figure 4.4: Histogram of the depth of different dim molecules across multiple samples with a smoothing fit applied to show any obvious peaks. The peaks on the smoothing fit are at 32 and 70 pm depth below the monolayer height.

This histogram shows a large distribution of measured depths for the dim C_{60} molecules with a peak at ≈ 70 pm and another slight peak at ≈ 32 pm. The smoothing curve is useful to show if any peaks are statistically significant when compared to the spread of data. Other peaks could also be identified at 48 pm, 63 pm and 100 pm but are not clear enough to be verifiable. The large distribution could be due to the change in state of the tip between images and sometimes even within an image. If the tip picked up a molecule while scanning this could impact the electronic response between tip and sample and alter the height observed. The peak at ≈ 32 pm corresponds to previous studies, where measurements of 35 pm and 40 pm were measured as the height difference between neighbouring C_{60} molecules with differing orientations^{[64][66]}. The peak around 70 pm height difference could correlate to previous measurements of 60 pm by Shin et al. ^[66] which corresponds to the difference in height of the monolayer and molecules sitting in vacancies of the gold surface below.

Bright C_{60} molecules

Fewer bright molecules were observed than the dim C_{60} molecules. This is likely due to a relatively high coverage of C_{60} and either too high or too low coverage of Au(111). If the C_{60} coverage was lower, instead of large islands forming, smaller clusters would form and would form around the elbow sites of the reconstruction as shown by Zhang ^[69]. If the gold adatom coverage was too high, instead of small clusters forming (on elbow sites) the adatoms would agglomerate at the step edges and form extended step

edges.

The few heights observed were grouped around certain sizes of: 45 pm 173 pm and 1.3 nm. The height of 45 pm is most likely due to the orientation of the molecule as it is a similar height difference to that observed for some dim molecules. Molecules that were raised by ≈ 173 pm were only found on samples where gold adatoms had also been deposited on top of the C_{60} molecules. On samples where gold adatoms were deposited small gold islands could be observed at elbow sites, the average height of these islands was calculated to be 179 pm. This height is similar to the height of some raised C_{60} molecules, therefore it is reasonable to attribute the bright molecules that are raised by 173 pm to gold islands sitting underneath the C_{60} island. This is similar to experiments undertaken previously that found C_{60} magic number clusters within a C_{60} matrix on HOPG [16]. The height of 1.3 nm is attributed to either a second layer C_{60} molecule forming on the first layer or a larger cluster of gold (greater than a single layer island) sitting underneath the monolayer of C_{60} raising the fullerene.

4.2.2 C_{60} molecules orientation

As discussed in section 2.4 there are multiple possible orientations of the C_{60} molecule with respect to the substrate it is adsorbed onto. These orientations can be observed via STM imagery as the electron orbitals of the C_{60} can be resolved due to their varying current density which is measured by the STM.










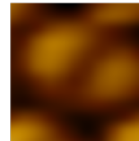
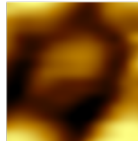

	3 lobes 'hexagon down'	2 lobes 'bridge down'	1 lobe 'pentagon down'	2 lobes rotated 'bridge down'
Diagram of C ₆₀ molecule				
Shape of electron density expected in STM images				
STM images				

Figure 4.5: A table showing diagrams of the C₆₀ molecule orientation, a simplified orbital structure diagram of what would be observed through the STM and STM images of the corresponding orientations.

The three lobe structure corresponds to the hexagon facet of the fullerene molecule being adjacent to the surface “hexagon down”. The two lobe structure represents a bond between facets binding to the surface (“bridge down”) and the single electron orbital corresponds to the pentagon facet (“pentagon down”) being adsorbed. Due to the C₆₀ molecule’s structure if a hexagon facet is facing the surface “hexagon down” it is also the face of the structure that is viewed at the top of the molecule. The same goes for pentagon facets and bridge sites facing the surface; the top most facet is the same facet as the bottom facet. Figure 4.6 shows some C₆₀ molecules with sub molecular resolution so that the different orientations can be identified.

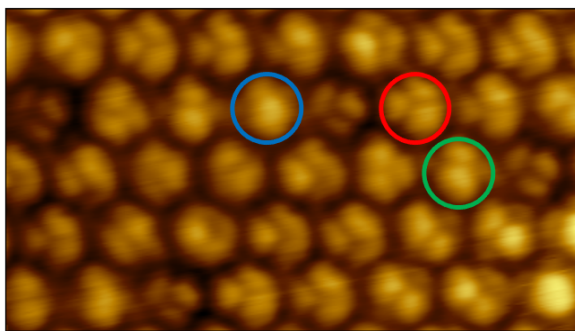


Figure 4.6: A 7.8×4.3 nm image (taken at 1.42 V and 123 pA) showing the electronic lobe structure of C_{60} molecules within a small island of C_{60} . The red circle represents the “hexagon down” orientation, the green represents the “bridge down” and the blue represents the “pentagon down” orientations.

The apparent heights of these C_{60} molecules varies within the island. In figure 4.7 an STM image and a corresponding height profile across one line of the image (indicated by a white line) is shown. Molecule 4 is considerably dimmer (0.12 nm lower) than the other molecules which only have 0.07 nm variation in height between them. When looking at the height profile measured in figure 4.7 it can be observed that the molecules with “hexagon down” orientation sit slightly lower than the “bridge down” molecules.

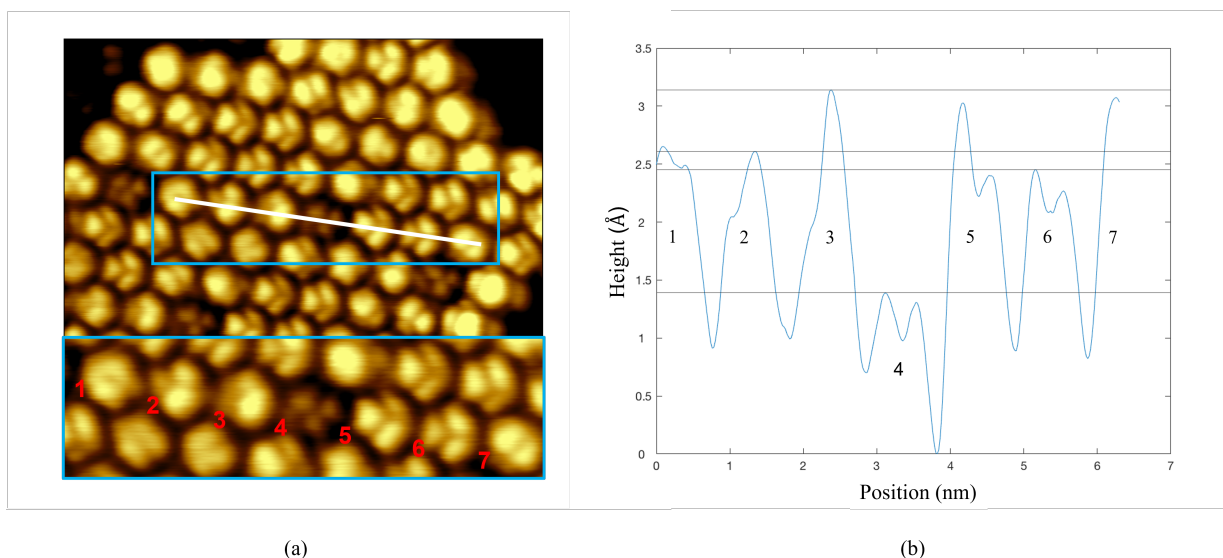


Figure 4.7: a) A 10×6 nm image taken at 1.42 V and 124 pA showing the orientation of C₆₀ molecules within an island. The blue box on the image corresponds to the enlarged image just below and the white line indicates the line that the height profile was obtained at. The molecules in the enlarged portion of a) are numbered and correspond to the numbers on the graph in b). b) A graph showing the height of multiple C₆₀ molecules along the line shown in a).

Molecule 4 in figure 4.7 can be treated as a dim molecule with the apparent height difference between it and the other molecules in the monolayer lying between 0.18 nm and 0.1 nm. 0.18 nm represents the height difference between the brightest molecule (molecule 3) to molecule 4, 0.12 nm and 0.1 nm represent the difference between molecule 2 to molecule 4 and molecule 6 to molecule 4 respectively. Molecule one two and seven show two lobe structure and hence have “bridge down” orientation. Molecules one and two have the same orientation where the two orbitals seen are perpendicular to the line shown in white on the image, whereas molecule seven has the two orbitals along the direction of the line. This could account for the height difference observed between the three molecules as molecule 1 and 2 are very similar in height but molecule 7 appears

much taller closer to the height of molecule 3. Due to the arrangement of molecules one and two, the brightest point could have been missed when measuring the height profile along the white line, due to the brightest lobe appearing off centre.

Molecules 4, 5 and 6 have 3 lobe structure hence the C_{60} molecule has a hexagon facet parallel to the surface in these instances. The height difference between molecules 5 and 6 is more likely to be due to the slight difference in orientation of the two hex down C_{60} molecules. As can be seen from the enlarged image at the bottom of figure 4.7a the three lobe shape is in the same orientation for both but the apparent brightness of the individual lobes is arranged differently. For molecule 5 the dimmest of the three lobes is the lobe closest to the top and for molecule 6 the brightness appears to be relatively even between the three lobes with possibly the left hand lobe appearing slightly dimmer. This difference in brightness of the image indicates that the molecules are slightly rotated compared to the surface; where molecule 5 is likely to be in between having the hexagon facet parallel to the substrate and a bridge site parallel to the substrate and molecule 6 is also rotated slightly towards a bridge site being parallel to the substrate but is rotated less than molecule 5 so the lobes have a more similar brightness within the molecule. Molecule 3 in this image could be due to the C_{60} molecule being in a “pentagon down” orientation or a bridge site orientation, if it is arranged so that the bridge is down the molecule would be rotated towards one of the pentagon facets so that there is one very bright orbital and the other is much dimmer. This is similar to what can be seen in the final column of the table in figure 4.5.

When comparing the apparent height data for the molecules shown in figure 4.7 it can be seen that the “bridge site” molecules and the “hexagon down” molecules have similar heights. When the C_{60} molecule is not sitting perfectly on one of the facets but is rotated the molecule appears brighter than its surrounding molecules. These results are similar to previous research of C_{60} molecules on surfaces, in work by Shin et al. the variation in height between a bright C_{60} molecule and a dim 3 lobe molecule was found to be between 0.095 nm and 0.1 nm ^[66]. In their work differences in height between 3 lobe and two lobe oriented C_{60} molecules was found to be 0.04 nm which corresponds nicely with the height between molecule 7 and molecule 6 which is approximately 0.05 nm in figure 4.7b. Other studies of C_{60} on Au(111) have found height variations of the bright and dim molecules of 0.09 nm ^[109] which also corresponds with the dim molecules’ height observed in this experiment.

C_{60} Dim orientation

Dim molecules within islands of C_{60} molecules were isolated and if the orientation could be analysed it was categorised into “hexagon down” , “pentagon down” and “bridge down” orientations. The results of this study are presented in a pie chart in figure 4.8 which shows the proportion of dim molecules in each orientation. The table in figure 4.5 shows diagrams of the C_{60} molecule in multiple orientations and the facets that correspond to the orbital appearance within the STM images highlighted. A simplified diagram of the lobe structure that is expected with each orientation and a corresponding

STM image for each orientation is also shown.

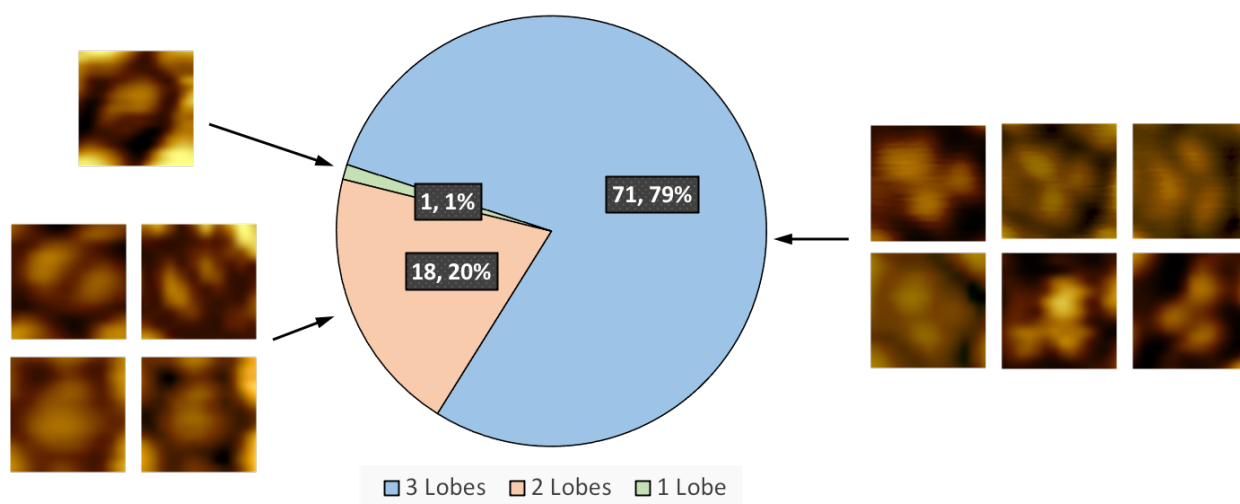


Figure 4.8: A pie chart showing the proportion of the orientations observed for dim molecules within multiple STM images. Each segment of the pie chart has examples taken from different STM images of the dim molecules as examples.

As can be seen from figure 4.8 the orientation that was most commonly observed in the dim C_{60} molecules was the 3 lobe or “hexagon down” orientation. The orientation with the pentagon facet adjacent to the surface was the least commonly observed and the second most common was the two lobe or “bridge down” orientation. These results correspond to previous work by Passens et al. that found for disordered $R30^\circ$ islands of C_{60} had 71% of molecules with “hexagon down” orientation^[110] Another study by Tang et al. found a similar result of 75% of molecules having three lobe structure in a disordered $R30^\circ$ monolayer^[65]. The C_{60} molecule with the “hexagon down” orientation could be most common due to the correlation between the 3 fold symmetry of the molecule in that orientation and the three fold symmetry of atop and hollow site binding positions on the gold substrate ^[13]. Previous studies have found that the difference

in binding energy of certain C_{60} molecules can be influenced by the orientation of the molecule from 140-240 meV per molecule^[111]. Therefore, if a particular orientation results in a lower binding energy that is expected to be the most dominant orientation observed which is the case for the three lobe structure or “hexagon down” orientation in this experiment.

Orientation on different phases

When C_{60} islands form on surfaces they can form with their packing at various orientations with respect to the packing direction of the substrate below. As discussed in section 2.4.1 the phases observed for C_{60} on Au(111) surfaces are $R0^\circ$ where the adlayer and substrate are arranged along the same direction; $R30^\circ$, $R34^\circ$ and $R14^\circ$ where there is a 30, 34 or 14 degree difference respectively between the orientation of the substrate and adsorbed C_{60} molecules. To work out the phase of the fullerene islands, the gold reconstruction can be compared against the packing orientation of the C_{60} island. The image below (figure 4.9) shows an image with $R30^\circ$, $R0^\circ$ and $R14^\circ$ phase islands which are detailed on the image.

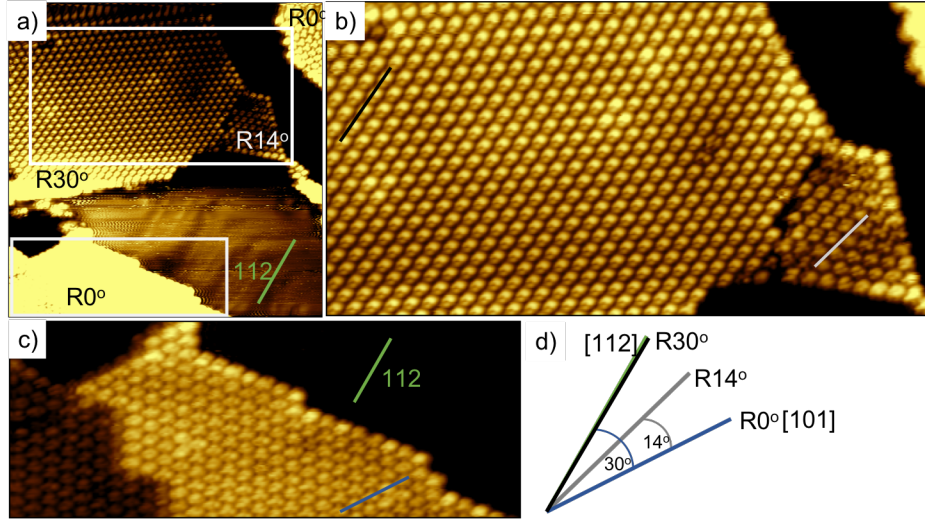


Figure 4.9: Images showing the different phases in one STM image of a C_{60} island on Au(111). a) A 40×40 nm image taken at 708mV and 112 pA of 0.6 ML coverage C_{60} . The white boxes correspond to the two enlarged areas b) 34×16.5 nm and c) 29×11 nm. The green line on image a) and c) corresponds to the direction of the reconstruction lines of the gold substrate. d) takes the four different lines (blue green black and grey) from the previous images and compares the angles between each of them and hence the phases of those islands.

The gold atoms are compressed along the $\langle 1\bar{1}0 \rangle$ crystal lattice vector which is perpendicular to the reconstruction lines that form. Since the C_{60} has HCP packing structure there are 3 lattice directions each 120 degrees from each other. When the C_{60} lattice is aligned with the DLs one of the lattice directions is along the $[11\bar{2}]$ direction (90° from the $[1\bar{1}0]$ direction) and thus 30° from the $[10\bar{1}]$ direction. In figure 4.9a the DL direction is highlighted with a green line showing its direction. The directions of each island's packing can be compared to the 112 direction and the angle between the lines measured. All islands' directions are shown in figure 4.9d where the angles comparing the directions are shown, the $R30^\circ$ direction is parallel to the DL direction.

As can be seen in figure 4.9 the $R30^\circ$ island has almost all C_{60} molecules in the same

orientation with respect to the surface. The C_{60} molecules have 2 orbitals one much larger than the other indicating that the molecule is sitting on a bridge site but is rotated so one of the faces is closer to the surface than the other. This rotated orientation has previously been observed on many surfaces such as silicon^[112], platinum^[60] and gold^[65]. The only deviations from this molecular orientation are two of the dim molecules shown on this island which appear to have a more even two lobe structure. The R14° island in figure 4.9b has more than one orientation in the island. Out of the 65 C_{60} molecules that make up the island there were 17 unidentifiable orientations, 24 molecules arranged “hexagon down”, 22 molecules “bridge down”, and 2 “pentagon down”. In other images where the phase of the islands was identifiable the proportion of each orientation was noted and collated in the graph shown in figure 4.10.

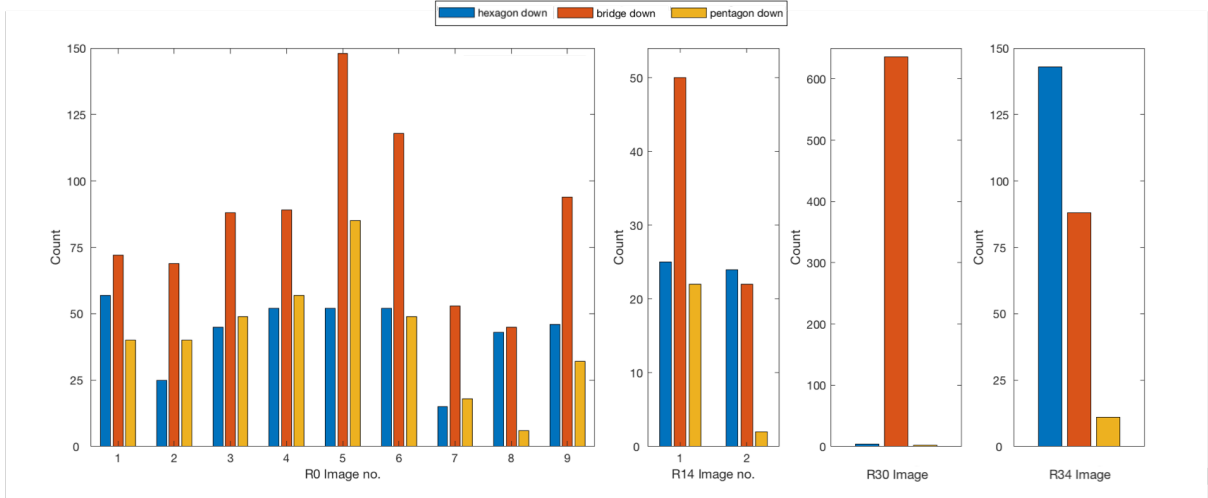


Figure 4.10: This figure shows the frequency of each orientation of C_{60} molecule for different phase islands of C_{60} . The first graph shows the data taken from various C_{60} islands with 0° phase difference to the gold lattice below. The second graph shows the data from two R14° islands and the final two graphs contain data collated from an R30° island and an R34° island.

More examples of in phase C_{60} islands ($R0^\circ$) were found while imaging the sample and for $R34^\circ$ and $R30^\circ$ only one example was found where the orientation of the fullerene molecules could be identified. As can be seen from figure 4.10 the $R0^\circ$ islands had more C_{60} with two lobe orbital structure (“bridge down”) than either “hexagon down” or “pentagon down”. For almost every image examined the “bridge down” orientation was the most frequently observed. The exceptions to this are one of the $R14^\circ$ images and the $R34^\circ$ image where the 3 lobe structure (“hexagon down”) is most frequent. Another anomaly when comparing the data is the observed frequency for the $R30^\circ$ island. This is the data for the island shown in figure 4.9b. This phenomenon where almost the entire island is comprised of one C_{60} molecule orientation was only observed in this instance and not duplicated. Since no further images of $R34^\circ$ had sub molecular resolution, it was not possible to corroborate this data. It is likely that the collected data for islands in phase with the gold atoms beneath is reliable as it was repeatedly observed that the bridge site is the most common adsorption site for the C_{60} molecules. The bridge site adsorbing to the gold substrate is frequently observed for all orientations, this could be due to the multiple possible angles the molecule can be adsorbed onto the surface and be classified in this way. The C_{60} molecule could have a two lobe structure where the molecule is comprised of two roughly even orbitals or could be uneven with one substantially larger than the other as seen in figure 4.9b. If the different types of two lobe C_{60} molecule were subcategorised additional trends could be observed. Previous work by Tang et al. that examined the orientation of C_{60} molecules on Au(111) found that the most commonly observed orientation in the $R30^\circ$ phase was the 3 lobe structure.

They also found that the $R0^\circ$ and the $R14^\circ$ had more variation and groups of molecules in specific arrangements tended to form^[65]. Shin et al. ^[66] found that for the $R30^\circ$ phase 80% of the molecules had the “hexagon down” orientation and the remaining 20% was the “bridge down” orientation. These results do not correlate with the results found in this chapter that the $R30^\circ$ island imaged contained mostly bridge site bonded C_{60} molecules. However, only one $R30^\circ$ island was examined in this study and had more islands with submolecular resolution been imaged the statistics could have varied drastically. The previous research showing that $R0^\circ$ and $R14^\circ$ have more variation than the $R30^\circ$ phase does correspond with the results obtained in this study.

4.3 Summary

Within this chapter the analysis of sub-monolayer coverage C_{60} on Au(111) was detailed. The overall appearance of the sample and the fullerenes’ behaviour on step edges was shown, the dim and bright molecules that appear in islands of C_{60} were discussed and the orientation of the C_{60} molecules was examined. The dim molecules were found to mostly be in a three lobe orientation where the hexagon facet of the C_{60} molecule bonds to the surface of the gold substrate. The orientation most commonly found for the C_{60} molecules in all but one phase of the C_{60} islands was found to also be the “hexagon down” orientation. The apparent height of different orientations was examined and it was found that the brightest molecules were oriented with a pentagon facing the surface; the two lobe and three lobe orientations had a similar height with the “hexagon down”

orientation being slightly lower than the “bridge down”. The depth of dim molecules observed was measured for multiple images and plotted in a histogram that showed the depths had a large variation with a peak around 70 pm depth. The results presented in this chapter were compared to the literature and in most cases the results follow what has previously been observed. A comparison of results presented in this chapter and the following chapters can be found in Chapter 7.

Chapter 5

Investigation of C_{60} on highly oriented pyrolytic graphite (HOPG)

In this chapter the investigation of a C_{60} /Au matrix on HOPG will be discussed. The previous chapter detailed the study of C_{60} on Au(111) which has also been examined in previous studies and magic number clusters were found to form on the surface. On HOPG surfaces C_{60} molecules are more mobile and therefore it is interesting to see if the C_{60} /Au clusters are stable on graphite similar to on Au(111). The Au(111) surface and Au cluster that sits at the centre of the magic number clusters have a strong interaction. Recreating these clusters on HOPG would decouple the clusters from the substrate and allow them to be studied individually. HOPG was selected as an alternative to the crystalline gold sample, as it has large flat terraces and a weak interaction with gold.

Within this chapter some C_{60} molecules were found to be raised above the average

height of the monolayer and the heights of these molecules and possible explanations will be discussed. The C_{60} molecules can also appear depressed when compared to the monolayer, these molecules are investigated and the results presented. The orientation of C_{60} molecules on the HOPG surface is also examined within this chapter.

5.1 Experimental Methods

Samples of HOPG were prepared according to the cleaving procedure laid out in section 3.2.1. C_{60} was then deposited onto the HOPG surface and gold adatoms were deposited after that (details of the evaporation techniques can be found in sections 3.2.3 and 3.2.4). The gold adatoms were deposited on a cooled (77 K) C_{60} /HOPG sample to prevent agglomeration on the surface. The C_{60} fullerene is very mobile on the graphite surface due to the weak bond between C_{60} and HOPG substrate (813 meV^[113]) the thermal diffusion barrier at room temperature is 13 meV. To accommodate for the surface diffusion of the fullerene molecules larger amounts of C_{60} are deposited (0.75-0.9 ML) compared to the amount that was deposited on gold surfaces (0.5-0.7 ML). Higher coverage of C_{60} results in larger islands of the molecule, this in turn allows for more stable imaging as the C_{60} - C_{60} bond is stronger (968 meV) than the C_{60} -HOPG (substrate) bond (813 meV)^[113]. At edges of large islands and for small groups of C_{60} on the surface, the scanning tunneling microscope (STM) tip can attract the fullerenes and drag them across the surface resulting in bright streaks in the STM images. An example of this combination of thermal and tip induced movement can be seen in figure 5.1.

Heights of the molecules and features discussed in the results section were calculated using Gwyddion's height profile tool. For a height profile, a snippet from one line of the STM image is taken and plotted so that just the relative heights of the features in question are shown. As the STM does not directly measure the height of the sample but the current or the height of the tip, electronic effects can influence height measurements taken on the surface.

5.2 Results and Discussion

A C_{60} Au matrix was deposited on the HOPG substrate, a typical image of the sample can be seen in figure 5.1. In this image large islands of C_{60} molecules can be seen with small gaps between where the HOPG surface is not covered by the fullerenes. The main golden colour of the image represents the C_{60} monolayer and the dark patches are the gaps between C_{60} islands, STM images represent different heights using a colour gradient. Dark areas of STM images correspond to the lowest points on the image and bright areas are the taller aspects of the image. The brighter shapes in the image are the second layer C_{60} islands (sitting on top of the first layer of C_{60}) in some places these 2nd layer molecules are dragged by the tip while scanning the surface and they appear distorted as a bright streak on the image. The height of the 1st layer C_{60} islands on the HOPG substrate was found to be 0.74 ± 0.15 nm and the 2nd layer C_{60} molecules were found to have an average height of 0.85 ± 0.15 nm.

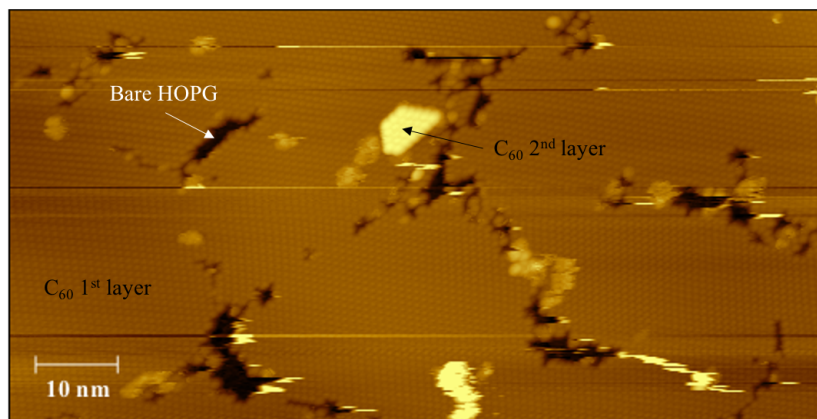


Figure 5.1: A 100×50 nm image of the C_{60} -Au HOPG surface. The C_{60} molecules cover the majority of the sample with the bare HOPG only visible through gaps in the C_{60} monolayer. This image was taken at 1.5 V and 152 pA with 0.75 ML C_{60} and 1 minute Au deposition.

5.2.1 Bright Molecules

The C_{60} -Au/HOPG samples had some brighter molecules (raised compared to the monolayer) present in the images of these samples. Height analysis was done on these samples and various heights for these raised molecules were found. Some were found to be the height of a second layer C_{60} molecule (≈ 1 nm) and for some the height difference was significantly smaller (≈ 0.25 nm). Figure 5.2a shows an area of a sample with 3 different heights of bright molecules. The large island in the centre is a second layer island and the two single bright molecules have differing heights. The height profiles taken on this sample are indicated by white lines on figure 5.2a and these height profiles are shown in figure 5.2b.

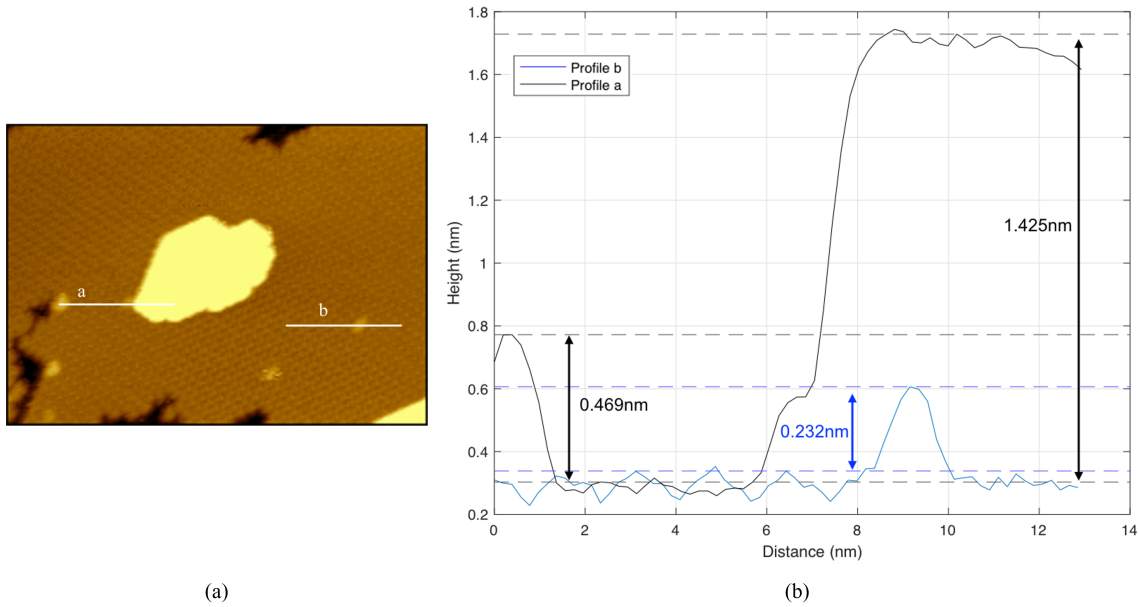


Figure 5.2: a) A 79x56 nm image of three types of bright features in an STM image of an HOPG sample with 0.75 ML C_{60} and 2 minutes Au deposition. Taken at 2.5 V and 110 pA.

b) The corresponding height profiles along the lines indicated on (a). The black line profile is taken along the line labeled a and the blue profile is taken along the profile b. Heights of the features are labeled on the figure.

The height of the molecule examined with profile b corresponds to previous studies of magic number clusters within a C_{60} monolayer where the C_{60} molecule is raised ≈ 0.24 nm (the height of a single layer gold island). The second layer island on the surface has a height of 1.4 nm compared to the first layer, this is higher than would be expected as C_{60} normally appears to be 0.7-1 nm on STM images^[16]. This height could be greater due to a larger gold island sitting below the C_{60} monolayer of at least 2 atomic layers in height (≈ 0.5 nm). Taking this into account the height of the second layer C_{60} molecule would be ≈ 0.9 nm which falls within previously observed heights for C_{60} molecules. The bright C_{60} molecule with a height of 0.47 nm could also be due to

a double layer of gold atoms underneath the C_{60} molecule or it could be due to the tip interacting more strongly with the molecule and moving it as it was scanning. The movement of molecules on the surface induced by the STM tip passing over them is more common in molecules at the edge of an island or at the edge of a second layer island. This is due to the molecules having less neighbouring molecules so therefore a weaker bond to the island than molecules that are surrounded by neighbours.

The heights observed over multiple samples were examined and a graph of these results can be found in figure 5.3. Figure 5.3 is a histogram of the different heights found on sample images, the red line on the histogram is a fit that smooths the shape of the data to make the statistically significant peaks observed more apparent. As can be seen from the figure there are several peaks, one at around 0.25 nm, possibly another at 0.8 nm and a peak at around 1.4 nm; the fit curve only highlights two peaks with the 0.8 nm peak being combined into the 0.25 nm peak.

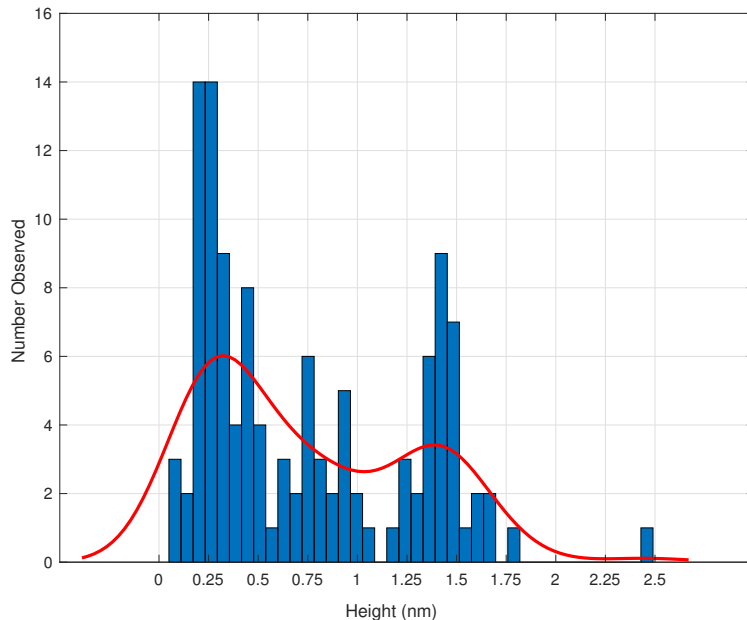


Figure 5.3: Histogram showing the number of bright molecules found at different heights. The red curve is a smoothing fit applied to show any major peaks detected.

The peak centred around 0.25 nm corresponds to the height of a single layer of gold atoms, therefore it is plausible that these raised molecules are the C_{60}/Au clusters contained within the matrix of the C_{60} monolayer. This agrees with previous data found by Guo et al. ^[16] where the height at the centre of the the C_{60}/Au clusters compared to the monolayer was found to be 0.27 nm. The peaks centred around 1.4 nm and 0.8 nm also correspond to previous studies of C_{60} on HOPG, where the height of a single molecule is ≈ 0.7 nm and a second layer would be roughly double that ^[16]. The molecules that are 1.4 nm above the first monolayer could be due either to: a large gold island sitting on the HOPG surface that lies underneath the C_{60} ; a double C_{60} layer island on top of the 1st layer molecules; or gold islands both underneath the first C_{60}

layer and interspersed between the first and second layers. Possible arrangements of C_{60} molecules and the gold islands is shown in figure 5.4.

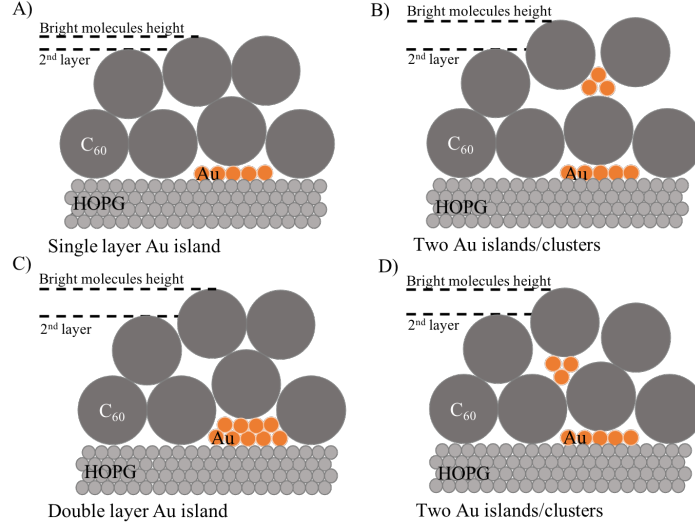


Figure 5.4: Diagram showing possible arrangements of the C_{60} molecules and the gold adatoms on the HOPG surface. Figure a) shows a single layer Au island and c) shows a double layer gold island sitting on the surface of the HOPG substrate. Diagrams b) and d) show two possible arrangements for two single layers of gold islands forming between the two C_{60} layers. These diagrams are for illustration purposes and the atoms shown are not to scale with one another.

The probability of double layer C_{60} islands forming on top of the first monolayer is unlikely due to the way the C_{60} monolayer forms (discussed in section 2.4.2). The third layer of C_{60} molecules can form on top of second layer islands but the area of the second layer island that the 3rd layer molecules cover is rarely the same size as the second layer [79]. If three layers were deposited it would usually be observed as a large first layer island, a smaller second layer island and an even smaller third layer island, appearing as a stepped surface. This makes it more probable that the 1.4 nm height observed corresponds to a double layer gold island or two single layer gold islands

sitting beneath or between the C_{60} layers. When deposited at room temperature the Au molecules coagulate on the HOPG surface forming large clusters. If, when depositing the gold onto the C_{60} /HOPG sample it was warmer than the expected 77 K, this could have lead to the formation of double layer Au islands.

The broadness of these peaks shows that there is a large distribution of the heights observed, this could be due to the STM tip's interaction with the surface. The STM tip can easily interact with the C_{60} molecules and often picks up a molecule while scanning, this can lead to streaks on the image or a change of state of the tip mid way through an image. When a C_{60} molecule is attached to the end of a tip the work function of the tip is altered; the tunneling current measured at each point of the sample is different from when a clean tip is used. It is possible that when scanning some of the images analysed, the tip picked up a C_{60} molecule and this changed the electronic interaction between the tip and the sample, leading to a wider range of heights being observed and broadening of the peaks observed in figure 5.3.

5.2.2 Dim molecules

The C_{60} monolayer also had dim molecules on the fullerene islands which can be seen in figure 5.5. This figure has three dim molecules and one raised molecule, the corresponding height profiles are shown in figure 5.6. Height profiles for dim molecules were taken for all images and were plotted in a histogram, this data can be seen in figure 5.7. The sample shown in both these figures has 1 minute Au deposition and 25 min

C_{60} deposition.

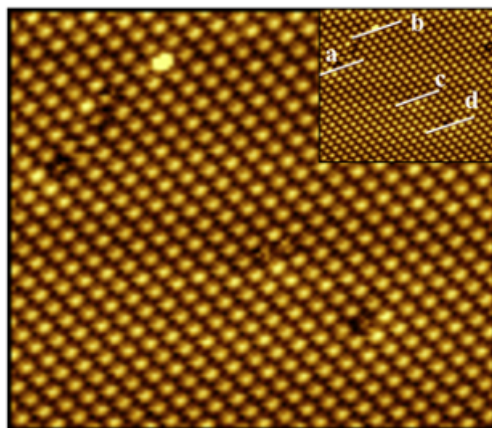


Figure 5.5: A 23x20 nm size image of the C_{60} monolayer on HOPG with dim molecules and one bright molecule. Taken at 1.5 V and 114 pA, the sample had 0.75 ML C_{60} deposition and 1 minute Au.

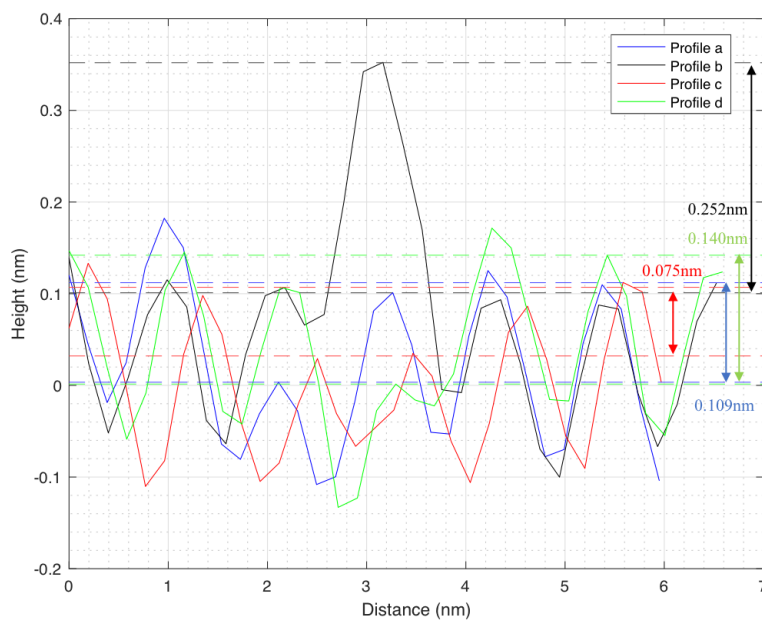


Figure 5.6: Height profiles a-d of the molecules labeled on 5.5. The heights of the features are labeled on the graph in the corresponding colour to each trace.

The height profiles of the dim molecules and bright molecule from figure 5.5 show

heights of -0.075 nm, -0.109 nm, -0.140 nm and +0.252 nm. The raised molecule, similar to results discussed in the previous section, is raised by the height of a single layer of gold atoms so this molecule can be assumed to be sitting on an Au layer.

One possible explanation for the dim molecules has previously been the orientation of the C_{60} molecule and the strength of its interaction with the surface dependant on orientation. The variety of heights measured could correspond to different orientations of the molecule, with the lowest apparent heights corresponding to the “hexagon down” arrangement, and the brightest being the pentagon facing down with the bond occurring on a bridge site in the middle height wise^[60] ^[114]. Diagram of the orientation of the C_{60} molecules with respect to the surface are shown previously in figure 2.8.

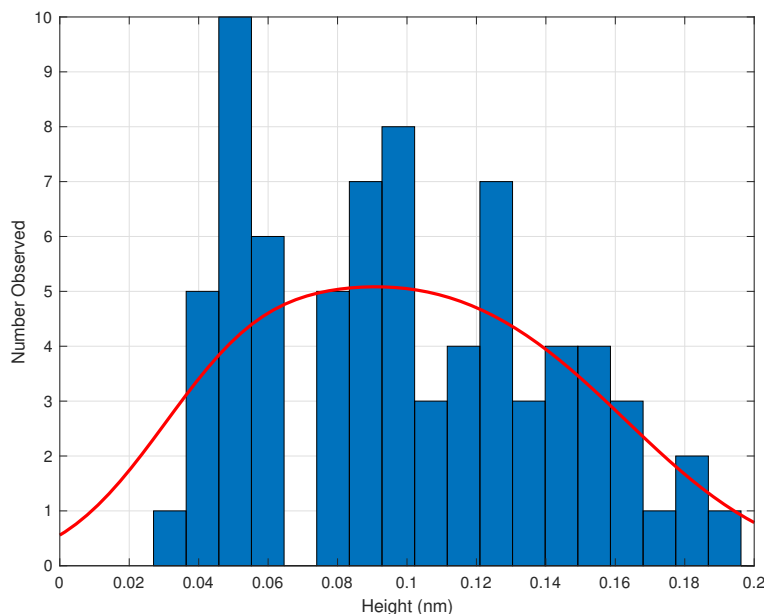


Figure 5.7: Histogram of the number of dim molecules found at different heights. The red curve is a smoothing fit that shows only one peak in the distribution.

As can be seen from figure 5.7 there is a large distribution of height difference between the dim molecules and the surrounding C_{60} molecules. The red curve is a smoothing fit that helps to identify any statistically significant peaks. This curve shows just one continuous peak for this data showing that no visible sub-grouping could be found of the heights observed. Previous studies have documented the height variation of C_{60} molecules in an island and found small height differences of around 0.04-0.06 nm that could be due to the orientation of the C_{60} molecule. C_{60} deposited on an FeO/Pt(111) ^[115] substrate and a plain Pt(111) ^[60] substrate both show 0.04 nm height difference between the brightest single orbital orientation (pentagon bound to substrate) and the dimmer 3 and 2 orbital orientations (hexagon facet bound and bridge site bound). C_{60} molecules on a Cd(0001) surface had a difference in height between dim and bright molecules of 0.06 nm ^[114]. When considering the heights observed within this experiment the smaller depth of the dim C_{60} molecules (<1 nm) could be attributed to the same phenomenon, where the orientation influences the height of the molecules.

Since the tip is not measuring the height directly but is measuring the apparent height based on the tunneling current, measured electronic differences can impact the height of a molecule. The “hexagon down” orientation forms a stronger bond with the surface so can therefore appear dimmer. When scanning at various biases the bright and dim molecules can swap or vary in height due to how the tip interacts with the molecules. When current flows from tip to sample and when the bias is reversed and the current flows from sample to tip the dim molecules can vary in height. No varied bias studies

were carried out on the samples made in this experiment due to poor tip stability.

Unfortunately, a large proportion of the STM images where the dim molecules are present have a double tip, this is a feature that sometimes occurs in STM imaging if the tip has more than one atomic peak at the apex. While scanning the surface of the sample the STM tip can pick up C_{60} molecules or other impurities and these can affect the tip shape and therefore the image it creates. If a tip has 2 peaks then current can pass through 2 routes to the surface and a structure on the surface can appear to be repeated in the images. The heights included in these calculations were in images where the double tip was not present or were taken from the same direction to eliminate the effects of the tip on the height profiles.

The larger height differences observed for some dim molecules don't align with previous measurements for orientations and since no bias studies were undertaken the electronic effects cannot be definitively cited as the cause. Another possibility for the height differences observed is a large gold coverage underneath the C_{60} monolayer. Since the gold adatoms bind underneath the C_{60} monolayer the coverage of these molecules cannot be estimated from these images. If a large amount of gold was deposited instead of the small amount intended, large gold islands could form underneath the C_{60} monolayer and the deeper dim molecules could be sitting on the bare HOPG rather than the Au adlayer. These dim molecules could also be due to impurities on the graphite or defects in its surface, while the bare HOPG was scanned before any deposition to check the sample, these impurities or defect sites cannot be ruled out. The height of one atomic

layer of HOPG is 0.34 nm so it follows that some of the deeper (>0.3 nm) dim molecules are related to impurities.

5.2.3 Orientation

A few STM images taken in these experiments showed possible orientations of some of the C_{60} molecules. In a couple of instances the dim molecules on the surface showed what could be interpreted as a three lobe structure, the hexagonal facet of the fullerene binding to the surface (section 2.4). If these images do represent a dim molecule with three orbitals then this corresponds to previous research that shows the bonding of hexagon down molecules is stronger than others therefore has a lower “height” on the STM image^[13]. The height observed of the three lobed molecules in the images below was between 100 – 125pm. Comparing this depth to the height of monatomic steps on gold (240pm) and HOPG (340pm^[116]) it is clear that these dim molecules are not caused by defects in a gold underlayer or in the HOPG substrate and are more likely to be caused by electronic effects such as orientation or binding site on the surface.

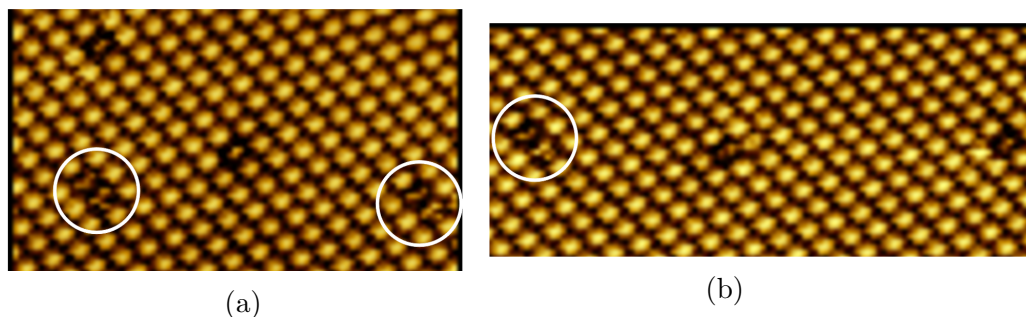


Figure 5.8: Images of the orientation of dim molecules in a C_{60} monolayer. a) 18x10 nm taken at 1.5 V and 114 pA. b) 21x8 nm taken at 1.5 V 114 pA. Both samples had 0.75 ML C_{60} and 1 minute Au deposition.

Very few scans with the orientations of the C_{60} molecules were able to be recorded in this experiment and the images which did contain orientations only had the orientations of a few molecules, the bulk monolayer orientations were not able to be imaged. Achieving these images would have been beneficial as it could have provided key information about the orientation of the C_{60} molecules in the C_{60}/Au clusters. A comparison could have been drawn with suggested orientations of the C_{60} molecules in clusters on Au(111). This inability to capture the orientation is likely due to the tip conditions whilst scanning. Jarvis et al. looked at the effect having a C_{60} molecule adsorbed on the end of a force microscopy tip affects the imaging and found that it was much harder to see the molecular orientation ^[117]. Another study that looked into the impact of C_{60} molecules adsorbed to the tip was the study by Chiutu et al.^[112] where a Si(111) surface was scanned with a C_{60} adsorbed to the end of a tip. This study found that the orientation of the C_{60} molecule on the tip could be determined by the change in the appearance of the silicon molecules on the surface. When the tip had a molecule with the bond between two hexagons facing the sample the silicon atoms appeared to have two lobes. When the pentagon face of the C_{60} molecule was facing the sample each silicon atom appeared to have 5 lobes. In both these cases the tip structure was impacting the resulting image by changing the appearance of the silicon molecules. Figure 5.9 shows the molecular orientation of the C_{60} molecule and the corresponding image of the Si sample.

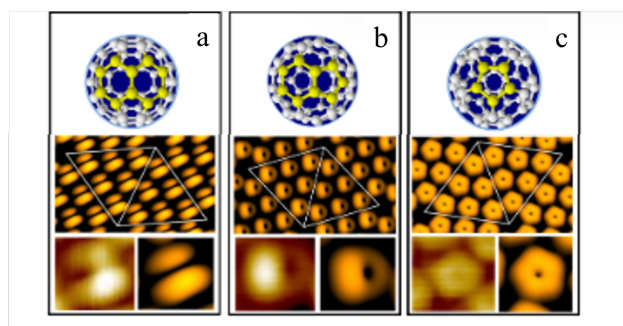


Figure 5.9: Figure showing the effect of a C_{60} molecule's orientation adsorbed on the STM tip when scanning Si(111). From [112]. The top image of a, b and c shows a model of the C_{60} molecule showing the face that is adjacent to the substrate in yellow: a) bridge site between two hexagons b) bridge between hexagon and pentagon facets and c) a pentagon facet bonded to the sample. The large STM image in the centre of a b and c is an STM image showing how these orientations appear in a scan. The bottom left image is a zoomed in version of the image above focusing on one molecule and the bottom right image is the same but with a higher contrast so the orbital shape can be more easily resolved.

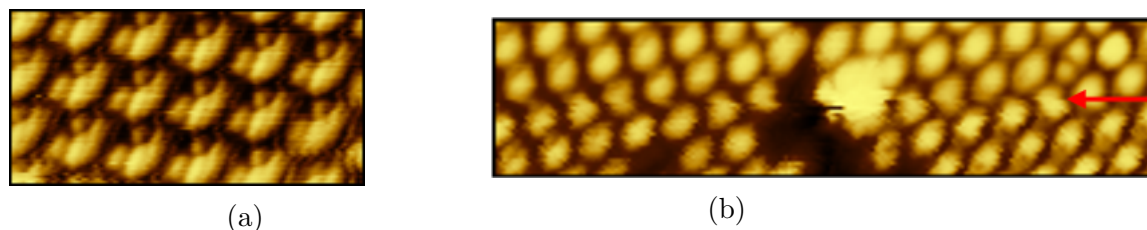


Figure 5.10: Image of C_{60} molecules on HOPG taken with C_{60} adsorbed onto the tip. a) 5.3×2.8 nm taken at 1 V and 112 pA on sample with 25 minutes C_{60} and 1 minute Au. b) 15.5×3.5 nm taken at 1.5 V and 146 pA on sample with 25 minutes C_{60} and 1 minute Au deposition, the red arrow indicates the line where the tip changed state.

The STM images in figure 5.10 show examples of the tip's geometry affecting the shape of the C_{60} molecules while scanning. This can be ascertained by comparing the shapes of the molecules observed with possible orientations of the C_{60} molecule. Figure 5.10a is probably the result of multiple molecules at the end of the STM tip as the shape of the molecules does not match up with any orientations of the C_{60} molecule. Figure

5.10b has molecules that look like the molecules in figure 5.9b and then the tip can be seen to change state within the image after scanning over the bright molecule in the centre of the image and the shape of the molecules changes.

5.3 Summary

This section contains a summary of the results discussed in this chapter, concluding remarks can be found in chapter 7. It was found that C_{60}/Au on HOPG samples contained both bright and dim molecules. Bright molecules were found to be 0.25 nm above the monolayer which corresponds to the height of a single layer gold underneath the molecule. Bright molecules were also found at 1.4 nm above the monolayer, which could correspond to a second layer C_{60} island with gold clusters underneath the two layers. Dim molecules were found to vary greatly in height, the smaller depths found are most likely related to the orientation of the C_{60} molecules. Some orientations were observed in the investigation of the C_{60}/Au HOPG samples, the orientations were seen for a few dim molecules which were more hexagon face bonded to the sample. In the next chapter the investigation into electronic details of both the $C_{60}/Au(111)$ sample (discussed in the previous chapter) and the $C_{60}/HOPG$ samples (considered in this chapter) will be discussed.

Chapter 6

Scanning Tunneling Spectroscopy

Studies of Au(111), HOPG and C₆₀ on Au(111).

This chapter details the investigation using Scanning Tunneling Spectroscopy, of the same samples detailed in chapters 4 and 5 with the aim of gaining more information about the samples. Au(111) samples with C₆₀ molecules adsorbed on the surface were investigated along with bare Au(111) and HOPG. The effect of the height of the tip while performing spectroscopy measurements, along with the polarity of the bias voltage was examined. On the bare Au(111) and the HOPG different lattice positions were studied and the difference of the conductivity at various sites was explored.

6.1 Experimental Method

The processes of tip etching and annealing discussed in section 3.3 were used within this chapter to produce the tips needed for spectroscopy measurements. Sample production techniques from section 3.2 were also used to create the samples for these experiments and experiments in the previous chapters. Details of the lock-in amplifier that is used for scanning tunneling spectroscopy (STS) to improve the signal to noise ratio in the spectra will be discussed along with the analysis techniques used.

6.1.1 STS Tips

STS experiments require a stable scanning tunneling microscope (STM) tip due to the small currents being measured during the I-V sweep. When scanning with an STM tip, molecules can be picked up and this can affect the stability of the tip. Changing the scanning voltage is often used while imaging to clean the tip, quick voltage pulses can help to remove adsorbates from the tip. The STS I-V spectra were achieved by holding the STM tip at a constant height and sweeping the voltage from a negative voltage to a positive voltage. It is therefore obvious how an unstable tip could dramatically affect measurements. If an adsorbed molecule is removed during the voltage sweep, effecting the electronic structure of the tip, it could change the electronic response measured.

The STM tips were prepared using the methods laid out in section 3.3 (etched using NaOH, recrystallised and annealed). Recrystallised tips were used in these experiments

due to their more uniform electronic structure, recrystallisation can also reduce the number of anomalous tips produced, when compared to non-recrystallised tungsten wire. This technique was inspired by the work of Greiner et al. ^[118], where the tips were used in field emission experiments, and the technique used by Alex Pattison ^[119], who used the recrystallised tips in STEM tomography experiments. Since the local density of states (LDOS) of the sample and the tip are measured during spectroscopy experiments, the crystalline structure of the tungsten is thought to be advantageous compared to amorphous tungsten wire.

Figure 6.1 shows an STM tip etched using tungsten wire with no additional processes completed (viewed through an optical microscope) and a tip that has been recrystallised and heated to remove the oxide layer before etching. As can be seen in the recrystallised and annealed wire the end of the wire is a different colour to the main part of the tungsten wire, this is due to the thick oxide layer being removed during the heating process.

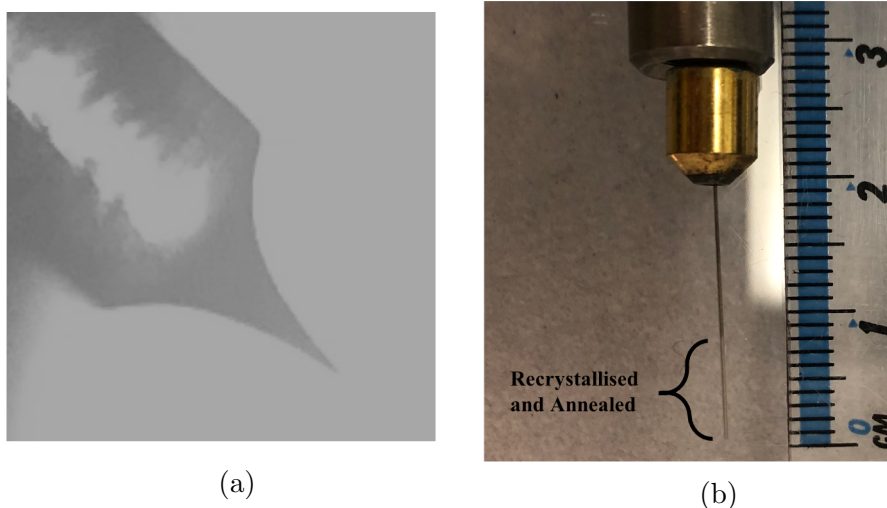


Figure 6.1: a) Image of an etched W tip magnified with an optical microscope, showing the basic shape of a good tip. b) Image of a recrystallised and heated wire in the wire etching holder, the brighter section at the end of the wire is where the tungsten oxide layers have been removed, it appears a brighter silver to the rest of the tungsten wire.

6.1.2 Lock-in

Lock-in amplifiers can be used to measure small signals where the signal to noise ratio is high. These amplifiers employ the use of a modulating reference signal (normally sinusoidal) that is combined with the tunneling current data from the STM. This is then compared to the reference signal, where constructive and destructive interference occur, amplifying the signal from the STM over any noise. The lock-in amplifier can also be used to extract an approximation of the first derivative of the current ($\frac{dI}{dV}$). When a sinusoidal voltage with amplitude V_{mod} and angular frequency ω is applied to the bias voltage (V_{bias}) the current observed is represented as $I(V_{bias} + V_{mod}\sin(\omega t))$ [87].

This can be expanded to equation 6.1 using a Taylor expansion:

$$I(V_{bias} + V_{mod}\sin(\omega t)) \approx I(V_{bias}) + \frac{dI(V_{bias})}{dV}V_{mod}\sin(\omega t) + \frac{dI^2(V_{bias})}{dV^2}V_{mod}^2\sin^2(\omega t) + \dots \quad (6.1)$$

The first harmonic of the modulated current ($\frac{dI(V_{bias})}{dV}V_{mod}\sin(\omega t)$) can be approximated to $\frac{dI}{dV}$ (when ω is small) and hence the lock-in can be used to extract this term from the current measured during spectroscopy. The frequency of the reference signal chosen was not a multiple of 50Hz to prevent amplifying any electronic noise that might be present.

6.1.3 Analysis

I-V spectra were taken and the $\frac{dI}{dV}$ spectra could then be produced by taking the first harmonic from the lock-in amplifier or by numerically differentiating the I-V data. The figure below 6.2a shows the current response to sweeping the voltage from -4 V to $+4$ V. The differentiated version of this spectrum is shown in 6.2b. The graphs presented here are used as examples, the results shown here will be discussed in more detail in section 6.2.2.

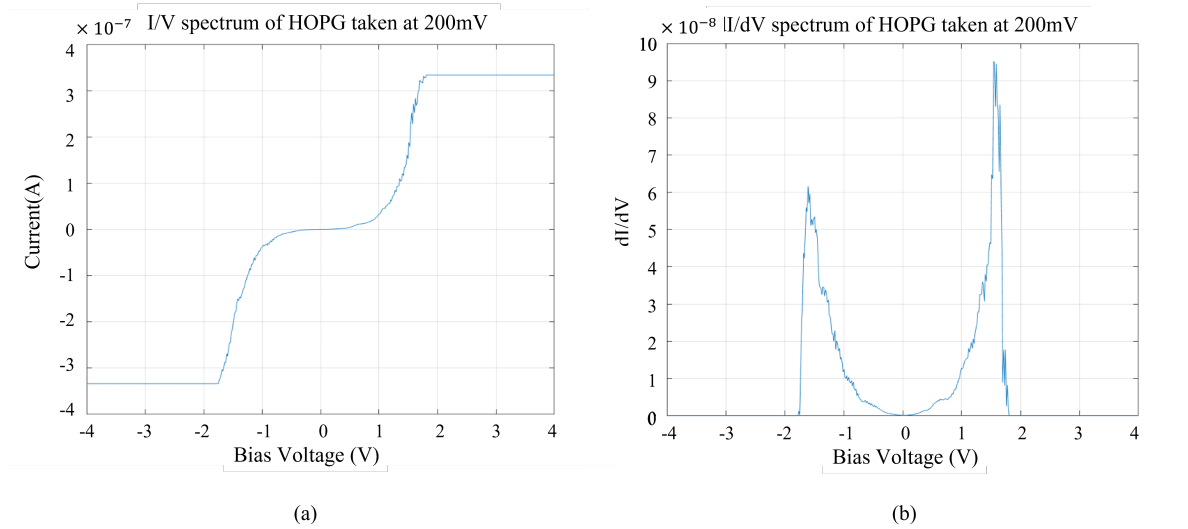


Figure 6.2: a) Graph of the IV sweep performed during the spectroscopy measurement. b) Graph showing $\frac{dI}{dV}$ against V for the same bias sweep as in a). The data for both these graphs was taken on the bare HOPG surface.

The I-V signal (figure 6.2a) saturates at 330 nA, this is due the STM pico-amplifier saturating at this current and is not a feature specific to this particular curve. Some of the graphs presented in the results section of this chapter are divided by I/V to normalise the data and allow for comparison between spectra. Most spectra presented in this chapter are calculated by averaging over multiple scans.

6.2 Results and Discussion

6.2.1 Spectroscopy measurements on Au(111)

Before spectroscopy of the C_{60} -Au samples can be examined the background needs to be investigated so any contributions from the substrate to the spectra can be negated. STS

spectra of the Au(111) surface have been studied previously and the spectra achieved by previous groups will be compared to the data extracted from this experiment. Figure 6.3 shows the STS spectrum averaged from 34 spectra taken on the Au(111) surface, the left hand side of the image is the $\frac{dI}{dV}$ spectrum and the right graph is the normalised spectrum ($\frac{dI}{dV}/(\frac{I}{V})$).

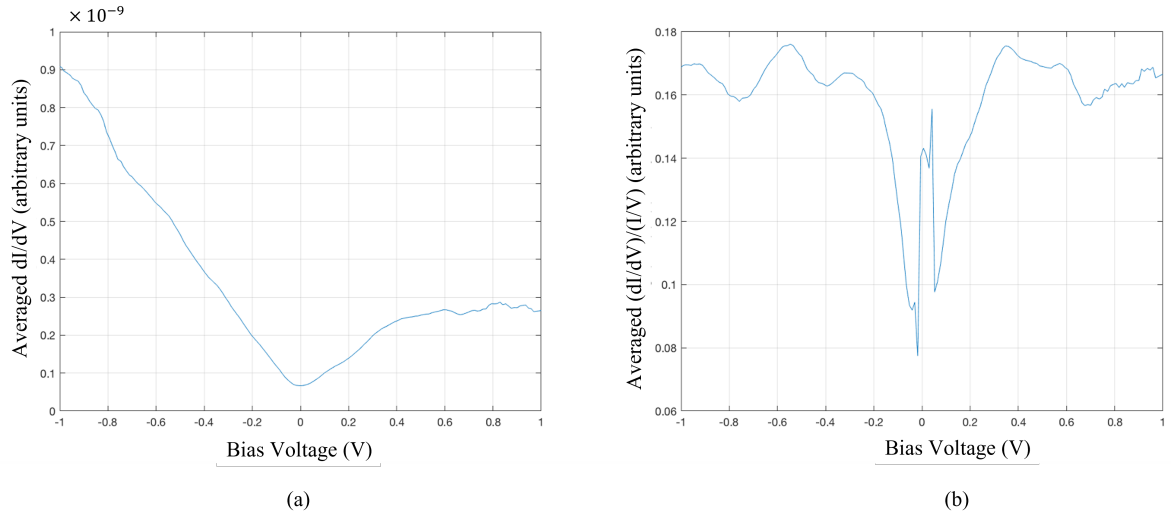


Figure 6.3: a) Graph showing the differential current vs voltage curve averaged from multiple Au(111) spectra. b) Graph showing the normalised differentiated current data for Au(111). The peaks observed on this graph are located at -0.53 V, -0.33 V, $+0.34$ V and 0.58 V. The spectrum was taken at 200 mV set-point voltage and 0.2 nA.

As can be seen from the $\frac{dI}{dV}$ (6.3a) spectra the conductance near zero volts is the lowest point on the graph which results in the large observed spike around zero volts when it is normalised (6.3b). While the conductivity does decrease as the voltage approaches zero the conductance ($\frac{dI}{dV}$) is never zero which would be the case if the sample was a semiconductor (the band gap of the material). The typical profile for metal STS spectra have small variations in conductivity, when compared to either semi metals or

semiconductors, with a slight dip around the fermi level (0 V) ^[120], this can be seen in figure 6.4.

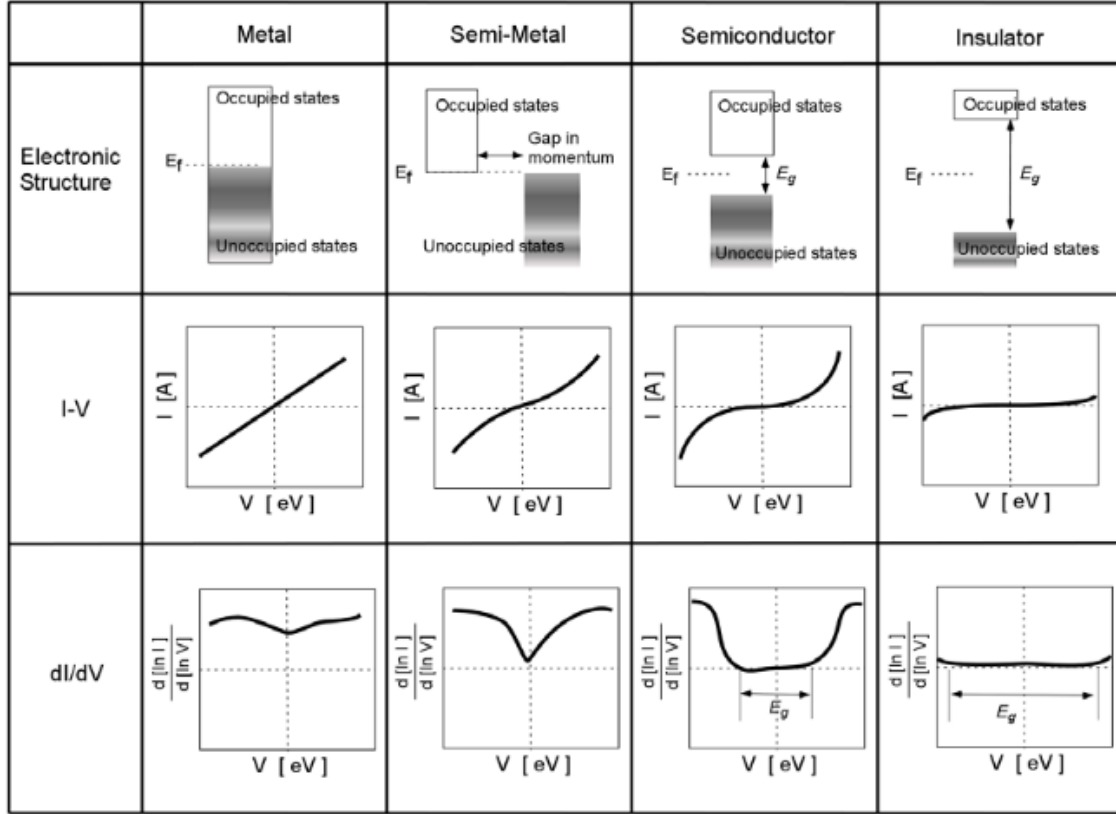


Figure 6.4: Figure showing the electronic structure, typical I-V and $\frac{dI}{dV}$ curves for metals, semi-metals, semiconductors and insulators. Image sourced from ^[120].

Au(111) has delocalised electrons on the surface that form a “free-like” electron surface state which is an example of a Shockley surface state, they can also be found on other metals such as copper and silver. The surface state peak for gold is located between -0.5 V and 0 V on the STS spectrum. For previous measurements in ultra high vacuum (UHV) it is observed closer to -0.5 eV below the fermi level (0 V) ^[121] whereas in air or liquid the energy is shifted higher towards zero (-0.43 eV in liquid ^[122] and -0.35 eV ^[123] and -0.2 eV^[124] in air). The only expected peak in the -1 to $+1$ range shown in figure

6.3 is the surface state peak at ≈ -0.5 eV, any other peaks are most likely due to the tip states or convolution of the tip and sample LDOS. The peaks observed on the positive side of the spectrum are most likely due to the tip DOS influencing the measurement, similar to the studies by Passoni et al.^[125], where a peak at 0.6 V was found to be a result of the tip states as opposed to the surface LDOS. Schouteden et al.^[126], found that a peak at -650 meV was also due to tip DOS as it was not present when different tips were used to perform spectroscopy on the same sample. The shape of the curve in figure 6.3a does not have good contrast between any potential peaks and the background signal. The contrast is improved when the STS spectrum is normalised in figure 6.3b and the peaks' positions can be more easily identified. Enhanced conductivity is observed at -0.53 V and -0.33 V, the peak at -0.53 V is most likely due to the surface state. There are other peaks on the positive side of the spectrum which are at similar positions of $+0.34$ V and $+0.58$ V which are most likely due to the tip density of states. The -0.33 V peak could also be due to tip states, however, a previous study by Reinert et al. found that a peak at -300 mV is also related to the Shockley state^[96]. Conversely, this peak could be due to defects or features of the Au(111) surface such as step edges or point defects. The spectra of varying lattice positions on the surface due to its reconstruction (face centered cubic (FCC), hexagonal close packed (HCP), discommensuration line (DL)) and the step edges will be examined in the next section.

Spectroscopy of Au(111) surface sites

The spectra on different lattice sites: the FCC sites; HCP sites; and DL lattice positions were treated separately and spectra were taken at each position. The DL's are the small ridges formed by the contraction of the surface, the FCC region is found between sets of DL's and the HCP region is found in the region between a pair of DL's. Further detail on these lattice positions can be found within the literature review chapter in section 2.2. Figure 6.5 shows the spectra produced at FCC sites, figure 6.6 shows the HCP spectra, the DL spectra is displayed in figure 6.7 and a normalised comparison of these graphs can be found in figure 6.8.

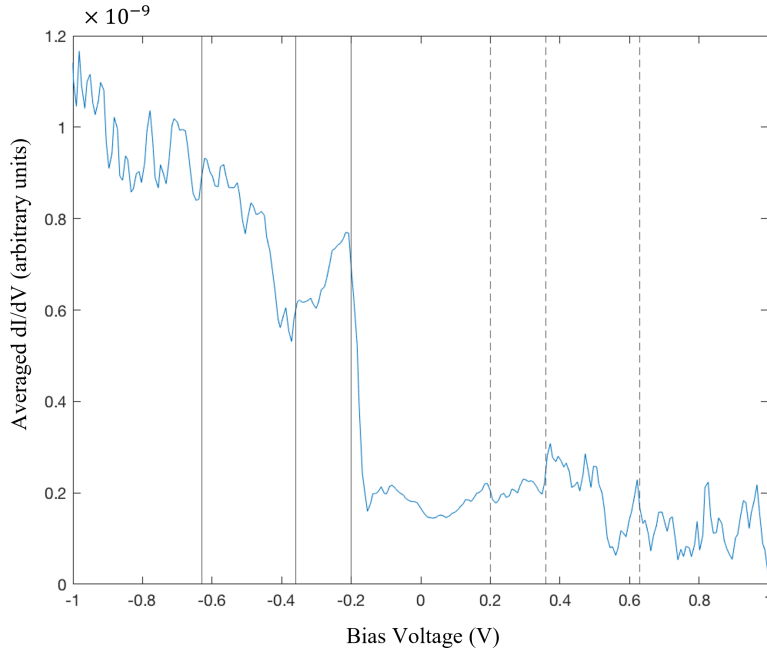


Figure 6.5: Graph showing the STS spectra averaged over 15 FCC positions on the Au(111) surface. The spectra were taken at 500 mV and 1 nA set-point. The surface state peaks on this graph are at approximately -0.36 V and -0.2 V. The vertical lines on the graph help to highlight peaks that are at similar voltages to experiments found in the literature and to guide the eye.

The positions of the peaks shown on this curve are at -0.2 V , -0.36 V , -0.63 V they are also reflected in the positive voltages with much smaller intensities. The peak at -0.63 V is most likely due to the tip density of states (DOS) and the small peaks in the positive voltage range of the graph could be due to a convolution of the sample and tip DOS.

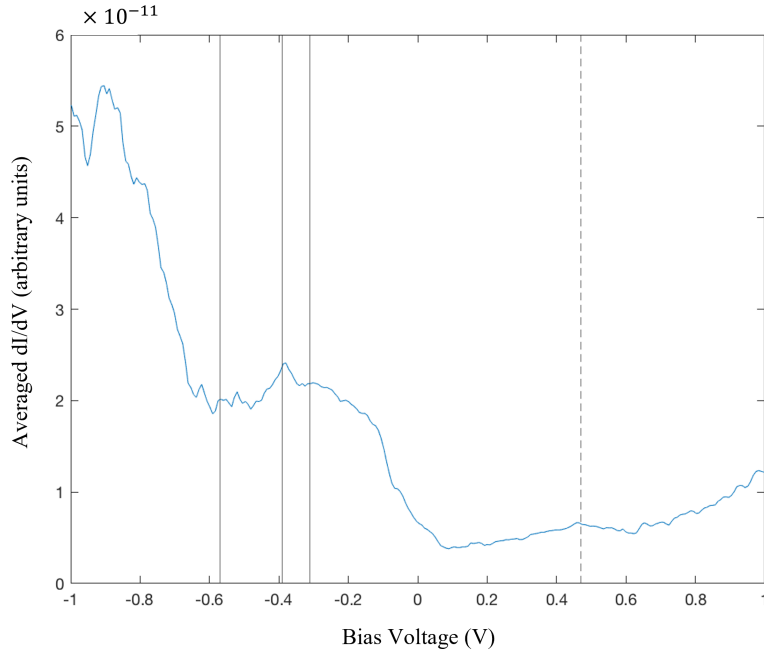


Figure 6.6: Graph showing STS data averaged from 26 HCP sites taken at 500 mV and 1 nA set-point. Main peaks observed in this spectrum are observed at -0.31 V and -0.39 V . The vertical lines on this graph are used as a guide to show the shape of the curve at certain voltages that have been previously associated to peaks or troughs in conductance

The positions of the peaks in this spectra are found at -0.31 V , -0.39 V , -0.57 V , -0.87 V , 0.47 V , 0.8 V . The peak at -0.39 V is most likely due to the surface state on the gold surface with the peak at 0.47 V due to the tip DOS.

The graph in figure 6.7 shows the spectra obtained when performing spectroscopy above

the surface of the reconstruction lines (DL's). The peaks found in this graph are located at -0.16 V, -0.31 V, -0.59 V, -0.74 V and -0.86 V, none of these peak positions correspond directly to peaks on the positive side of the graphs where the peaks are located at 0.37 V, 0.61 V, 0.48 V, 0.8 V and 0.71 V. The peaks found at positive voltages are relatively evenly spaced and look like oscillations, similar to the results found near step edges or in quantum corrals ^[91]. These peaks could be the result of the tip density of states or perhaps an unstable tip influencing the oscillations of the tip DOS. The peak at -0.31 V is most likely to be the Shockley state surface peak, it is shifted from the 0.5 V that was previously observed in the FCC spectra but similar to the value seen in the HCP graph.

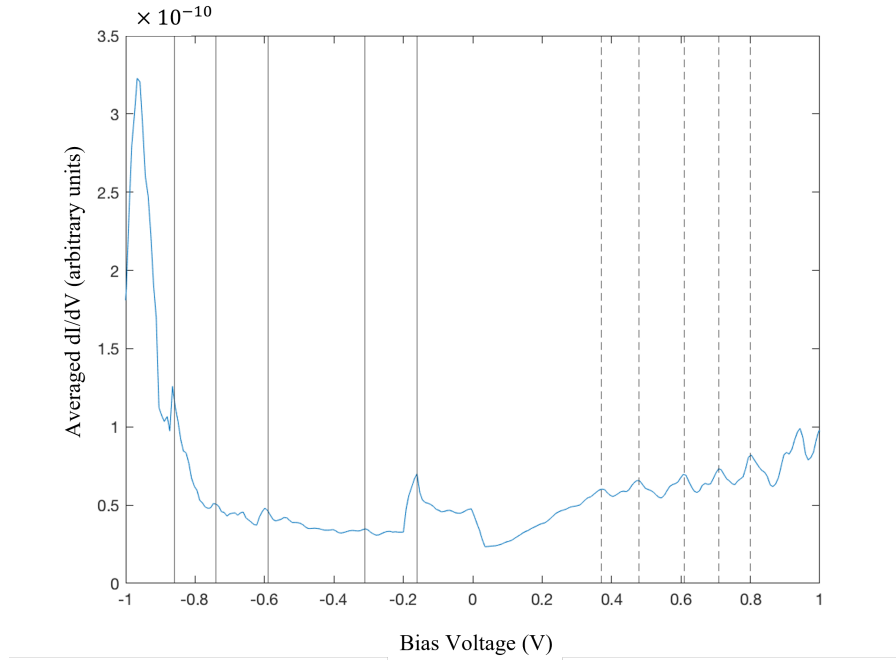


Figure 6.7: Graph showing the averaged STS data from DL sites averaged over 22 spectra, taken at 500 mV 1 nA . Peaks of this spectra are highlighted with vertical lines on the graph indicating their position. The -0.31 V peak is due to the surface state of the gold.

The comparison of these spectra can be obtained when the spectra are normalised, as shown in figure 6.8. The spectra are offset from each other to improve readability and so that the bias voltage that the peaks occur at can be easily compared.

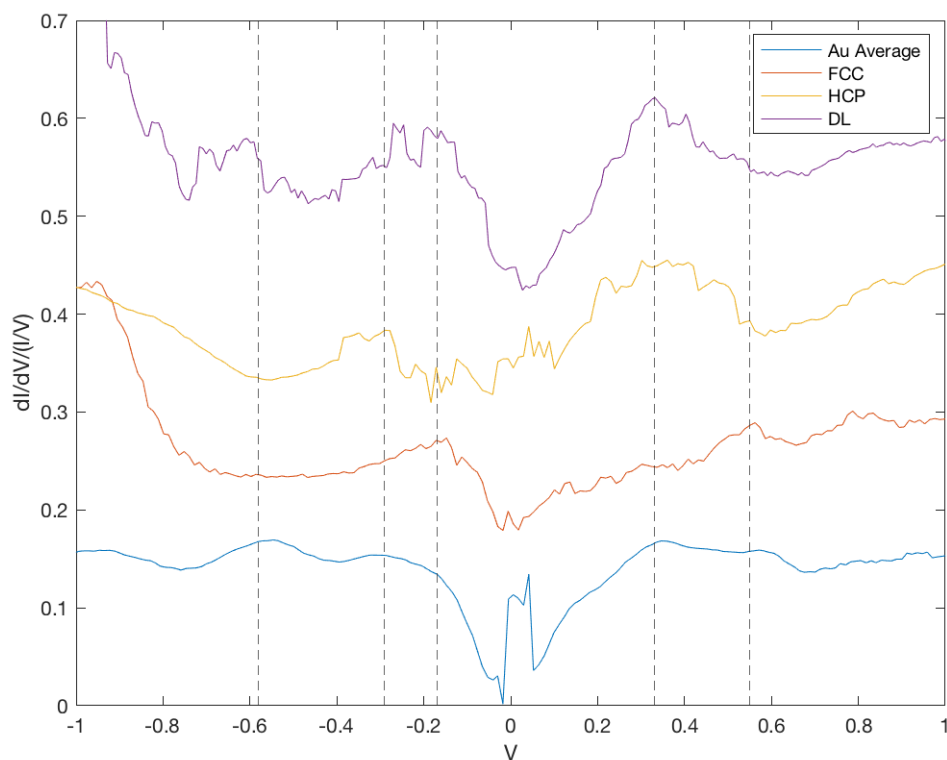


Figure 6.8: Graph showing the comparison between FCC HCP DL and an averaged spectra over various positions of Au(111) surface. Peaks highlighted are at -0.6 V, -0.3 V, -0.2 V, 0.34 V and 0.57 V

When comparing the spectra averaged from the multiple positions on the Au(111) surface (blue curve) with the HCP(yellow), FCC(red) and DL (purple) lattice sites spectra, the components of the individual sites' curves can also be seen in the averaged spectra. The Au(111) averaged spectrum would be expected to show all the components of the other site positions if those individual results were averaged to create the Au

curve, however, the Au(111) curve presented here is the average of spectra taken on a different day and not a composite of the lattice site positions shown here.

As can be seen in the $\frac{dI}{dV}$ spectra (figure 6.5) and the normalised curve (figure 6.8), the FCC and the HCP spectra show surface state peaks at differing voltages. The HCP sites display a peak at -0.35 V whereas the FCC sites do not and instead show a peak around -0.2 V which the HCP curve does not. The HCP peak at -0.3 V could be the same peak as the 0.2 V peak in the FCC spectrum that has shifted to a slightly lower energy, or this could just be due to noise affecting the signal and making the voltage of the peak hard to determine. The DL curve has similarities to both the HCP and FCC curves. Both DL and FCC have peaks at -0.2 V, the HCP and DL have peaks at -0.35 V and 0.3 V respectively. The Au curve shares a peak at -0.6 V with the DL curve along with the previously mentioned -0.2 V and -0.3 V peaks. The averaged Au spectra, DL and the FCC spectra all show a peak at around -0.6 V which is either not present or is shifted in the HCP spectra. This energy below the fermi level is unlikely to be due to the surface state so can therefore be attributed to the tip.

Spectroscopy of Au(111) step edges

The step edges of the Au(111) surface have also been examined in this study. Work by Avouris et al. showed that the spectrum found when scanning the Au(111) terraces differed from the spectrum achieved on atomic steps ^[127], this has also been shown in other studies^[91], ^[122], ^[124]. The gold spectra from figure 6.3 was averaged from multiple

terrace sites on the gold surface. This is compared to the spectra produced at the top and bottom edge of a step in figure 6.9. From this image it can be seen that the top edge curve has a roughly similar shape and intensity to the terrace spectra (average Au). The bottom edge spectra however has a much lower intensity and no obvious peaks when compared to the gold terrace spectra. This is the same phenomenon observed in previous work where the surface state peak is diminished or not present in the vicinity of step edges as the step behaves like a potential barrier^[91]. The two edge spectra also appear to have more oscillations in the curve particularly after -0.5 V, this could be due to the step acting as a potential barrier where the wavefunction of the surface electrons are reflected from the step. Work by Avouris et al. found that at 0K the magnitude of the LDOS oscillations adjacent to a step could be up to 40% of the LDOS measured on a flat terrace surface^[127].

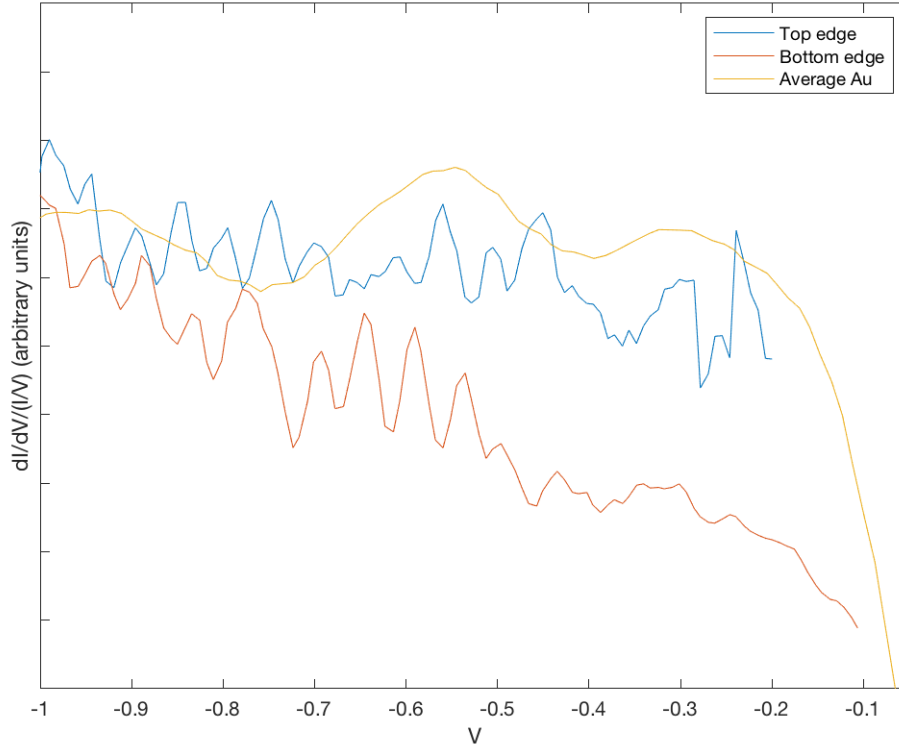


Figure 6.9: Graph showing STS of step edge sites and the averaged Au signal from figure 6.3 taken at multiple points on a terrace. The terrace spectra taken at 500 mV 1 nA averaged over 34 spectra, and the step edge spectra taken at 500 mV 1 nA averaged over 18 spectra (upper edge) and 10 spectra (bottom edge).

The top edge of the step and the lower edge of the step were probed separately to produce the spectra seen in figure 6.10. As discussed in section 2.2.1 the $\{111\}$ micro-faceted Au(111) steps are more abundant on the surface due to the FCC structure of these steps. Following that, it is logical to assume the step STS profiles should hold similarity to the FCC spectra since they have the same packing structure. However, it has previously been found that the step spectra have lower intensity peaks than terrace spectra as the steps act as a potential barrier for the surface electrons^[46] (figure 6.9).

The spectra from the upper edge of the steps in this experiment appears similar to the shape previously observed in the HCP and FCC regions, whereas the spectra from the lower step edge appears not to have a surface state peak in figure 6.10 or if present the feature is of low contrast to the background data.

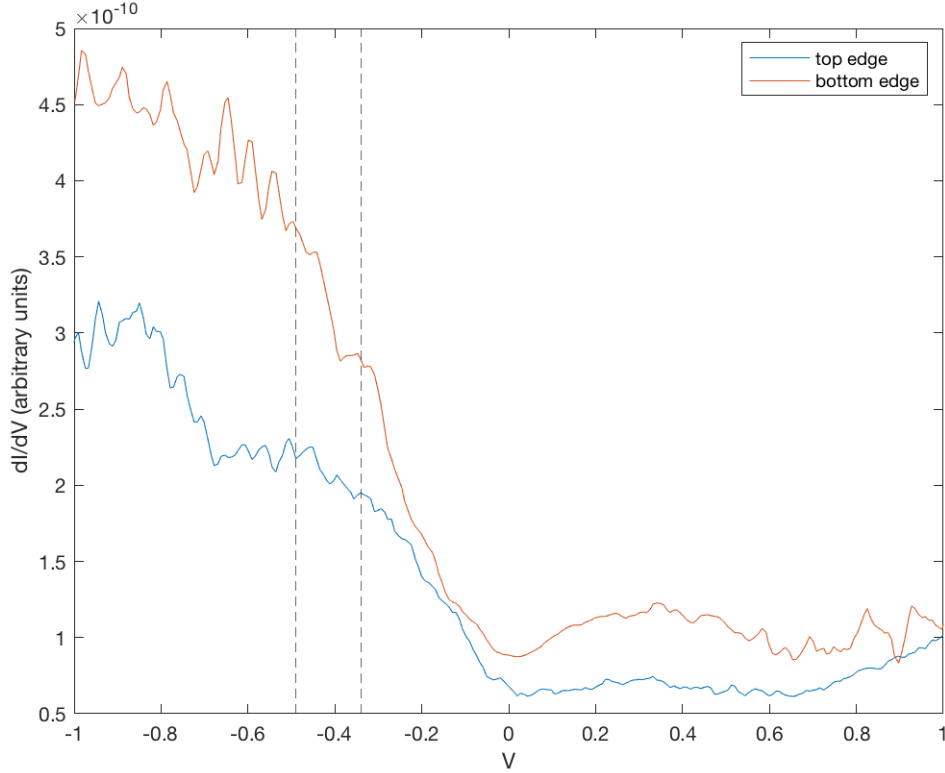


Figure 6.10: STS taken at the top and bottom of a step on the Au(111) surface. Spectra taken at 500 mV and 1 nA averaged from 18 and 10 data sets respectively. The peak positions are at -0.49 V (lower step edge) and -0.34 V (upper edge).

The top edge spectrum show a peak at -0.49 V and the highest contrasting peak in the bottom edge spectrum was at -0.34 V. The background signal makes determining the peaks more challenging, the spectra are normalised so that any peaks are clearer (shown in figure 6.11).

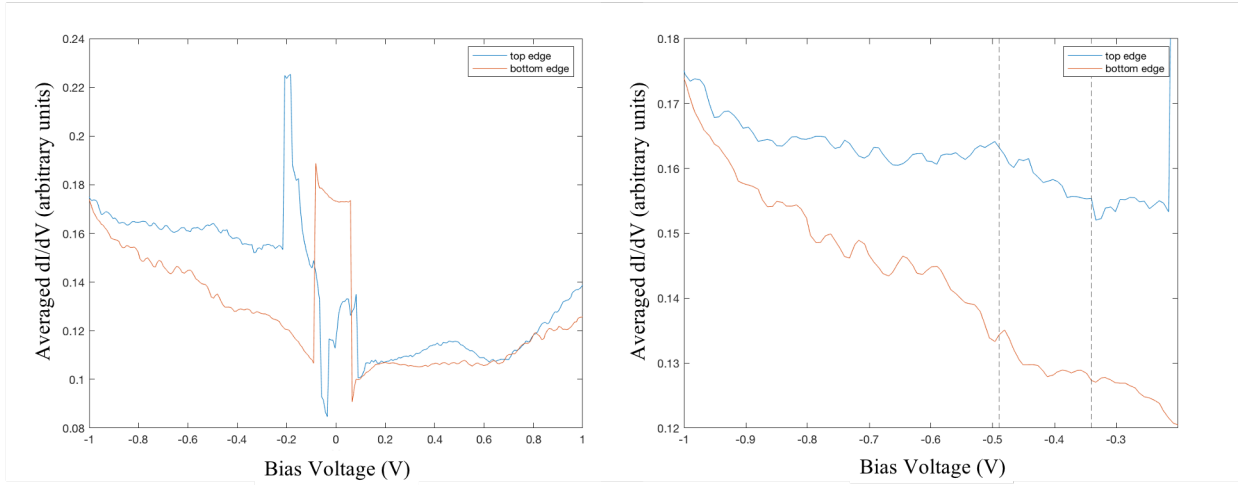


Figure 6.11: a) Graph of normalised edge spectra from -1 V to 1 V. b) Enlarged portion of (a) from -1 V to -0.2 V with peaks highlighted at -0.49 V and -0.34 V. Upper step edge spectra averaged over 18 curves, taken at 500 mV 1 nA. Lower edge spectra averaged over 10 curves, taken at 500 mV 1 nA.

The edge STS spectra are shown in figure 6.10 unnormalised and again in figure 6.11a where the spectra are normalised. The vertical lines on figure 6.10b show the positions of the peak and trough on the top edge curve (blue). The normalised spectrum has a large abnormality around zero volts which overshadows the other data so the negative bias response is presented in figure 6.11b for clarity. When comparing the upper and lower edge of the step it can be seen that the peaks observed in figure 6.10 are more prominent in figure 6.11b. The peak position of the lower step edge is similar to that of the surface state peak observed at the HCP sites. The upper step edge has a peak at -0.5 V which agrees with previous studies but not with the previously measured spectra for FCC surface sites which it should also correspond to. It could be argued that there is also a peak around -0.25 V for the upper step curve and that corresponds well to the peak observed at -0.2 V in the FCC spectra. The purpose of this study was

to develop a comprehensive understanding of the Au(111) spectra for later comparison to spectra from C₆₀-Au samples.

6.2.2 HOPG

Similarly to Au(111), HOPG was studied so that any electronic effects of the graphite when performing spectroscopy of other adlayers on a HOPG substrate can be subtracted from the signal. An averaged spectra of HOPG can be seen in figure 6.12. This spectrum aligns with spectra previously observed ^{[101][128][129]} where around zero the graph forms a v like shape. Graphite has a characteristic STS profile of a semi metal; where the the density of states decreases near the fermi level but does not reach zero. The dip in LDOS is more pronounced than the spectra produced from a metal substrate but less than for a semiconductor where a band gap can be seen ^[120](illustrated in figure 6.4). Similarly to other results on HOPG the increase in LDOS on one side of the spectra in figure 6.12 is sharper than the other. For graphene the spectrum is more symmetrical where both sides of the v shape curve have a similar gradient ^[128].

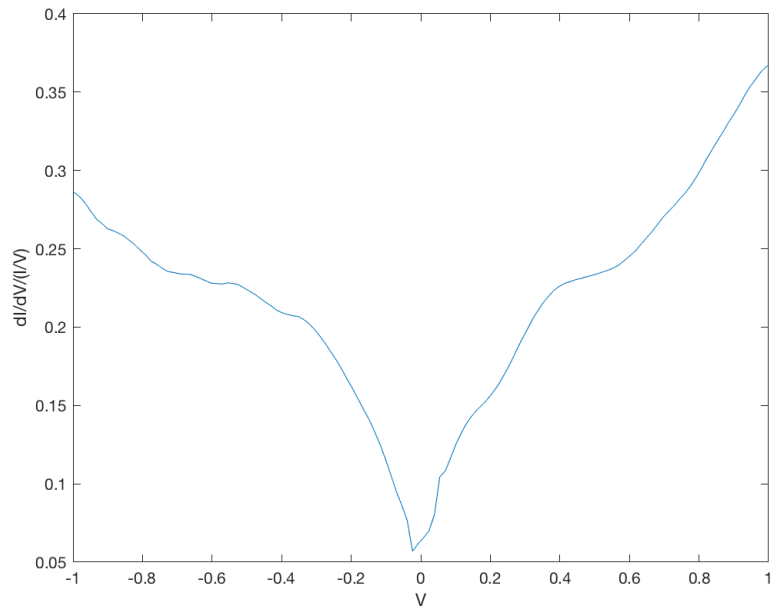


Figure 6.12: STS profile from the HOPG surface averaged over 34 spectra and taken at 100 mV and 1 nA set-point.

STS spectra were produced on HOPG at a variety of voltages, these curves can be seen in figure 6.13.

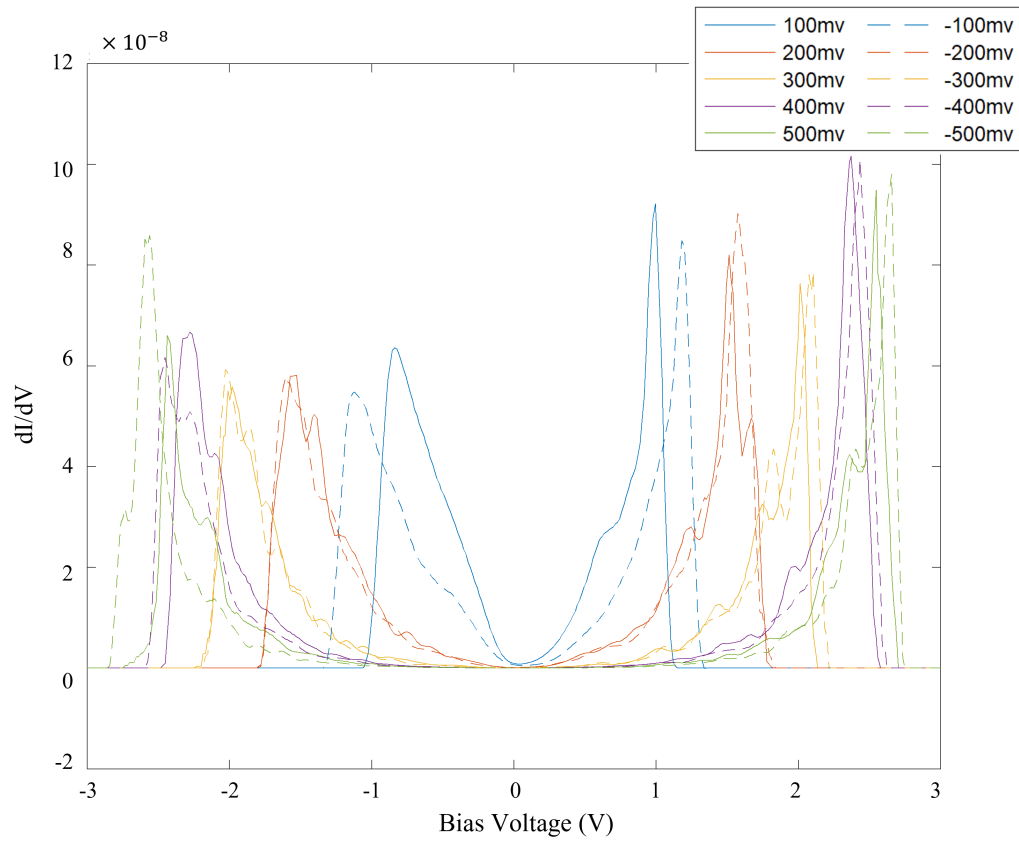


Figure 6.13: Graph showing STS curves on HOPG at different set-point voltages. The positive and negative biases are shown in the same colour with the positive bias as a solid line and the negative bias presented as a dashed line.

The set-point voltage that the spectrum is performed at corresponds to the fixed height of the tip while completing the voltage sweep. The higher the voltage the greater the distance from the STM tip to the surface. spectra were taken at 100 mV increments from 100 mV to 1 V set-point, figure 6.13 shows the results for 100-500 mV (600 mV-1 V spectra are not included on this graph to improve readability). Similar experiments have been performed before ^{[100][130]} where instead of the bias set-point used to denote the height of the STM tip the set-point current is used instead. The set-point current is

highest when the tip is closest to the sample so high current corresponds to the lowest voltages seen in the data presented from these experiments.

In figure 6.13, as the set-point voltage is increased (tip to sample distance increased) the distance between the left hand peaks (negative applied bias) and the right hand peaks (positive applied bias) for each voltage increases. The section of the graph where the $\frac{dI}{dV}$ value is ≈ 0 (similar to a band gap) increases in size with the increasing magnitude of the set-point voltage. This corresponds to data observed by Söde et al. ^[130] who found that increasing the current set-point that the spectrum was taken at on graphene nanoribbons, led to a shift of the peaks when compared to spectra taken at a higher set-point current.

The effects observed in the work by Kusunoki et al. ^[100] where the increasing voltage led to deformation of HOPG (discussed in section 2.6.3) were not seen in this investigation of voltage effects. It can be assumed that during these spectroscopy measurements the tip did not induce any deformation of the HOPG surface layer. Since all curves presented in this section do not follow a perfect v shaped curve it is clear they are not from graphene layers that have detached from the surface of HOPG but rather STS profiles of the HOPG surface.

It can be seen that the positive bias set-point voltages produce similar data to the negative bias voltage set-points, as all curves of the same colour are clustered in their pairs on the graph. The ± 100 mV spectra are not quite aligned with each other and are shown in more detail in figure 6.14a.

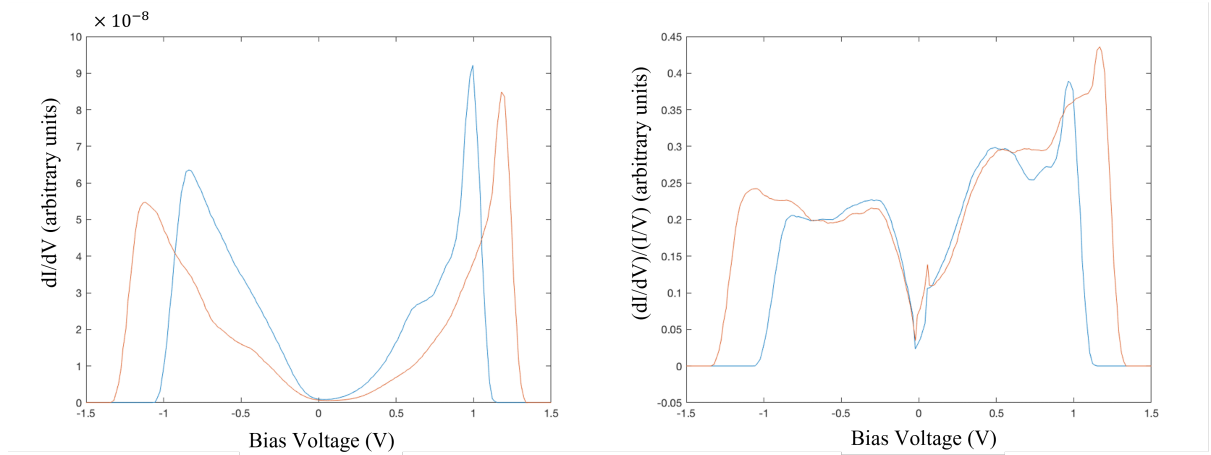


Figure 6.14: Graphs showing the unnormalised (left) and normalised (right) STS spectra taken at positive and negative 100 mV set-point voltages and 1 nA . The blue line represents +100 mV and the red line represents -100 mV.

In figure 6.14 it can be seen that the curve taken at the negative bias and the curve taken at the positive bias appear to be mirror images of each other. This is easiest to observe in figure 6.14a by observing the slight dip in the curve at around 0.6 V on the blue curve and -0.6 V on the orange. This is due to the direction the current flows between the tip and the sample; when a positive voltage is applied the current flows from the sample to the tip and when a negative bias is applied the current flows in the other direction from tip to sample. Therefore, at the same voltage set-point but different polarities the data is either representing electrons tunneling into the tip from the sample or from the tip to the sample. This phenomenon is also observed in other studies such as work done by Zhang et al. ^[68] where the spectra are taken on graphene on SiO₂ at various voltages. When the bias voltage is negative the peaks appear on the opposite half of the graph to when the bias voltage is positive.

The results presented above are from single spectra, multiple measurements were taken at 100, 200 and 300 mV and averaged for each voltage to give a more comprehensive view of the effects of set-point voltage. These results are illustrated in figure 6.15.

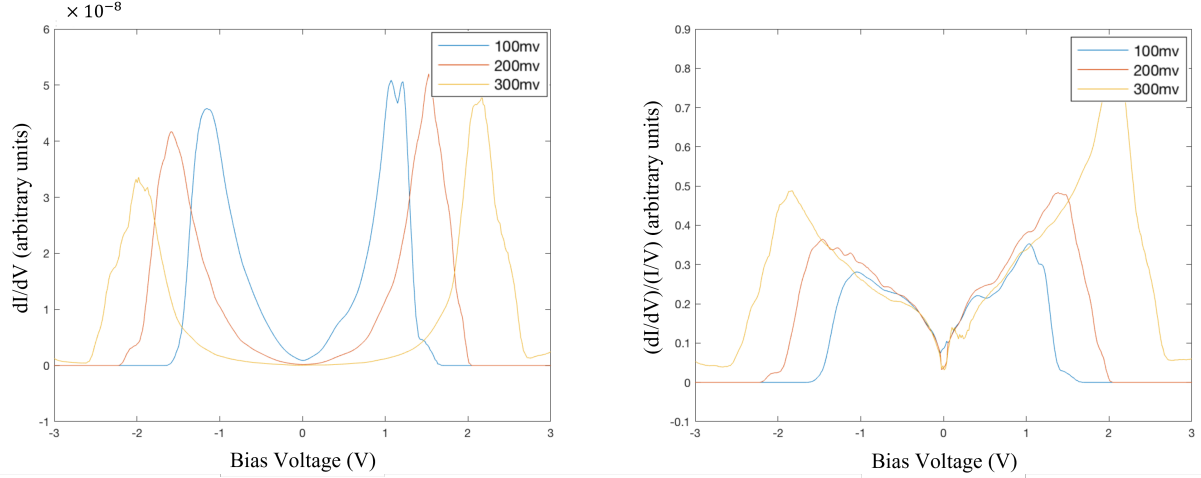


Figure 6.15: Graph showing the curves averaged over multiple spectra taken at 300 mV 200 mV and 100 mV set-point voltages and 1 nA. a) differential current b) normalised differential current.

All spectra taken in this experiment were performed at 77K. Previous research ^[131] has shown that scanning at lower temperatures can increase the detail seen in the spectra. In the study by Yin et al. they looked at 100K, 78K and 7.8K and though in all three spectra the energies of the peaks were identifiable, the spectrum at 7.8K provided the most detail. Using their observations as a basis it can be assumed that the spectra observed in these experiments can be relied upon but may have a larger error than if the spectra were taken at lower temperatures. From this investigation into the bare HOPG substrate it can be assumed the spectra represent the HOPG surface and not any graphene layer that has detached from the surface. Deformation of the surface by

the tip causing the detachment of a graphene sheet was also not observed. It can also be seen that varying the set-point voltage can affect the energy that conductance is enhanced at (shifting of peaks).

Atomic resolution and STS

Scanning the HOPG surface can sometimes result in atomic resolution of the surface layer, figure 6.16 is an example of this type of image. The left hand image shows a triangular lattice the right hand image shows the carbon atoms in a hexagonal lattice, the hexagonal lattice is misshapen due to thermal drift whilst scanning.

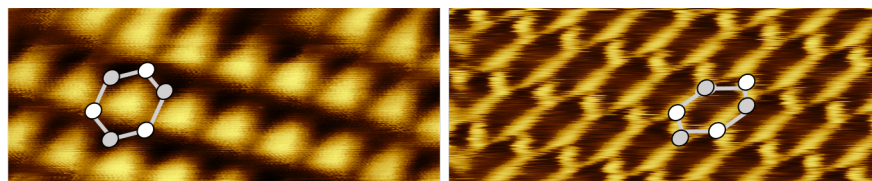


Figure 6.16: Image showing the HOPG surface atoms. The left hand image shows the triangular lattice and the right hand side image shows the hexagonal lattice, over both images a diagram of 6 carbon atoms is superimposed to show the rough positions of the atoms that make up the image.

The triangular lattice that is observed when scanning graphite with the STM can be explained by the structure of graphite. The unit cell for the arrangement of the carbon atoms that make up the graphite surface layer (graphene) is shown in figure 6.17. The unit cell is made up of two different atoms shown in white and black (grey in figure 6.16) which form two different triangular lattices ^[132].

One of the atoms (B in figure 6.17) is positioned directly on top of the atom below it and

the other is positioned in a hollow site (no atom directly below). This causes the white atoms to appear brighter in the STM image due to the higher LDOS contributed to by the atom below. When the bias of the tunnel current is reversed the other triangular lattice (black) can be seen instead ^[133].

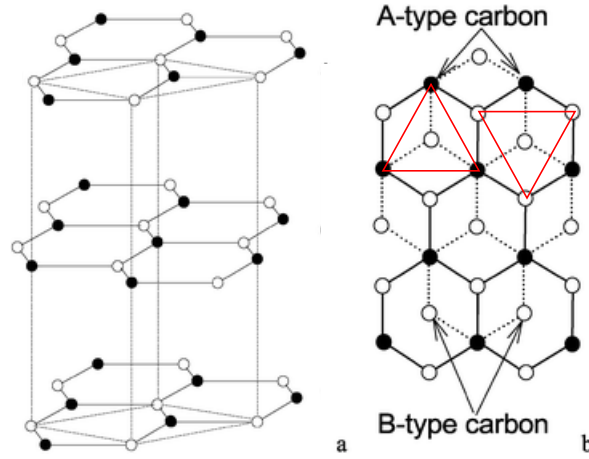


Figure 6.17: Image showing the layers of carbon atoms, their arrangement and the top down view of the surface layer of carbon atoms. The A type atoms are shown as black dots and the B type atoms are shown as white dots. The unit cells for A and B atoms are shown with red triangles. Adapted from [134].

The data in figure 6.18a and fig 6.18b show the differences when spectra are taken above the two different atoms in the unit cell (A or B). it also shows the A and B atoms and at positive and negative applied bias.

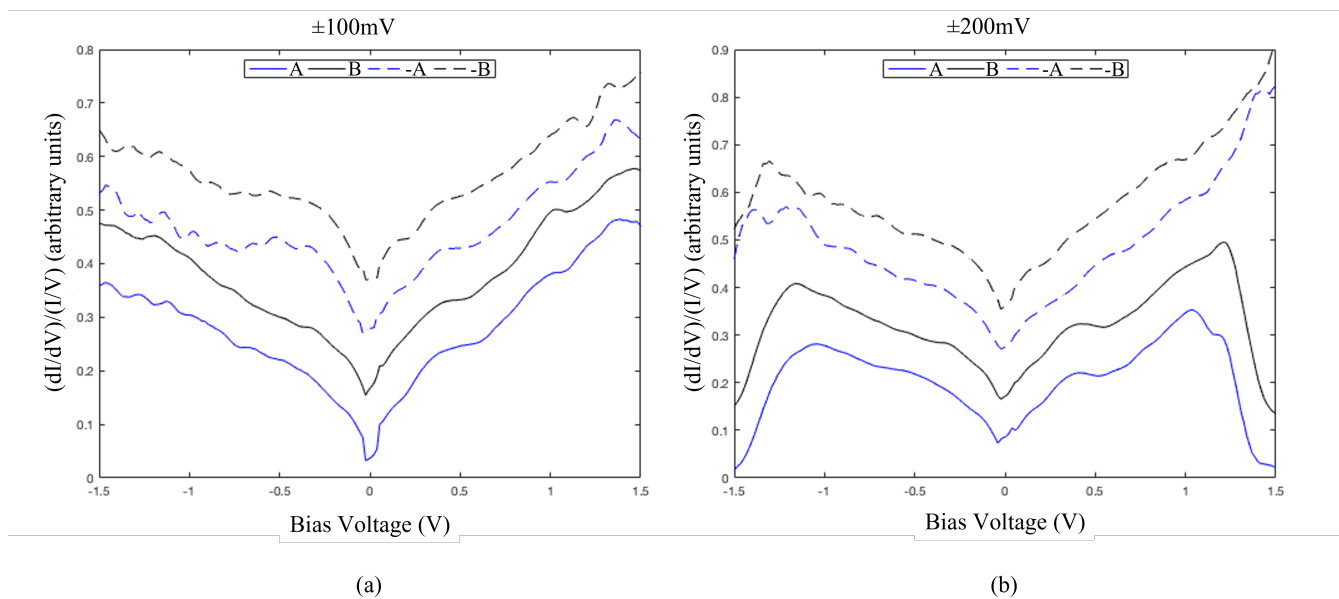


Figure 6.18: a) Graph showing the averaged spectra produced for -100 mV and 100 mV on the two types of triangular lattice. b) Graph showing the averaged spectra produced for -200 mV and 200 mV on the two triangular lattice atoms. Peaks have been shifted vertically for clarity.

Similarly to the previous investigation of applied bias polarity on HOPG spectra, the $+100$ and -100 mV spectra should mirror each other along $x=0$. The solid black and blue curves that represent the A and B lattices at positive bias show a similar shape with a peak deviating from the v shape at around 0.4 V . The blue curve has the shoulder like peak at an energy slightly closer to the fermi level than the black curve. The curves taken at negative bias are shown with a dashed line, these appear to be slightly broader curves than the positive bias spectra. The shoulder is less distinct in the negative bias spectra and appears to be closer to -0.25 V than -0.4 V .

The curves taken at $+or-200\text{ mV}$ are broader than the curves taken at 100 mV , this is due to the height of the tip while performing the spectroscopy, discussed in the

previous section. The positive bias curves show the same behaviour as the positive curves at 100 mV. The shoulder appears at approximately 0.4 V with the blue curve appearing a touch closer to zero volts than the black, a second peak on the positive side of the graph appears at 1 V. Spectra taken with a negative sample bias have a more exaggerated shape at negative voltages, the shoulder peak also appears to be shifted closer to the fermi level than -0.4 V appearing around -2.5 V.

Work by Teobaldi et al. ^[135] investigated the difference in conductance of the two carbon atom types in HOPG. It was found that the atom sitting directly on top of an atom in the layer below (A type) had a higher LDOS than the atom that sits in a hollow site (B type). This was previously known to be the case at lower bias voltages near the fermi level ^[136], Teobaldi et al. showed that at larger bias voltages the effect is still present and the B type atoms have a smaller LDOS when a positive bias is applied. When the polarity is reversed the B type atoms have a higher LDOS than the A type this corresponds with what was observed in STM images where at one polarity one lattice is bright and the other dim, this then switches with the reversed polarity.

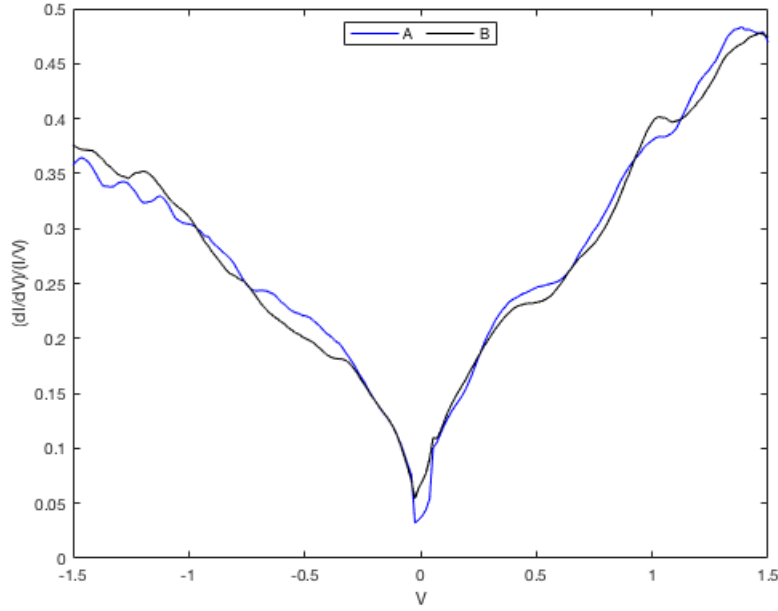


Figure 6.19: Graph showing the spectra of A and B atom types taken at 200 mV 1 nA set-point.

The data in figure 6.18b and figure 6.18a do not correlate with these results, but for both set-point voltages the B atoms have lower conductance at energies close to the fermi level but as the applied voltage increases in magnitude the B atoms have a higher conductance than their counterpart. This is demonstrated more clearly in figure 6.19. At voltages approaching zero (0 to -1 V and 0.1 to 1 V) the blue curve lies above the black curve, this stays constant on the right hand side of the graph except for a couple of crossings of the black and blue curves. At larger negative bias the black curve has a higher conductance than the blue curve. This replicates data taken by Teobaldi et al.^[135] who found that near zero the A type atoms had a stronger $\frac{dI}{dV}$ response and away from zero the B type overtook the A type atoms.

Patil et al. ^[132] examined the conductance of differing points on superlattices on graphite. Superlattices are formed when multiple layers are stacked in various angles so that certain atoms appear brighter due to atoms beneath them. For graphite these superlattices are also referred to as moiré patterns as they behave similarly to the moiré pattern that can be observed in watered silks. It was found that there are electronic differences between bright and dark spots on the superlattices shown in figure 6.20. The single layer superlattices shown in figure 6.20a and b are formed by a single layer of graphene on top of graphite. For the triangular lattice observed in figure 6.20a there is very little difference between the two atomic sites, whereas for the hexagonal lattice in figure 6.20b the electronic difference is much larger.

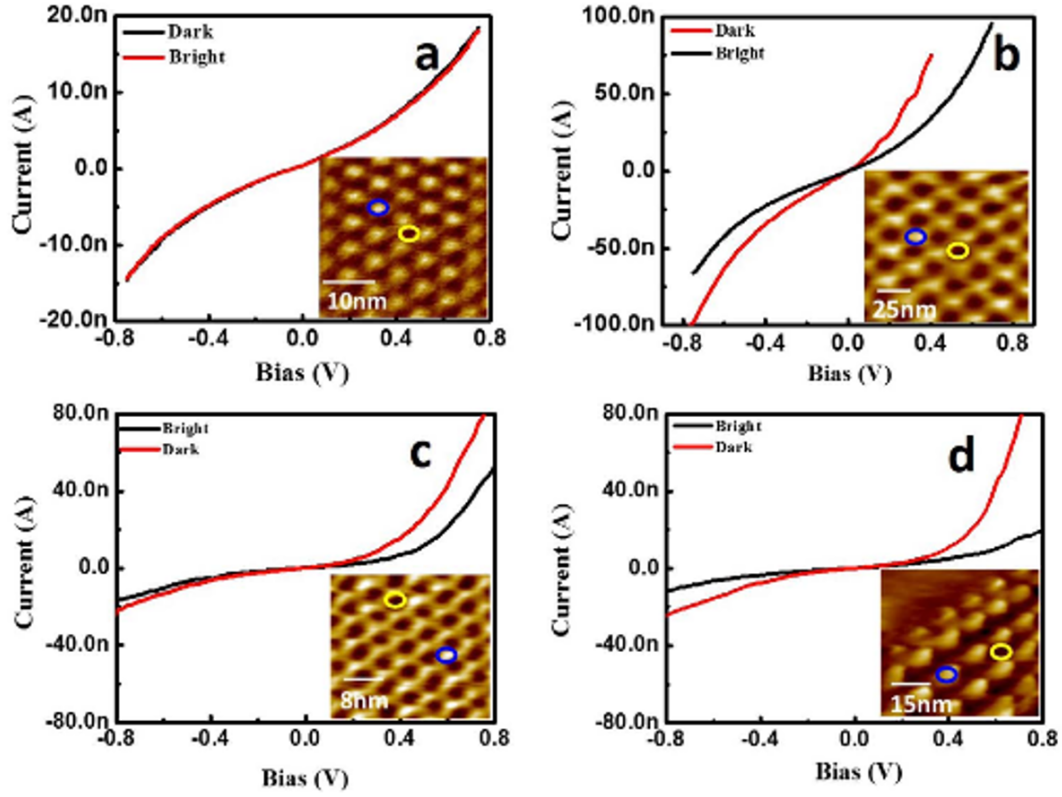


Figure 6.20: Graph showing the I-V response at bright and dim spots on 1 layer (a and b) 2 layer (c) and 3 layer (d) superlattice lattices. The Blue circle shows the position where the red curve was taken and the yellow circle shows the position of where the black curve was measured. Image sourced from [132].

Andrei et al. ^[128] compare the conductance of graphite with triangular and hexagonal lattices observed by STM, where the hexagonal lattice has a v shaped $\frac{dI}{dV}$ curve and the triangular lattice has a slightly distorted shape. In this case the shape of the $\frac{dI}{dV}$ spectra can be used to identify if the graphite is similar to bulk graphite (like the spectrum observed for the triangular lattice) or whether it is more likely to be due to a graphene sheet that has detached from the surface. In the case of a detached sheet of graphene the spectra would appear almost perfectly v shaped.

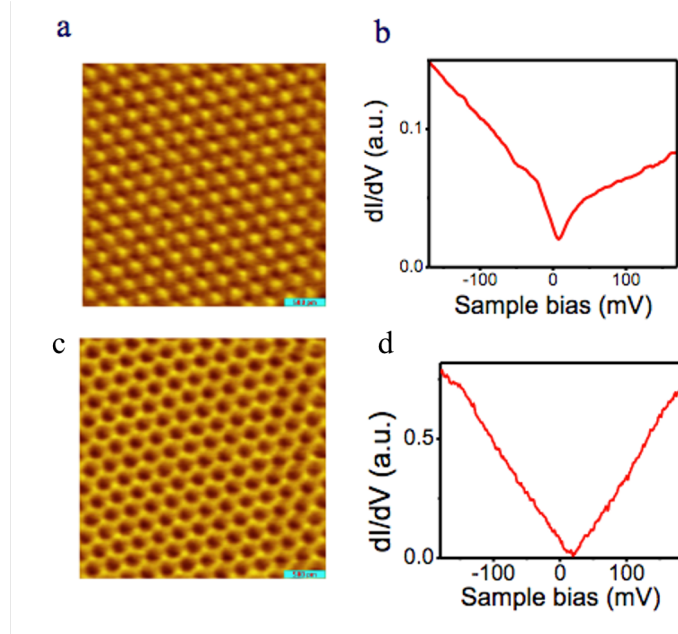


Figure 6.21: Images of triangular lattice and hexagonal lattice observed via STM imaging and the corresponding $\frac{dI}{dV}$ spectra for each lattice. a) triangular lattice b) spectra from the triangular lattice area c) hexagonal lattice d) spectra from the hexagonal lattice.

When comparing the differences observed in conductance in the two different atomic positions from this experiment and previous research, it can be seen that the spectra achieved do represent differing lattice sites. The STS data for the A type atoms (atop site) shows a larger conductance response than the B type atom (hollow site) at energies close to the fermi level; as energy increases this switches so that the B type atom has a larger conductance measured. This information can be taken into account when depositing monolayers on top of the graphite sample, as the lattice site has an effect on the conductance measured so could potentially affect results. None of the spectra taken in this experiment showed detached graphene layers, as all the spectra deviated from the perfect v shaped curve expected for graphene.

6.2.3 C₆₀ on Au(111)

Once the spectra for base samples of highly oriented pyrolytic graphite (HOPG) and Au(111) were obtained, the spectroscopy for C₆₀ on Au and C₆₀ on HOPG could be analysed. For Au(111) substrate if a peak is present between -0.5 V and 0 V this could be due to the gold surface state peak. On HOPG any deviation from the v shaped curve expected from graphite would be due to the adsorbate on the substrate.

Figure 6.22 and 6.23 show the two investigations of C₆₀ molecules on Au(111). As can be seen from the figures the response is not consistent across the two investigations. However, Pascual et al. ^[137] performed spectroscopy on a C₆₀ monolayer on Ag(110) and found that the LDOS is not consistent across the sample. The position of the C₆₀ molecules, both in terms of gold lattice site they are sitting on and the orientation of the C₆₀ molecule, has previously been shown to affect the spectra produced by STS^{[138][139][140][141]}. Both spectra in 6.22 and 6.23 are analysed below and compared to previous research.

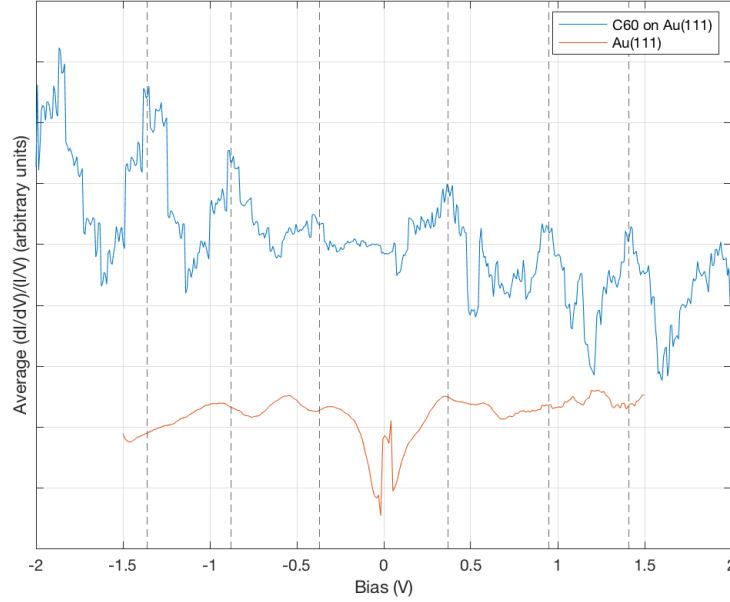


Figure 6.22: Figure showing graphs of the STS spectra from C_{60} molecules adsorbed on the Au(111) substrate, averaged from 9 spectra taken at 700 mV 0.2 nA set-point.

The peaks in figure 6.22 are highlighted with a dashed line and are located at -1.36 V, -0.88 V, -0.37 V, 0.37 V, 0.95 V, 1.41 V. The spectrum for Au(111) is displayed below the C_{60} spectrum for comparison; the only peak position that aligns is at 0.4 V therefore this peak on the spectrum could be due to the Au(111) surface state. Previous studies of C_{60} on Cu(100)^[138] and Cu(111)^{[140][142]} have observed peaks closest to the fermi level (lowest unoccupied molecular orbital (LUMO)) at 0.4 V for Cu(100) and 0.7 V or 0.8 V for Cu(111). Other peaks have been found at 1.5 V, 2.1 V and 1.8 V but these peaks have been found to depend on the orientation of the molecule, for example the peak at 1.5 V was only observable directly above the centre of the C_{60} molecule but was not present if the STS was taken off-centre. Similar studies on Au(111) have LUMO peaks

at 0.7 V^{[141][24]}, 0.6 V^[139], and 0.84 V^[24]. Further peaks were observed at 2 V, 1.1 V and in all studies a peak around -1.7 V was observed. This peak is due to the band structure of the C_{60} molecule and this -1.7 V peak represents the highest occupied molecular orbital (HOMO). The gap between the HOMO and LUMO states in previous studies of C_{60} on Au(111) was observed to be ≈ 2.3 -2.8 V. Comparing this data to the graph in figure 6.22 there is a peak at around -1.8 V which could correspond to the HOMO peak for C_{60} , there is however not a substantial peak observed around 0.7 V. The peaks in this graph are spaced quite evenly which leads to the conclusion that these peaks are not due to the sample LDOS but instead from electronic oscillations due to an unstable tip or contributions from the tip DOS.

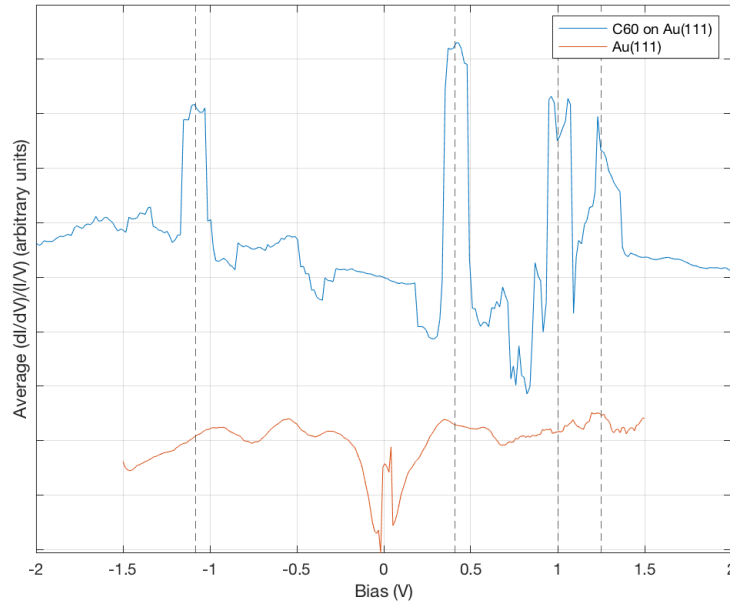


Figure 6.23: Figure showing a graph of the STS spectra from C_{60} molecules adsorbed on the Au111 substrate. The data was averaged from 3 data sets taken at 1.5 V 0.2 nA set-point.

The results displayed in figure 6.23 are less evenly spaced so are less likely to be due to electronic noise. Peaks on this graph are observed at -1.08 V, 0.41 V, 1 V and 1.25 V. Comparing the C_{60} on Au(111) curve to the averaged gold curve below it can be seen that the peaks at 0.4 V, 1.25 V and -1.1 V align relatively well with the Au(111) curve. A peak is not observed at -1.7 V in this spectra. However, this spectrum was taken above a large island of C_{60} molecules, this has previously been found to shift the energy of this peak away from the fermi level when compared to single C_{60} molecules' spectra. It is unlikely that this spectrum is a result of probing the C_{60} molecules' LDOS as the peak energies are not observed at similar energies to previous work. If the spectrum did represent the C_{60} LDOS, the 0.4 V peak could be due to the Au(111) surface state and the LUMO peak would be the amplified conductance at 1 V. The HOMO would be at -1.1 V, this would lead to a LUMO-HOMO gap of 2.1 V which is slightly smaller than that observed previously.

Unfortunately the STS of isolated magic number clusters was not taken during this experiment. When the STS experiments were taking place the magic clusters could not be located on the sample. The orientation of the individual C_{60} molecules was unable to be studied in detail by STS, so the spectra above represent the C_{60} monolayer as opposed to specific sites on the C_{60} molecules.

6.3 Summary

The STS experiments detailed in this chapter will be summarised here; conclusions for the whole thesis can be found in chapter 7. The STS measurements of the Au(111) surface illustrated the difference in spectra produced from measuring different lattice sites on the sample. The difference between FCC, HCP and DL spectra was subtle but the difference between the top edge of the step (which behaved in a similar way to the terrace sites) and the lower edge of the step was much larger. The results from the Au(111) experiment correlate to the previous work done on Au(111) and provided a good basis for examining C₆₀ monolayers on the Au(111) substrate. Although the C₆₀ on graphite sample was not studied by STS, the investigation of bare HOPG provided a good insight into the electronic structure of the substrate. The HOPG experiment demonstrated some operating principles of STS: set point voltage and its relationship with the spectra produced was investigated along with the polarity of the bias voltage applied. It was found that as the set-point voltage is increased the conductance peaks become broader and the energy that the peaks occur at shifts away from the fermi level. STS measurements were performed while the STM had atomic resolution and the two types of graphite unit cell were examined and compared. It was found that the A and B type carbon atoms produced slightly differing STS curves, the comparison of this experimental data to theoretical studies shows a strong correlation between the measurements from this experiment and previous density functional theory (DFT) calculations. Finally, the C₆₀ Au(111) sample measurements were discussed and

while the data collected does not perfectly match up with previous studies, the results could represent peaks that occur at shifted energies due to the C_{60} molecules that were studied being a component of a monolayer not a cluster or individual molecules.

Chapter 7

Conclusion

Within this thesis the experiments of C_{60} on Au(111) and HOPG using STM and STS were discussed. This work follows on from previous studies where magic number clusters were produced on reconstructed Au(111) surfaces and within a C_{60} matrix on HOPG surfaces. The STM investigations examined the orientation of the C_{60} molecules on both substrates and detailed the characteristics of the bright and dim molecules within the monolayers deposited. STS investigations were undertaken for the bare Au(111) and HOPG surfaces and some investigation of the C_{60} monolayers on Au(111) was also undertaken. The STS experiments on HOPG highlighted the impact of the set point voltage and the polarity of the bias applied on the STS spectra. The STS spectra showed differences when taken at two different points on the unit cell for HOPG and at different locations on the reconstruction for Au(111). The spectroscopy data collected for both gold and HOPG correlated with previous studies and provided a good background

spectra for comparing the Au/C₆₀ spectra to.

7.1 STM investigation of C₆₀ on Au(111)

The study of samples with C₆₀ deposited onto Au(111) confirmed and built upon previous work. The C₆₀ molecules formed islands nucleated from steps on the Au(111) surface. At sub-monolayer coverage the C₆₀ formed islands in some areas and in other areas only the face centered cubic (FCC) packed areas of steps were decorated with fullerenes. Within the islands, bright and dim molecules were observed at varying heights compared to the monolayer surface.

The dim molecules' heights were found to have a large distribution of depths from 0.02 nm to 0.1 nm. The deeper molecules are thought to be due to the fullerene in question sitting within vacancies in the gold surface layer directly below the C₆₀ island. The smaller differences in height between the average of the monolayer and the dim molecules is thought to be due to the orientation of the C₆₀ molecule and variations in the electron density of the sample. The most commonly observed height difference between dim molecules and bright molecules was found to be 0.03 nm and 0.07 nm. The 0.07 nm height corresponds to previously measured differences in height for C₆₀ molecules on surfaces due to differences in orientation of the molecule.

Both orientation of the molecule and the adsorption site of the surface can impact the apparent height measured with the STM. Since the STM does not directly measure

height but probes the LDOS of the sample, any electronic effects can impact the apparent height of the molecule measured. The electron density is not consistent across the whole C_{60} molecule since there are two bond lengths (bonds between two hexagons and a bond between a hexagon and a pentagon) that make up the structure. The bond between two hexagons (6:6) is 1.4 \AA and the bond between a hexagon and pentagon (6:5) is 1.45 \AA in length, the shorter 6:6 bond leads to a higher electron density on those bonds. When the electron density across the fullerene is modelled, the pentagon rings of the molecule are electron deficient and the hexagons are electron rich. When a hexagon facet binds to the substrate, the bond formed can be stronger due to the higher electron density of that facet in comparison with a pentagon facet binding to the surface. LaRocca et al. found that the binding energy can vary by 140-240 meV between orientations^[111]. Comparing results from previous experiments to the results collected within chapter 4 it is suggested that the dim molecular heights and the broad range of the distribution measured is due to a combination of orientation of the fullerene and the adsorption site the molecule sits on.

The raised (bright) molecules within the monolayer were found at 0.045 nm, 0.173 nm and 1.3 nm heights compared to the average monolayer. The heights of gold islands measured at elbow sites on the sample was approximately 0.17 nm, it can be assumed that the molecules raised by this height are due to a gold island sitting below the monolayer. The 1.3 nm height difference is attributed to either a larger cluster of gold sitting beneath the monolayer or to a second layer C_{60} molecule adhering on top of the

first layer.

The height difference of 0.045 nm is most likely due to the orientation of the molecule as it is of a similar scale to the depths measured previously for dim molecules and corresponds to previously observed height of 0.04 nm^[66].

When examining the orientation of the molecules, height profiles could be taken and the heights of each orientation could be measured and compared. From this study the height variation in the average monolayer was 0.1 nm where the “bridge down” and the “hexagon down” molecules had similar heights and the “pentagon down” molecule was the tallest. The height difference measured between bridge and hexagon adsorption facets was found to be approximately 0.04 nm; this corresponds to one of the most common heights observed when measuring the bright molecules’ heights. It can therefore be assumed that the hypothesis that the 0.045 nm height difference observed is due to the orientation of the C₆₀ molecule is correct.

The majority of dim molecules observed had a hexagon down orientation (80%) with bridge down orientation being the second most commonly observed (20%). The orientations of the C₆₀ molecules in islands was investigated over multiple images and it was found that the hexagon down orientation was the most commonly observed orientation. The phase of each C₆₀ island where the orientation was analysed was calculated and the impact of the phase on C₆₀ orientation was examined. It was found that the majority of islands, independent of phase, had “hexagon down” as the most commonly observed and “bridge down” the second most commonly observed. The exceptions to this were the

R14° island and the R30° island which had bridge down as a more commonly observed orientation.

7.2 STM investigation of C₆₀ on HOPG

C₆₀ was deposited onto HOPG and Au adatoms were deposited subsequently to create a C₆₀/Au matrix on HOPG. The C₆₀ molecules form a monolayer and the Au atoms are small enough to diffuse through the C₆₀ cages. The Au atoms can then agglomerate to form islands and clusters underneath the the C₆₀ layer, or the gold atoms can form magic number clusters with the C₆₀ - where one C₆₀ molecule is raised due to gold adsorbed underneath it. Examining the results from this experiment it can be ascertained that the C₆₀/Au matrix was formed. Bright molecules on the monolayer surface were analysed and the comparative heights were clustered in two groups of 0.24 nm and 1.4 nm height differences. The 0.24 nm height increase corresponds with the height of a single layer of gold atoms, it can therefore be assumed that the molecules that are raised by this amount are due to a single layer of gold sitting underneath the raised molecule. The larger height difference of 1.4 nm could correspond to second layer C₆₀ islands sitting above the C₆₀ surface with a gold cluster or island also contributing to the height increase of the molecules. Dim molecules within the C₆₀ monolayer were also investigated in this chapter and the height differences most commonly observed were 0.05 nm, 0.1 nm and 0.13 nm. An atomic step in HOPG has been found to be 0.34 nm when measured by STM ^[116] and as stated previously the gold atomic step

height is 0.24 nm^[30]. When comparing the heights of the dim molecules observed, it is clear that the most common heights are not due to vacancies in a large gold island or defects in the HOPG surface. The dim molecules' heights are thought to be due to the orientation of the C₆₀ molecules. Previous work has shown that molecular orientation can account for height differences between 0.04 nm and 0.09 nm^[66]. This accounts for the peak observed in the distribution of heights observed (figure 5.7) at 0.05 nm.

The orientation of fullerenes was also investigated in this experiment and it was found that only dim molecules' orientation was easily observable on HOPG and that all orientations observed had a three lobe structure. This suggests that the dim molecules are bound with the hexagon facet attached to the HOPG surface. No other orientations were easily distinguished in the STM images which could be a result of C₆₀ molecules contaminating the tip.

7.3 Comparison of results from C₆₀ on HOPG and Au(111)

When comparing the results from chapter 4 and chapter 5 it can be seen that the heights observed for dim and bright molecules are similar between samples increasing the validity of the conclusions drawn. The dim molecules' depths observed for HOPG were 0.05 nm, 0.1 nm and 0.13 nm and for Au(111) they were 0.03 nm and 0.07 nm. The height differences observed are assumed to be related to the orientations of the

C₆₀ molecules. Bright C₆₀ molecules were found at 0.24 nm and 1.4 nm on HOPG and 0.045 nm, 0.17 nm and 1.3 nm on Au(111). The 0.24 nm and 0.17 nm heights correspond to the molecules being raised by a gold island underneath the C₆₀ monolayer. The 1.3 nm and 1.4 nm heights are also considered to be due to the same phenomenon, a larger gold cluster forming underneath the molecule raising it by a larger amount than a single layer of gold. The height difference could also be contributed to by a second layer C₆₀ island forming in these areas.

On both HOPG and Au(111) the orientations observed most commonly were the 3 lobe orientation (“hexagon down”) this was the case for the dim molecules on both samples. Orientations of molecules within the island as a whole were not able to be analysed for HOPG, but for gold it was shown that “hexagon down” is the most prominent orientation. The ease of determining orientation on Au(111) compared to HOPG can be explained by the energies of the C₆₀ molecules on both substrates at 77 K. The C₆₀ molecule on gold forms a stronger bond than when the fullerene is deposited on HOPG. The gold bond is ionic in nature and 0.8 electrons are shared between the gold surface and the C₆₀ molecule^[143]. For C₆₀ on HOPG the bond is very similar to the bond between graphene layers, the van der Waals interaction has 0.85 eV strength^[144]. From this it can be assumed that the C₆₀ is more mobile on HOPG than on gold, at the same temperature the gold would provide a stronger interaction with the fullerenes and would result in less movement of the molecules than the HOPG. At room temperature the C₆₀ molecules are mobile on both HOPG and Au(111) and the orientation cannot

be imaged as the molecules rotate freely. At 77 K the molecules should be ‘pinned’ to the surface as they have less kinetic energy. If the samples were to be imaged at lower temperatures than 77 K it may improve the ability to determine the orientation of the C_{60} molecules on HOPG.

7.4 STS investigation of Au(111), HOPG and C_{60} on Au(111)

The STS investigation on Au(111) examined the different spectra produced at different packing sites on the surface. It was found that the FCC sites and discommensuration line (DL) sites both shared a peak at -0.2 V and the hexagonal close packed (HCP) sites had a peak at -0.3 V. These peaks are assumed to be due to the surface state electrons and this peak is commonly referred to as the Shockley state. The position of these peaks is different from some of the literature which places the Shockley state at closer to -0.5 V, however, studies have also shown that the surface state can result in a peak at around -0.3 V^[96]. The step edges of the sample were also examined with STS measurements and the spectra taken from the top edge of the step and the lower edge were compared. The spectra from the top edge of the step appeared very similar in shape to the averaged Au curve, whereas the lower edge step spectra did not resemble the shape for the averaged spectra on the sample. The position of the surface state peak also differed between the top and lower edge steps, with the top edge having the

peak positioned at -0.3V and the bottom edge peak was shifted to a lower voltage. The intensity of the bottom edge spectra was lower than the top edge which was to be expected, since previous work has shown that the presence of a step acts as a potential barrier and impacts the LDOS of the sample in areas near the step. ^{[90][92]} The top edge of the step behaves in the same way as other areas of the sample and the electron density is unhindered by the step.

The STS investigation of HOPG examined the two different lattices that make up HOPG and how the difference in site affects the spectra produced. The impact of set point and other settings relating to the technique of STS were also examined in this experiment. The averaged spectra produced for HOPG match what is expected for graphite and were not the symmetrical V shaped curves expected for a layer of graphene. The comparison of the shape of the spectra to previously measured data allowed for classification of the surface. In some STM imaging the atomic structure of graphite could be seen, this can appear similar to when a sheet of graphene has detached from the HOPG surface due to attraction between the tip and the graphene layer. Both images appear to have a hexagonal lattice pattern. The STS data could be used to determine that the images were of the structure of the graphite and not a detached graphene sheet. If the spectra were more symmetrical and followed more closely to the V shape expected for graphene then the conclusion drawn would have been different. The impact of tip set point on STS was investigated and it was found that at smaller set point voltages (smaller tip sample distances) the peaks observed

were closer in energy to the fermi level and as the voltage is increased the peaks shift further away from the fermi level. These results are in accordance with work by Söde et al. where the same phenomenon was observed^[130]. The final STS experiment on HOPG was the influence of lattice site of the LDOS. It is known that the different lattice sites on HOPG (A and B atoms) have similar LDOS at energies near the fermi level. The two curves observed in this chapter were similar at low voltages and the A type atom had a higher conductance measured than the B type atoms. However, at larger negative biases the B type atom shows a higher conductance, this correlates with previous data taken by Teobaldi et al.^[135].

The STS experiment of the C_{60} molecules was only performed on Au(111). Unlike the studies of bare Au(111) and HOPG spectra produced were not consistent between experiments. It is therefore harder to draw any firm conclusions from this study. If the spectra are assumed to be viable, then peaks at -0.37 V could correspond to contributions from the Au(111) surface peak and the LUMO and HOMO peak positions could be identified at 1 V and -1.1 V respectively. This HOMO LUMO gap is smaller than the previously measured gap of 2.3-2.8 V observed for C_{60} on Au(111). It is possible that the spectra produced show the LDOS of the tip and convolutions between the tip DOS and the sample LDOS. This requires more measurements to determine which if any peaks are due to the LDOS of the C_{60} molecules.

7.4.1 Comparison of STS and STM Investigations

The STS experiments show the impact of binding site on the LDOS and contribute to the hypothesis that the heights observed of the C_{60} molecule can be impacted by the binding site that they bond with. Unfortunately detailed analysis of the C_{60} molecules on both substrates was unable to be performed by STS and so no further conclusions about the arrangement of C_{60} molecules in magic number clusters was able to be drawn.

7.5 Suggestions for future work

To build upon the work previously done in the literature and knowledge gained in the experiments detailed in this thesis more experiments could be carried out. Further investigations into the local density of states (LDOS) of the C_{60} molecules within magic number clusters could help to improve the theorised arrangement of the C_{60} molecules and the gold islands that make up the clusters. Within this work no sub cluster LDOS of the clusters was able to be obtained and extracting this information could inform the models of the arrangements within the clusters. Orientation of the molecules within the clusters were not examined in this work and this would also aid in the understanding of the formation of the C_{60} clusters, both within a matrix and isolated on the Au(111) surface. Scanning the C_{60} -Au clusters on both gold and highly oriented pyrolytic graphite (HOPG) at low temperatures with a very stable tip would be able to illustrate the sub molecular orbitals and therefore the orientation of the C_{60}

molecules that form the magic number cluster. Low temperature studies of the samples examined within this experiment would also be beneficial to reduce the kinetic energy of the fullerenes and improve the contrast (reduce the noise) in STS measurements. Liquid helium measurements often provide the best stability and lowest signal to noise ratio therefore providing a more accurate representation of the LDOS within the STS measurements. These suggestions would build upon the work presented in this thesis to hopefully provide a fuller picture of the clusters that have been studied in this case.

Bibliography

- [1] G. Binnig and H. Rohrer, “SCANNING TUNNELING MICROSCOPY,” *Surface Science*, vol. 126, pp. 236–244, 1983.
- [2] A. Ulman, “Formation and structure of self-assembled monolayers,” *Chemical Reviews*, vol. 96, no. 4, pp. 1533–1554, 1996.
- [3] I. H. Campbell, J. D. Kress, R. L. Martin, D. L. Smith, N. N. Barashkov, and J. P. Ferraris, “Controlling charge injection in organic electronic devices using self-assembled monolayers,” *Applied Physics Letters*, vol. 71, pp. 3528–3530, jun 1997.
- [4] F. Rissner, G. M. Rangger, O. T. Hofmann, A. M. Track, G. Heimel, and E. Zojer, “Understanding the electronic structure of metal/SAM/organic-semiconductor heterojunctions,” *ACS Nano*, vol. 3, pp. 3513–3520, nov 2009.
- [5] L. Bardotti, B. Prével, M. Treilleux, P. Mélinon, and A. Perez, “Deposition of preformed gold clusters on HOPG and gold substrates: Influence of the substrate on the thin film morphology,” *Applied Surface Science*, vol. 164, pp. 52–59, sep

2000.

- [6] R. V. Lapshin, “Automatic lateral calibration of tunneling microscope scanners,” *Review of Scientific Instruments*, vol. 69, no. 9, pp. 3268–3276, 1998.
- [7] J. Christopher Love, Lara A. Estroff, Jennah K. Kriebel, , Ralph G. Nuzzo, and George M. Whitesides, “Self-Assembled Monolayers of Thiolates on Metals as a Form of Nanotechnology,” *Chemical Reviews*, vol. 105, no. 4, pp. 1103–1169, 2005.
- [8] H. Martin, “Buckminster fuller’s geodesic dome and other forward-looking architecture,” *Architectural Digest*, 2016.
- [9] H. W. Kroto, J. R. Heath, S. C. O’Brien, R. F. Curl, and R. E. Smalley, “C₆₀: Buckminsterfullerene,” *Nature 1985 318:6042*, vol. 318, no. 6042, pp. 162–163, 1985.
- [10] S. F. A. Acquah, A. V. Penkova, D. A. Markelov, A. S. Semisalova, B. E. Leonhardt, and J. M. Magi, “Review—The Beautiful Molecule: 30 Years of C₆₀ and Its Derivatives,” *ECS Journal of Solid State Science and Technology*, vol. 6, pp. M3155–M3162, mar 2017.
- [11] H. Park, J. Park, A. K. L. Lim, E. H. Anderson, A. P. Alivisatos, and P. L. McEuen, “Nanomechanical oscillations in a single-C₆₀ transistor,” *Nature 2000 407:6800*, vol. 407, no. 6800, pp. 57–60, 2000.
- [12] A. Montellano, T. Da Ros, A. Bianco, and M. Prato, “Fullerene C₆₀ as a multi-

- functional system for drug and gene delivery,” *Nanoscale*, vol. 3, no. 10, pp. 4035–4041, 2011.
- [13] X. Q. Shi, M. A. Van Hove, and R. Q. Zhang, “Survey of structural and electronic properties of C_{60} on close-packed metal surfaces,” *Journal of Materials Science*, vol. 47, no. 21, pp. 7341–7355, 2012.
- [14] Y. C. Xie, L. Tang, and Q. Guo, “Cooperative assembly of magic number C_{60} -Au complexes,” *Physical Review Letters*, vol. 111, no. 18, 2013.
- [15] M. Rokni Fard, *Study of fullerenes on Au (111) surfaces using STM*. PhD thesis, University of Birmingham, 2018.
- [16] L. Guo, Y. Wang, D. L. Bao, H. H. Jia, Z. Wang, S. Du, and Q. Guo, “On-surface synthesis of size-and shape-controlled two-dimensional Au: Nanoclusters using a flexible fullerene molecular template,” *Nanoscale*, vol. 12, no. 42, pp. 21657–21664, 2020.
- [17] H. W. Kroto and D. Walton, “Fullerene.” Encyclopedia Britannica (online) <https://www.britannica.com/science/fullerene> [accessed on 03/8/21], 2004.
- [18] S. Iijima, “Helical microtubules of graphitic carbon,” *Nature* 1991 354:6348, vol. 354, no. 6348, pp. 56–58, 1991.
- [19] K. S. Novoselov, A. K. Geim, S. V. Morozov, D. Jiang, Y. Zhang, S. V. Dubonos, I. V. Grigorieva, and A. A. Firsov, “Electric Field Effect in Atomically Thin Carbon Films,” *Science*, vol. 306, no. 5696, pp. 666–669, 2004.

- [20] N. S. Sariciftci, “Role of Buckminsterfullerene, C₆₀, in organic photoelectric devices,” *Progress in Quantum Electronics*, vol. 19, no. 2, pp. 131–159, 1995.
- [21] B. Kraabel, D. McBranch, N. S. Sariciftci, D. Moses, and A. J. Heeger, “Ultrafast spectroscopic studies of photoinduced electron transfer from semiconducting polymers to C_{60} ,” *Physical Review B*, vol. 50, no. 24, p. 18543, 1994.
- [22] R. D. Bolskar, “Gadofullerene MRI contrast agents,” 2008.
- [23] R. Bakry, R. M. Vallant, M. Najam-ul Haq, M. Rainer, Z. Szabo, C. W. Huck, and G. K. Bonn, “Medicinal applications of fullerenes,” *International Journal of Nanomedicine*, vol. 2, no. 4, p. 639, 2007.
- [24] G. Schull and R. Berndt, “Orientationally ordered (7×7) superstructure of C₆₀ on Au(111),” *Physical Review Letters*, vol. 99, no. 22, p. 226105, 2007.
- [25] “Wikipedia - Fullerene.” <https://en.wikipedia.org/wiki/Fullerene> [Accessed on 6/8/21].
- [26] J. J. Ramsden, “Carbon-based nanomaterials and devices,” *Nanotechnology*, pp. 231–244, 2016.
- [27] P. Yang, D. Li, V. Repain, C. Chacon, Y. Girard, S. Rousset, A. Smogunov, Y. J. Dappe, C. Barreateau, and J. Lagoute, “C₆₀ as an atom trap to capture Co adatoms,” *Journal of Physical Chemistry C*, vol. 119, no. 12, pp. 6873–6879, 2015.

- [28] L. Guo, Y. Wang, D. Kaya, Z. Wang, M. Zhang, and Q. Guo, “Self-build of C₆₀-C₇₀ molecular heterojunctions on highly oriented pyrolytic graphite,” *Applied Surface Science*, vol. 538, 2021.
- [29] . M. J. Ford, , R. C. Hoft, and A. McDonagh, “Theoretical Study of Ethynylbenzene Adsorption on Au(111) and Implications for a New Class of Self-Assembled Monolayer,” *Journal of Physical Chemistry B*, vol. 109, no. 43, pp. 20387–20392, 2005.
- [30] J. V. Barth, H. Brune, G. Ertl, and R. J. Behm, “Scanning tunneling microscopy observations on the reconstructed Au(111) surface: Atomic structure, long-range superstructure, rotational domains, and surface defects,” *Physical Review B*, vol. 42, no. 15, p. 9307, 1990.
- [31] “Face Centered Cubic.” <https://www.corrosionpedia.com/definition/1592/face-centered-cubic-fcc> [Accessed on 6/8/21].
- [32] “Hexagonal Close Packed.” <http://lamp.tu-graz.ac.at/~hadley/ss1/problems/hcp/Q.php>[Accessed on 6/8/21].
- [33] M. S. Wartak and C. Fong, “Field guide to solid state physics.” SPIE digital library https://www.spiedigitallibrary.org/ContentImages/ebooks/FG43/Images/FG43_ch010.jpg [accessed on 6/8/21].
- [34] Crljen, P. Lazić, D. Šokčević, and R. Brako, “Relaxation and reconstruction on (111) surfaces of Au, Pt, and Cu,” *Physical Review B - Condensed Matter and*

Materials Physics, vol. 68, no. 19, 2003.

- [35] N. Takeuchi, C. T. Chan, and K. M. Ho, “Au(111): A theoretical study of the surface reconstruction and the surface electronic structure,” *Physical Review B*, vol. 43, no. 17, p. 13899, 1991.
- [36] F. Hanke and J. Björk, “Structure and local reactivity of the Au(111) surface reconstruction,” *Physical Review B*, vol. 87, no. 23, p. 235422, 2013.
- [37] D. Fujita, K. Amemiya, T. Yakabe, H. Nejoh, T. Sato, and M. Iwatsuki, “Observation of two-dimensional Fermi contour of a reconstructed Au(111) surface using Fourier transform scanning tunneling microscopy,” *Surface Science*, vol. 423, no. 2, pp. 160–168, 1999.
- [38] F. Grillo, H. Früchtl, S. M. Francis, and N. V. Richardson, “Site selectivity in the growth of copper islands on Au (111),” *New Journal of Physics*, vol. 13, p. 13044, 2011.
- [39] R. Fard, “Biased Ostwald ripening in site-selective growth of two-dimensional gold clusters,” *The Journal of Physical Chemistry*, vol. 122, no. 14, pp. 7801–7805, 2018.
- [40] V. Repain, J. M. Berroir, S. Rousset, and J. Lecoer, “Interaction between steps and reconstruction on Au(111),” *EPL (Europhysics Letters)*, vol. 47, no. 4, p. 435, 1999.
- [41] K. Morgenstern, J. Kibsgaard, J. V. Lauritsen, E. Lægsgaard, and F. Besen-

- bacher, “Cobalt growth on two related close-packed noble metal surfaces,” *Surface Science*, vol. 601, no. 9, pp. 1967–1972, 2007.
- [42] C. Wu and M. R. Castell, “Ultrathin Oxide Films on Au(111) Substrates,” *Springer Series in Materials Science*, vol. 234, pp. 149–168, 2016.
- [43] J. A. Meyer, I. D. Baikie, E. Kopatzki, and R. J. Behm, “Preferential island nucleation at the elbows of the Au(111) herringbone reconstruction through place exchange,” *Surface Science*, vol. 365, no. 1, pp. L647–L651, 1996.
- [44] V. Repain, J. M. Berroir, S. Rousset, and J. Lecoeur, “Growth of self-organized cobalt nanostructures on Au(111) vicinal surfaces,” *Surface Science*, vol. 447, no. 1-3, pp. L152–L156, 2000.
- [45] S. Rousset, V. Repain, G. Baudot, Y. Garreau, and J. Lecoeur, “Self-ordering of Au(111) vicinal surfaces and application to nanostructure organized growth,” *Journal of Physics: Condensed Matter*, vol. 15, no. 47, p. S3363, 2003.
- [46] T. Michely and G. Comsa, “Temperature dependence of the sputtering morphology of Pt(111),” *Surface Science*, vol. 256, no. 3, pp. 217–226, 1991.
- [47] S. Huang, J. E. Weis, S. Costa, M. Kalbac, and M. S. Dresselhaus, “Properties of Carbon: An Overview,” in *Advances in Electrochemical Science and Engineering*, vol. 16, pp. 1–29, wiley, 2016.
- [48] M. INAGAKI, “Highly Oriented Graphites,” in *New Carbons - Control of Structure and Functions*, pp. 30–57, Elsevier, 2000.

- [49] M. F. Juarez, S. Fuentes, G. J. Soldano, L. Avalle, and E. Santos, “Spontaneous formation of metallic nanostructures on highly oriented pyrolytic graphite (hopg): an ab initio and experimental study,” *Faraday Discuss.*, vol. 172, 2014.
- [50] S. Okita and K. Miura, “Molecular Arrangement in C₆₀ and C₇₀ Films on Graphite and Their Nanotribological Behavior,” *Nano Letters*, vol. 1, no. 2, pp. 101–103, 2001.
- [51] M. F. Luo, Z. Y. Li, and W. Allison, “Initial stages of C₆₀ thin film growth on graphite,” *Surface Science*, vol. 402-404, pp. 437–440, 1998.
- [52] W. W. Pai, H. T. Jeng, C. M. Cheng, C. H. Lin, X. Xiao, A. Zhao, X. Zhang, G. Xu, X. Q. Shi, M. A. Van Hove, C. S. Hsue, and K. D. Tsuei, “Optimal electron doping of a C₆₀ monolayer on Cu(111) via interface reconstruction,” *Physical Review Letters*, vol. 104, no. 3, p. 036103, 2010.
- [53] M. Sogo, Y. Sakamoto, M. Aoki, S. Masuda, S. Yanagisawa, and Y. Morikawa, “C₆₀ adsorbed on platinum surface: A good mediator of metal wave function,” *Journal of Physical Chemistry C*, vol. 114, no. 8, pp. 3504–3506, 2010.
- [54] M. Moalem, M. Balooch, A. V. Hamza, W. J. Siekhaus, and D. R. Olander, “Surface mobility of C₆₀ on SiO₂,” *The Journal of Chemical Physics*, vol. 99, no. 6, pp. 4855–4859, 1993.
- [55] U. D. Schwarz, W. Allers, G. Gensterblum, J. J. Pireaux, and R. Wiesendanger, “Growth of C₆₀ thin films on GeS(001) studied by scanning force microscopy,”

Physical Review B, vol. 52, no. 8, pp. 5967–5976, 1995.

- [56] P. A. Brühwiler, A. J. Maxwell, P. Baltzer, S. Andersson, D. Arvanitis, L. Karlsson, and N. Mårtensson, “Vibronic coupling in the photoemission bands of condensed C_{60} ,” *Chemical Physics Letters*, vol. 279, no. 1-2, pp. 85–91, 1997.
- [57] R. Felici, M. Pedio, F. Borgatti, S. Iannotta, M. Capozzi, G. Ciullo, and A. Stierle, “X-ray-diffraction characterization of Pt(111) surface nanopatterning induced by C_{60} adsorption,” *Nature Materials*, vol. 4, no. 9, pp. 688–692, 2005.
- [58] H. I. Li, K. Pussi, K. J. Hanna, L. L. Wang, D. D. Johnson, H. P. Cheng, H. Shin, S. Curtarolo, W. Moritz, J. A. Smerdon, R. McGrath, and R. D. Diehl, “Surface Geometry of C_{60} on Ag(111),” *Physical Review Letters*, vol. 103, no. 5, p. 056101, 2009.
- [59] M. Stengel, A. D. Vita, and A. Baldereschi, “Adatom-vacancy mechanisms for the $C_{60}/Al(111)(6 \times 6)$ reconstruction,” *Physical Review Letters*, vol. 91, no. 16, p. 166101, 2003.
- [60] C. Liu, Z. Qin, J. Chen, Q. Guo, Y. Yu, and G. Cao, “Molecular orientations and interfacial structure of C_{60} on Pt(111),” *Journal of Chemical Physics*, vol. 134, no. 4, p. 044707, 2011.
- [61] T. Hashizume, K. Motai, X. D. Wang, H. Shinohara, Y. Saito, Y. Maruyama, K. Ohno, Y. Kawazoe, Y. Nishina, H. W. Pickering, Y. Kuk, and T. Sakurai, “Intramolecular structures of C_{60} molecules adsorbed on the Cu(111)-(1 \times 1) sur-

- face,” *Physical Review Letters*, vol. 71, no. 18, pp. 2959–2962, 1993.
- [62] E. I. Altman and R. J. Colton, “Nucleation, growth, and structure of fullerene films on Au(111),” *Surface Science*, vol. 279, no. 1-2, pp. 49–67, 1992.
- [63] R. Sk, S. Arra, B. Dhara, J. S. Miller, M. Kabir, and A. Deshpande, “Effect of Cyano Substitution on the Step-Edge Adsorption of Copper Phthalocyanine on Au(111),” *Journal of Physical Chemistry C*, vol. 122, no. 22, pp. 11848–11854, 2018.
- [64] J. A. Gardener, G. A. Briggs, and M. R. Castell, “Scanning tunneling microscopy studies of C₆₀ monolayers on Au(111),” *Physical Review B - Condensed Matter and Materials Physics*, vol. 80, no. 23, p. 235434, 2009.
- [65] L. Tang, Y. Xie, and Q. Guo, “Complex orientational ordering of C₆₀ molecules on Au(111),” *Journal of Chemical Physics*, vol. 135, no. 11, p. 114702, 2011.
- [66] H. Shin, A. Schwarze, R. D. Diehl, K. Pussi, A. Colombier, E. Gaudry, J. Ledieu, G. M. McGuirk, L. N. Serkovic Loli, V. Fournée, L. L. Wang, G. Schull, and R. Berndt, “Structure and dynamics of C₆₀ molecules on Au(111),” *Physical Review B - Condensed Matter and Materials Physics*, vol. 89, no. 24, p. 245428, 2014.
- [67] Megan Grose, “Investigation of c₆₀ and c₇₀ and platinum on an au(111) surface,” Master’s thesis, University of Birmingham, 2016.
- [68] X. Zhang, F. Yin, R. Palmer, and Q. Guo, “The C₆₀/Au(111) interface at room

- temperature: A scanning tunnelling microscopy study,” *Surface Science*, vol. 602, no. 4, pp. 885–892, 2008.
- [69] X. Zhang, L. Tang, and Q. Guo, “Low-Temperature Growth of C_{60} Monolayers on Au(111): Island Orientation Control with Site-Selective Nucleation,” *J. Phys. Chem C*, vol. 114, no. 14, pp. 6433–6439, 2010.
- [70] Y. C. Xie, M. Rokni Fard, D. Kaya, D. Bao, R. E. Palmer, S. Du, and Q. Guo, “Site-Specific Assembly of Fullerene Nanorings Guided by Two-Dimensional Gold Clusters,” *Journal of Physical Chemistry C*, vol. 120, no. 20, pp. 10975–10981, 2016.
- [71] M. Rokni-Fard and Q. Guo, “Biased Ostwald Ripening in Site-Selective Growth of Two-Dimensional Gold Clusters,” *Journal of Physical Chemistry C*, vol. 122, no. 14, pp. 7801–7805, 2018.
- [72] D. Kaya, D. Bao, R. E. Palmer, S. Du, and Q. Guo, “Tip-triggered Thermal Cascade Manipulation of Magic Number Gold-Fullerene Clusters in the Scanning Tunnelling Microscope,” *Nano Letters*, vol. 17, no. 10, pp. 6171–6176, 2017.
- [73] D. Kaya, J. Gao, M. R. Fard, R. E. Palmer, and Q. Guo, “Controlled Manipulation of Magic Number Gold-Fullerene Clusters Using Scanning Tunneling Microscopy,” *Langmuir*, vol. 34, no. 28, pp. 8388–8392, 2018.
- [74] M. Rokni-Fard and Q. Guo, “Stability of $(C_{60})_m$ - Au_n Magic Number Clusters,” *Journal of Physical Chemistry C*, vol. 123, no. 30, pp. 18482–18487, 2019.

- [75] H. Jia, Q. Guo, and S. Du, “Thermally Driven Diffusion of a Magic Number Gold-Fullerene Cluster on a Au(111) Surface,” *Journal of Physical Chemistry C*, vol. 124, no. 18, pp. 9990–9995, 2020.
- [76] H. Liu and P. Reinke, “C₆₀ thin film growth on graphite: Coexistence of spherical and fractal-dendritic islands,” *Journal of Chemical Physics*, vol. 124, no. 16, p. 164707, 2006.
- [77] S. Suto, A. Kasuya, C. W. Hu, A. Wawro, K. Sakamoto, T. Goto, and Y. Nishina, “Initial stage of C₆₀ film growth and reaction on Si(111)7×7 and graphite surfaces studied by HREELS-STM,” *Thin Solid Films*, vol. 281-282, no. 1-2, pp. 602–605, 1996.
- [78] R. Lüthi, E. Meyer, H. Haefke, L. Howald, W. Gutmannsbauer, and H. J. Güntherodt, “Sled-type motion on the nanometer scale: Determination of dissipation and cohesive energies of C₆₀,” *Science*, vol. 266, no. 5193, pp. 1979–1981, 1994.
- [79] S. Szuba, R. Czajka, A. Kasuya, A. Wawro, and H. Rafii-Tabar, “Observation of C₆₀ film formation on a highly oriented pyrolytic graphite substrate via scanning tunnelling microscopy,” *Applied Surface Science*, vol. 144-145, pp. 648–652, 1999.
- [80] H. Yu, J. Yan, Y. Li, W. S. Yang, Z. Gu, and Y. Wu, “Scanning tunneling microscopy of C₆₀ on graphite,” *Surface Science*, vol. 286, no. 1-2, pp. 116–121, 1993.

- [81] D. J. Kenny and R. E. Palmer, “Nucleation and growth of C₆₀ thin films on graphite,” *Surface Science*, vol. 447, no. 1, pp. 126–132, 2000.
- [82] M. Schmid, “The Scanning Tunneling Microscope.” 2005, TU Wien, <http://www.iap.tuwien.ac.at/www/surface/stm{ }gallery/stm{ }schematic>[Accessed on 30/01/2018].
- [83] J. Bardeen, “Tunnelling from a many-particle point of view,” *Physical Review Letters*, vol. 6, no. 2, pp. 57–59, 1961.
- [84] C. J. Chen, *Introduction to Scanning Tunneling Microscopy*. Oxford University Press, 2007.
- [85] A. D. Gottlieb and L. Wesoloski, “Bardeen’s tunnelling theory as applied to scanning tunnelling microscopy: A technical guide to the traditional interpretation,” *Nanotechnology*, vol. 17, no. 8, pp. R57–R65, 2006.
- [86] S. Lounis, “Theory of Scanning Tunneling Microscopy 1.” online, 2014.
- [87] A. L. Vázquez de Parga and R. Miranda, *Scanning Tunneling Spectroscopy*, pp. 2313–2321. Springer Netherlands, 2012.
- [88] D. A. Bonnell, ed., *Scanning Tunneling Microscopy and Spectroscopy. Theory, Techniques, and Applications*, ch. 4. VCH Publishers, 1993.
- [89] “Wikipedia - HOMO and LUMO.” <https://en.wikipedia.org/wiki/HOMO{ }and{ }LUMO>[accessed on 18/9/21], 2021.

- [90] M. P. Everson, “Effects of surface features upon the Au(111) surface state local density of states studied with scanning tunneling spectroscopy,” *Journal of Vacuum Science & Technology B: Microelectronics and Nanometer Structures*, vol. 9, no. 2, p. 891, 1991.
- [91] M. P. Everson, R. C. Jaklevic, and W. Shen, “Measurement of the local density of states on a metal surface: Scanning tunneling spectroscopic imaging of Au(111),” *Journal of Vacuum Science & Technology A: Vacuum, Surfaces, and Films*, vol. 8, no. 5, pp. 3662–3665, 1990.
- [92] L. C. Davis, M. P. Everson, R. C. Jaklevic, and W. Shen, “Theory of the local density of surface states on a metal: Comparison with scanning tunneling spectroscopy of a Au(111) surface,” *Physical Review B*, vol. 43, no. 5, pp. 3821–3830, 1991.
- [93] W. Chen, V. Madhavan, T. Jamneala, and M. F. Crommie, “Scanning Tunneling Microscopy Observation of an Electronic Superlattice at the Surface of Clean Gold,” *Physical Review Letters*, vol. 80, no. 7, pp. 1469–1472, 1998.
- [94] Z. Hussain and N. Smith, “Determination of the $E(k_{\parallel})$ relation for a surface state on Au(111),” *Physics Letters A*, vol. 66, no. 6, pp. 492–494, 1978.
- [95] R. Paniago, R. Matzdorf, G. Meister, and A. Goldmann, “Temperature dependence of Shockley-type surface energy bands on Cu(111), Ag(111) and Au(111),” *Surface Science*, vol. 336, no. 1-2, pp. 113–122, 1995.

- [96] F. Reinert and G. Nicolay, “Influence of the herringbone reconstruction on the surface electronic structure of Au(111),” *Applied Physics A*, vol. 78, no. 6, pp. 817–821, 2004.
- [97] A. P. Labonté, S. L. Tripp, R. Reifengerger, and A. Wei, “Scanning tunneling spectroscopy of insulating self-assembled monolayers on Au(111),” *Journal of Physical Chemistry B*, vol. 106, no. 34, pp. 8721–8725, 2002.
- [98] K. Katoh, Y. Yoshida, M. Yamashita, H. Miyasaka, B. K. Breedlove, T. Kajiwara, S. Takaishi, N. Ishikawa, H. Isshiki, F. Z. Yan, T. Komeda, M. Yamagishi, and J. Takeya, “Direct observation of lanthanide(III)-phthalocyanine molecules on Au(111) by using scanning tunneling microscopy and scanning tunneling spectroscopy and thin-film field-effect transistor properties of Tb(III)- and Dy(III)-phthalocyanine molecules,” *Journal of the American Chemical Society*, vol. 131, no. 29, pp. 9967–9976, 2009.
- [99] B. Koslowski, A. Tschetschetkin, N. Maurer, E. Mena-Osteritz, P. Bäuerle, and P. Ziemann, “Terthiophene on Au(111): A scanning tunneling microscopy and spectroscopy study,” *Beilstein Journal of Nanotechnology*, vol. 2, no. 1, pp. 561–568, 2011.
- [100] K. Kusunoki, I. Sakata, and K. Miyamura, “Interaction between Tip and HOPG Surface Studied by STS,” *Analytical Sciences*, vol. 17, pp. 1267–1268, 2001.
- [101] R. Houbertz, U. Weber, and U. Hartmann, “Scanning tunneling spectroscopy on

- Au thin film structures deposited on highly oriented pyrolytic graphite,” *Applied Physics A: Materials Science and Processing*, vol. 66, no. SUPPL. 1, pp. 149–152, 1998.
- [102] R. Klingeler, C. Breuer, I. Wirth, A. Blanchard, P. S. Bechthold, M. Neeb, and W. Eberhardt, “Scanning tunneling spectroscopy of small Ce-doped endohedral fullerenes on HOPG,” *Surface Science*, vol. 553, no. 1-3, pp. 95–104, 2004.
- [103] A. Stróżecka, J. Mysliveček, and B. Voigtländer, “Scanning tunneling spectroscopy and manipulation of C_{60} on Cu(111),” *Applied Physics A: Materials Science and Processing*, vol. 87, no. 3, pp. 475–478, 2007.
- [104] Á. J. Pérez-Jiménez, J. J. Palacios, E. Louis, E. SanFabián, and J. A. Vergés, “Analysis of scanning tunneling spectroscopy experiments from first principles: The test case of C_{60} adsorbed on Au(111),” *ChemPhysChem*, vol. 4, no. 4, pp. 388–392, 2003.
- [105] X. Lu, M. Grobis, K. H. Khoo, S. G. Louie, and M. F. Crommie, “Charge transfer and screening in individual C_{60} molecules on metal substrates: A scanning tunneling spectroscopy and theoretical study,” *Physical Review B - Condensed Matter and Materials Physics*, vol. 70, no. 11, 2004.
- [106] A. Warren, A. Nylund, and I. Olefjord, “Oxidation of tungsten and tungsten carbide in dry and humid atmospheres,” *International Journal of Refractory Metals and Hard Materials*, vol. 14, pp. 345–353, jan 1996.

- [107] C. D. Reddy, Z. G. Yu, and Y. W. Zhang, “Two-dimensional van der Waals C₆₀ molecular crystal,” *Scientific Reports*, vol. 5, pp. 1–7, jul 2015.
- [108] S. Guo, D. P. Fogarty, P. M. Nagel, and S. A. Kandel, “Thermal diffusion of C₆₀ molecules and clusters on Au(111),” *Journal of Physical Chemistry B*, vol. 108, no. 37, pp. 14074–14081, 2004.
- [109] E. I. Altman and R. J. Colton, “Determination of the orientation of C₆₀ adsorbed on Au(111) and Ag(111),” *Physical Review B*, vol. 48, no. 24, pp. 18244–18249, 1993.
- [110] M. Paßens and S. Karthäuser, “Interfacial and intermolecular interactions determining the rotational orientation of C₆₀ adsorbed on Au(111),” *Surface Science*, vol. 642, pp. 11–15, 2015.
- [111] G. C. La Rocca, “Anisotropic C₆₀–C₆₀ intermolecular potential,” *EPL*, vol. 25, no. 1, pp. 5–10, 1994.
- [112] C. Chiutu, A. M. Sweetman, A. J. Lakin, A. Stannard, S. Jarvis, L. Kantorovich, J. L. Dunn, and P. Moriarty, “Precise orientation of a single C₆₀ molecule on the tip of a scanning probe microscope,” *Physical Review Letters*, vol. 108, no. 26, 2012.
- [113] P. Gravi, M. Devel, P. Lambin, X. Bouju, C. Girard, and A. Lucas, “Adsorption of c₆₀ molecules,” *Physical Review B*, vol. 53, 1996.
- [114] Y. Shang, Z. Wang, D. Yang, Y. Wang, C. Ma, M. Tao, K. Sun, J. Yang, and

- J. Wang, "Orientation ordering and chiral superstructures in fullerene monolayer on Cd (0001)," *Nanomaterials*, vol. 10, no. 7, pp. 1–10, 2020.
- [115] Z. Qin, C. Liu, J. Chen, Q. Guo, Y. Yu, and G. Cao, "Molecular orientation and lattice ordering of C₆₀ molecules on the polar FeOPt(111) surface," *Journal of Chemical Physics*, vol. 136, no. 2, p. 114702, 2012.
- [116] H. Lee, H. B. R. Lee, S. Kwon, M. Salmeron, and J. Y. Park, "Internal and external atomic steps in graphite exhibit dramatically different physical and chemical properties," *ACS Nano*, vol. 9, no. 4, pp. 3814–3819, 2015.
- [117] S. P. Jarvis, M. A. Rashid, A. Sweetman, J. Leaf, S. Taylor, P. Moriarty, and J. Dunn, "Intermolecular artifacts in probe microscope images of C₆₀ assemblies," *Physical Review B - Condensed Matter and Materials Physics*, vol. 92, no. 24, p. 241405, 2015.
- [118] M. Greiner and P. Kruse, "Recrystallization of tungsten wire for fabrication of sharp and stable nanoprobe and field-emitter tips," *Review of Scientific Instruments*, vol. 78, no. 2, p. 026104, 2007.
- [119] A. J. Pattison, *Applying Automation and Machine Learning to Scanning Transmission Electron Microscopy*. PhD thesis, School of Physics and Astronomy, University of Birmingham, 2020.
- [120] R. M. Overney, *Nanoscience on the tip, a workshop in scanning probe microscopy*. University of Washington, NUS UNIQUE, 2007.

- [121] P. Heimann, H. Neddermeyer, and H. F. Roloff, “Ultraviolet photoemission for intrinsic surface states of the noble metals,” *Journal of Physics C: Solid State Physics*, vol. 10, no. 1, p. L17, 1977.
- [122] B. Hulsken, J. W. Gerritsen, and S. Speller, “Measuring the Au(111) surface state at the solid-liquid interface,” *Surface Science*, vol. 580, no. 1-3, pp. 95–100, 2005.
- [123] P. J. Kowalczyk, M. Puchalski, W. Kozłowski, P. Dabrowski, Z. Klusek, and W. Olejniczak, “Investigation of the Shockley surface state on clean and air-exposed Au (111),” *Applied Surface Science*, vol. 254, no. 15, pp. 4572–4576, 2008.
- [124] R. Rösch and R. Schuster, “Tunneling spectroscopy of clean and adsorbate-covered gold surfaces in humid air, measured with fast bias voltage ramps,” *Surface Science*, vol. 631, pp. 105–111, 2015.
- [125] M. Passoni, F. Donati, A. Li Bassi, C. S. Casari, and C. E. Bottani, “Recovery of local density of states using scanning tunneling spectroscopy,” *Physical Review B - Condensed Matter and Materials Physics*, vol. 79, no. 4, p. 045404, 2009.
- [126] K. Schouteden and C. Van Haesendonck, “Narrow Au(111) terraces decorated by self-organized Co nanowires: A low-temperature STM/STS investigation,” *Journal of Physics Condensed Matter*, vol. 22, no. 25, p. 255504, 2010.
- [127] P. Avouris, “Real space imaging of electron scattering phenomena at metal surfaces,” *Journal of Vacuum Science & Technology B: Microelectronics and*

Nanometer Structures, vol. 12, no. 3, p. 1447, 1994.

- [128] E. Y. Andrei, G. Li, and X. Du, “Electronic properties of graphene: A perspective from scanning tunneling microscopy and magnetotransport,” 2012.
- [129] T. Matsui, H. Kambara, Y. Niimi, K. Tagami, M. Tsukada, and H. Fukuyama, “STS observations of landau levels at graphite surfaces,” *Physical Review Letters*, vol. 94, no. 22, p. 226403, 2005.
- [130] H. Söde, L. Talirz, O. Gröning, C. A. Pignedoli, R. Berger, X. Feng, K. Müllen, R. Fasel, and P. Ruffieux, “Electronic band dispersion of graphene nanoribbons via Fourier-transformed scanning tunneling spectroscopy,” *Physical Review B - Condensed Matter and Materials Physics*, vol. 91, no. 4, p. 045429, 2015.
- [131] R. Yin, Y. Zheng, X. Ma, Q. Liao, C. Ma, and B. Wang, “Clarifying the intrinsic nature of the phonon-induced gaps of graphite in the spectra of scanning tunneling microscopy/spectroscopy,” *Physical Review B*, vol. 102, no. 11, p. 115410, 2020.
- [132] S. Patil, S. Kolekar, and A. Deshpande, “Revisiting HOPG superlattices: Structure and conductance properties,” *Surface Science*, vol. 658, pp. 55–60, 2017.
- [133] R. C. Tatar and S. Rabii, “Electronic properties of graphite: A unified theoretical study,” *Physical Review B*, vol. 25, no. 6, pp. 4126–4141, 1982.
- [134] A. S. Milev, N. H. Tran, G. S. Kannangara, and M. A. Wilson, “Unoccupied electronic structure of ball-milled graphite,” *Physical Chemistry Chemical Physics*, vol. 12, no. 25, pp. 6685–6691, 2010.

- [135] G. Teobaldi, E. Inami, J. Kanasaki, K. Tanimura, and A. L. Shluger, “Role of applied bias and tip electronic structure in the scanning tunneling microscopy imaging of highly oriented pyrolytic graphite,” *Physical Review B - Condensed Matter and Materials Physics*, vol. 85, no. 8, p. 085433, 2012.
- [136] D. Tomnek and S. G. Louie, “First-principles calculation of highly asymmetric structure in scanning-tunneling-microscopy images of graphite,” *Physical Review B*, vol. 37, no. 14, pp. 8327–8336, 1988.
- [137] J. I. Pascual, J. Gómez-Herrero, D. Sánchez-Portal, and H. P. Rust, “Vibrational spectroscopy on single C₆₀ molecules: The role of molecular orientation,” *Journal of Chemical Physics*, vol. 117, no. 21, pp. 9531–9534, 2002.
- [138] N. Néel, J. Kröger, L. Limot, and R. Berndt, “Conductance of oriented C₆₀ molecules,” *Nano Letters*, vol. 8, no. 5, pp. 1291–1295, 2008.
- [139] C. Rogero, J. I. Pascual, J. Gómez-Herrero, and A. M. Baró, “Resolution of site-specific bonding properties of C₆₀ adsorbed on Au(111),” *Journal of Chemical Physics*, vol. 116, no. 2, pp. 832–836, 2002.
- [140] J. A. Larsson, S. D. Elliott, J. C. Greer, J. Repp, G. Meyer, and R. Allenspach, “Orientation of individual C₆₀ molecules adsorbed on Cu(111): Low-temperature scanning tunneling microscopy and density functional calculations,” *Physical Review B - Condensed Matter and Materials Physics*, vol. 77, no. 11, 2008.
- [141] I. Fernández Torrente, K. J. Franke, and J. Ignacio Pascual, “Spectroscopy of

- C_{60} single molecules: The role of screening on energy level alignment,” *Journal of Physics Condensed Matter*, vol. 20, no. 18, p. 184001, 2008.
- [142] M. Jung, D. Shin, S. D. Sohn, S. Y. Kwon, N. Park, and H. J. Shin, “Atomically resolved orientational ordering of C_{60} molecules on epitaxial graphene on Cu(111),” *Nanoscale*, vol. 6, no. 20, pp. 11835–11840, 2014.
- [143] C. Tzeng, W. Lo, J. Yuh, R. Chu, and K. Tsuei, “Photoemission, near-edge x-ray-absorption spectroscopy, and low-energy electron-diffraction study of on Au(111) surfaces,” *Physical Review B - Condensed Matter and Materials Physics*, vol. 61, pp. 2263–2272, jan 2000.
- [144] H. Ulbricht, G. Moos, and T. Hertel, “Interaction of [Formula presented] with Carbon Nanotubes and Graphite,” *Physical Review Letters*, vol. 90, p. 4, mar 2003.